Université de Montréal

Forme et évolution des barres branchiales et des osselets de la classe Enteropneusta (Phylum Hemichordata)

par

Charles Larouche-Bilodeau

Département de sciences biologiques
Faculté des Arts et des Sciences
Superviseur: Prof. Christopher B. Cameron

Thèse présentée à la Faculté des études supérieures
en vue de l'obtention du grade de PhD.
en sciences biologiques

15 septembre 2021

Université de Montréal
Département de sciences biologiques, Faculté des Arts et des Sciences

Cette thèse intitulée

Forme et évolution des barres branchiales et des osselets de la classe Enteropneusta (Phylum Hemichordata)

Présentée par

Charles Larouche-Bilodeau

A été évaluée par un jury composé des personnes suivantes

Annie Angers
Président-rapporteur

Christopher Cameron
Directeur de recherche

Pierre-Luc Chagnon
Membre du jury

Imran Rahman
Examinateur externe

Résumé

Pour bien comprendre comment les espèces actuelles ont évolué, il est important d'étudier certains groupes clés. Ces groupes clés sont parfois bien négligés au profit d'autres groupes apparentés. L'embranchement Hemichordata forme, avec Echinodermata, le clade Ambulacraria. Ce dernier, avec l'embranchement Chordata, forme le super-embranchement Deuterostomia. Parmi les deutérostomes, la classe d'hémichordé Enteropneusta est souvent considérée comme étant la plus ressemblante au dernier ancêtre commun des deutérostomes. Les entéropneustes partagent en effet plusieurs caractéristiques avec Chordata et Ambulacraria et en étudiant celles-ci on peut reconstruire et comprendre leurs états ancestraux.

Dans le chapitre d'introduction, j'aborde la morphologie générale des hémichordés et leurs relations évolutives avec les deux autres embranchement deutérostomes. Je présente aussi les caractéristiques qu'ils partagent avec les échinodermes et les cordés. J'aborde ensuite les formes que prennent les parties dures chez les animaux et en particulier chez les deutérostomes.

Dans le chapitre deux, j'examine et décris la forme et la composition chimique des osselets chez huit espèces d'hémichordé. Cette étude représente un énorme bond dans nos connaissances sur la biominéralisation chez les hémichordés, car jusqu'à présent les osselets n'avaient été décrits que chez deux espèces, et la composition chimique déterminée chez une seule d'entre elle. J'interprète également ces données dans un contexte évolutif, car les osselets d'hémichordé sont probablement homologues au squelette des échinodermes. Ce chapitre est important, car il nous donne une hypothèse sur l'origine des osselets chez le dernier ancêtre commun des ambulacraires.

Dans le chapitre trois, je quantifie l'asymétrie dans les fentes pharyngiennes de populations de deux espèces d'entéropneustes et d'une espèce de cordé non-vertébré. En mettant ces différents nivaux de symétrie en parallèle avec leur comportement alimentaire, les résultats supportent l'hypothèse de l'alimentation par filtration comme rôle initial des fentes pharyngiennes chez les deutérostomes et que la perte de cette fonction induit du bruit développemental, une vestigialisation ou une perte des fentes branchiales.

Dans le chapitre quatre, J'utilise la micro-tomographie aux rayons-X pour décrire une espèce d'hémichordé qui était jusqu'à présent un *numen nudum*. Cette nouvelle technique est comparée avec l'histologie traditionnelle afin de prouver qu'elle pourrait être utilisée dans les futures études taxonomiques sur les hémichordés.

Dans le chapitre cinq, je présente quelques expériences qui ont dû être exclues des chapitres précédents car elles ont donné des résultats négatifs non-publiables. Je discute des raisons pour lesquelles ces expériences ont échoué ainsi que quelques pistes de solutions possibles pour qui voudrait tenter de les refaire. Ensuite je récapitule les résultats des chapitres précédents pour montrer comment étudier les hémichordés peut encore nous apprendre beaucoup sur d'autres groupes pourtant déjà très étudiés.

Mots-clés:

Deuterostomia, Hemichordata, Enteropneusta, Ambulacraria, Chordata,

biominéralisation, osselet dermique, asymétrie fluctuante, taxonomie, évolution.

Summary

The phylum Hemichordata forms, with Echinodermata, the group Ambulacraria that in turns forms with Chordata, the Deuterostomia. Among deuterostomes, the hemichordate class Enteropneusta is often viewed as the group that most closely resembles the last common ancestor of deuterostomes. Enteropneusts indeed share many traits with the other two deuterostome phyla and by studying them, we can infer the ancestral states of those traits.

In the first chapter, I present the general morphology of hemichordates and their relationships with the other two deuterostome phyla. I also discuss the shared traits between the hemichordates, the echinoderms and the chordates. Last, I present the varied shapes that hard parts can take in animals, with a focus on deuterostomes.

In chapter two, I describe the shape and mineral composition of ossicles in eight enteropneust species. This study is a major leap in our understanding of biomineralization in Hemichordata since up to this point ossicles were only described in two species and the mineral composition determined for only one. I discuss these results in an evolutionary context since hemichordate ossicles are probably homologous with echinoderm skeletal ossicles. This chapter is significant because it provides a hypothesis on the origin of ossicles in the last common ancestor of ambulacrarians.

In chapter three, I quantify the level of asymmetry of the pharyngeal slits in populations of two species of enteropneusts and the invertebrate cephalochordate *Branchiostoma floridae*. We found that adults of these species display fluctuating asymmetry in the gills and that this asymmetry is lower in filter feeding. This is significant because it supports

the hypothesis that filter feeding is an ancestral feature of deuterostomes and that the loss of this function increases developmental noise, vestigiality, or loss of the gills.

In chapter four, I use X-ray microtomography to describe the enteropneust *Balanoglossus occidentalis* that was heretofore a *nomen nudum*. This new technique is compared with traditional histology to show that it is a viable tool in hemichordate taxonomical studies.

In chapter five, I present a few experiments that had to be excluded from the other chapters because they gave negative, unpublishable results. I discuss the probable causes of their failures and potential ways to solve these issues for those who would want to pursue them further. Finally, I summarise the results of the previous chapters to show how studying hemichordates can still teach us a lot about the origin and evolution of the better studied deuterostome phyla.

Keywords:

Deuterostomia, Hemichordata, Enteropneusta, Ambulacraria, Chordata, biomineralization, dermal ossicles, fluctuating asymmetry, taxonomy, evolution.

Table des matières

Liste of tables

Liste des figures

Remerciements

Je tiens, tout d'abord, à remercier mes parents, Carole Larouche et Jean Bilodeau, qui ont su me supporter durant toute ma scolarité. Grace à eux j'ai pu me concentrer a 100% à mes études tout en sachant qu'ils seraient là pour moi en cas de besoin. Je tiens aussi à remercier ma conjointe, Audrey Martel, qui m'a toujours poussé à me dépasser et à ne jamais abandonner et qui a gracieusement accepté de corriger la qualité de mon français dans cette thèse. Sans eux ce projet ne serait probablement jamais arrivé à terme.

Je vous aime.

Je veux aussi remercier mon directeur de recherche, Christopher B. Cameron, pour son support, ses conseils et les opportunités qu'il m'a données tout au long de mon cheminement.

Thank you Chris.

Je remercie également Louise Peletier et Rui Tahara pour leur aide avec les microscopes électroniques et leurs suggestions pour mes protocoles.

Finalement, je veux remercier tous les enseignants et professeurs qui m'ont guidé depuis l'école primaire jusqu'à aujourd'hui et en particulier : Martin Coutu, Pierre Lancup, Simon-Philipe Lebel, Colin Favret et Christopher B. Cameron.

Merci à tous!

1. Introduction

1.1 Hemichordata

1.1.1 Relations

Le petit phylum Hemichordata, membre du clade Deuterostomia, a longtemps été vu comme un groupe très basal de la lignée évolutive des chordés, les protochordés, bien qu'ils soient plus proches parents des échinodermes que des chordés (Fig. 1.1, Cannon *et al.*, 2009). Hemichordata et Echinodermata partagent un plan d'organisation corporel tricoelomé et un stade larvaire de type dipleurula, et forment le clade Ambulacraria qui est traditionnellement reconnu comme le groupe frère de Chordata (Cameron, 2005). Certaines analyses moléculaires placent toutefois le groupe des Xenacoelomorphes comme groupe frère des ambulacraires, et les protostomiens comme groupe frère des chordés (Kapli *et al.*, 2020). Morphologiquement, les hémichordés partagent, avec les chordés, un pharynx avec des branchies, une queue post-anal et un processus de neurulation similaire (Lowe *et al.*, 2004; Ruppert, 2005; Gonzalez, & Cameron, 2009; Miyamoto & Wada, 2013). Le phylum Hemichordata est formé de deux classes et d'une espèce énigmatique aux affinités incertaines. Les membres de la classe Enteropneusta sont des vers marins solitaires fouisseurs ou épibenthiques (Cameron, 2005). Cette classe est elle-même divisée en quatre familles: Harrimaniidae, Spengelidae, Ptychoderidae et Torquaratoridae (Cameron, 2018). Les membres de la classe Pterobranchia sont des animaux marins, suspensivores, benthiques et coloniaux ou agrégés qui sont répartis en deux familles : Cephalodiscidae et Rhabdopleuridae, avec un seul genre chacun (Mitchell et al. 2013). Finalement, la famille monotypique Planctosphaeridae inclut uniquement *Planctosphaera pelagica* (Spengel, 1932) une larve tornaria géante avec un stade adulte inconnu qui fut étudié vivante une seule fois (il est assumé qu'elle est la larve d'un entéropneuste encore inconnu) (Hart et al.,

1994). Ce phylum souvent négligé a une aire de répartition très vaste, des océans polaires aux eaux équatoriales et des zones littorales aux plaines abyssales (Osborn et al, 2011, Tassia et al., 2016). L'anatomie des hémichordés est relativement simple avec un plan de corps en trois parties : le prosome (Le proboscis ou le bouclier céphalique), le mésosome (le collet) et le métasome (le tronc) (Cameron, 2018).

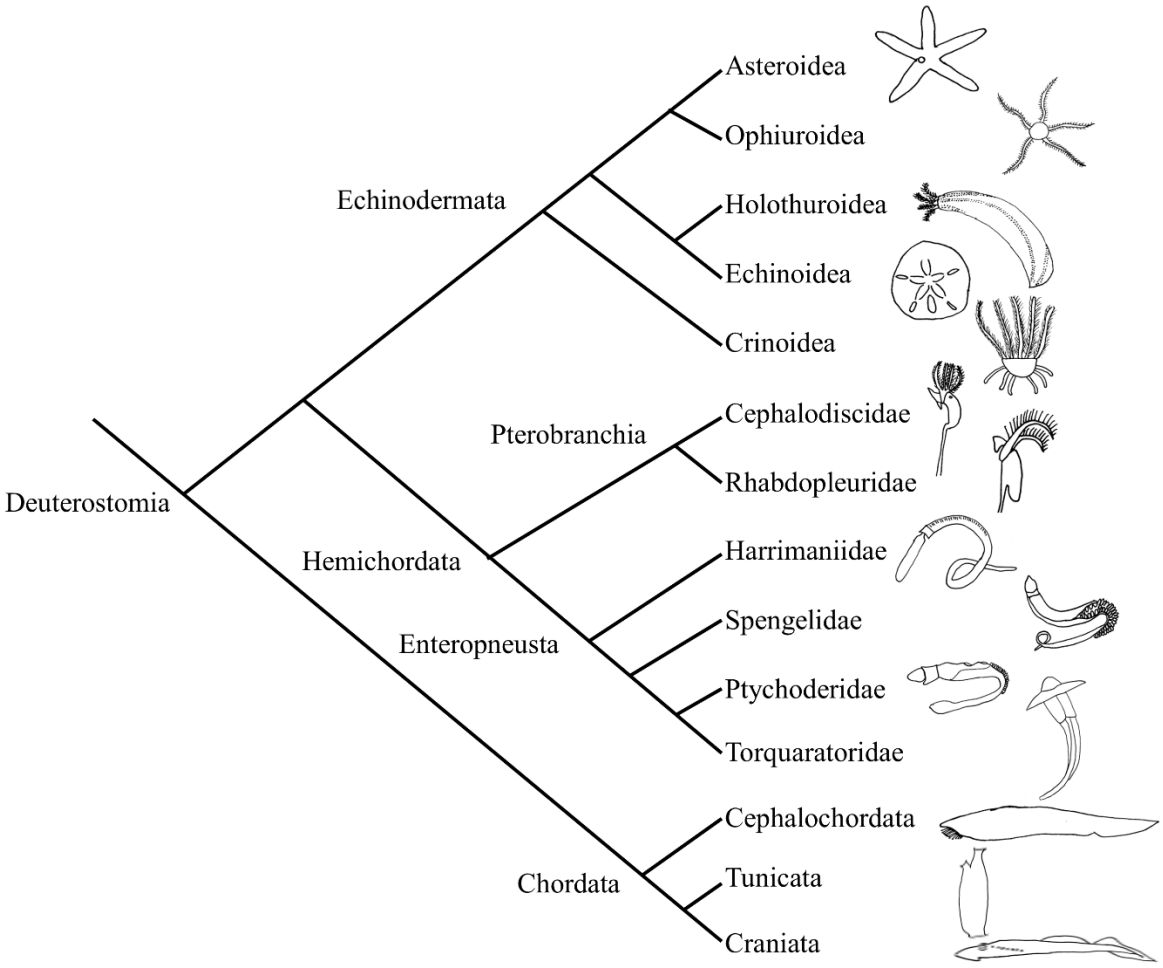

Figure 1.1 Arbre phylogénétique du clade Deuterostomia basé sur (Röttinger & Lowe, 2012; Cameron, 2018)

1.1.2. Enteropneusta

Chez les entéropneustes, le prosome est un proboscis musculeux et fortement cilié impliqué dans le fouissage et dans l'alimentation détritivore chez certaines espèces (Fig. 1.2; Balser et Ruppert, 1990). Dans le proboscis, il y a le complexe cœur-glomérule qui pompe et filtre le sang, qui est supporté par la stomochorde et qui est un homologue supposé du complexe axial des échinodermes (Fig. 1.2; Balser et Ruppert, 1990; Turbeville et al., 1994; Mayer et Bartolomaeus, 2003, Ezhova & Malakhov, 2020). Le glomérule est l'organe qui filtre le sang et crée l'urine primaire qui s'accumule dans le cœlome du proboscis (le protocoel,

Fig. 1.2). Celle-ci est ensuite excrétée par le pore situé sur le pédoncule du proboscis (Fig. 1.2; Balser et Ruppert, 1990; Mayer et Bartolomaeus, 2003). La stomochorde est aussi impliquée dans le mécanisme d'excrétion (Balser et Ruppert, 1990; Mayer et Bartolomaeus, 2003). Elle a longtemps été considérée comme un homologue ou un précurseur de la notochorde, mais les données moléculaires et développementales supportent maintenant une relation avec des structures dérivées du pharynx chez les vertébrés (Ruppert, 2005; Satoh et al., 2014). Le proboscis possède aussi un organe cilié préoral impliqué dans l'alimentation par filtration (Fig. 1.2; Burdon-Jones, 1962; Gonzalez & Cameron, 2009; Cameron, 2018).

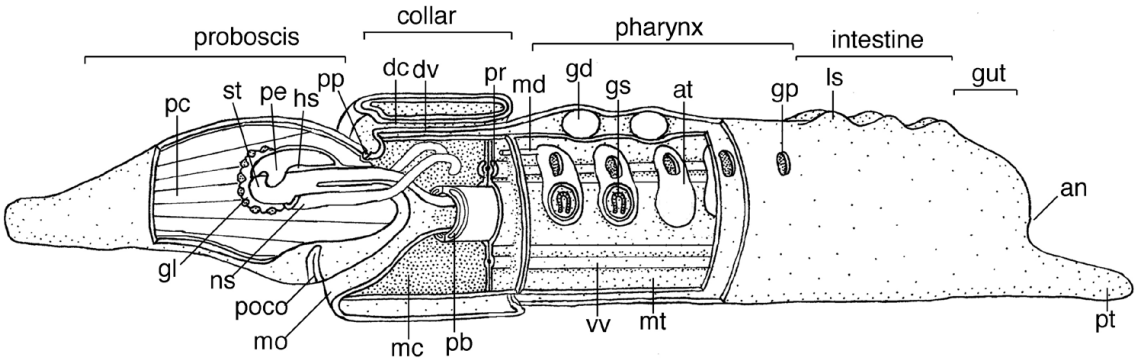

Figure 1.2 Illustration généralisé de la morphologie d'un enteropneust (adapté de Cameron 2005, fig. 1 & Cameron 2018, fig. 1). **an,** Anus; **at,** atrium; **dc,** corde neural dorsale; **dv**, vaisseaux sanguin dorsal; **gd,** gonade; **gl,** glomérule; **gp,** pore branchial; **gs,** fente branchiale; **hs,** sinus cardiaque; **ls,** diverticule hépatique; **mc,** mesocoel; **md,** canal du collet; **mo,** bouche; **mt,** métacoel; **ns,** squelette du proboscis; **pb,** cœlome peribuccal; **pc,** protocoel; **pe,** péricarde; **pt,** queue post-anal; **poco,** organe cilié préoral; **pp,** pore du proboscis; **pr,** cœlome perihaemal; **st,** stomochorde; **vv,** vaisseau sanguin ventral.

Le proboscis est lié au collet par un petit pédoncule qui contient une structure squelettique en forme de Y appelée le squelette du proboscis (Miyamoto et Wada, 2013; Cameron, 2018). Le collet contient essentiellement la bouche et un tube neural dorsal qui pourrait avoir un lien évolutif avec le tube neural des chordés (Miyamoto et Wada, 2013). Le collet possède également une paire de « canaux du collet » qui s'ouvrent généralement dans la première poche pharyngienne et permettent l'échange de liquide entre le mesocoel et l'environnement (Willey 1899; Deland et al., 2010; Ezhova & Malakhov, 2015).

Les entéropneustes possèdent un pharynx perforé de fentes branchiales dans la région la plus antérieure de leur tronc (Cameron, 2002; Gonzalez et Cameron 2009). Ces branchies permettent d'expulser l'eau des sédiments capturés par le mucus et le proboscis ou de filtrer les particules en suspension. Quelques espèces peuvent faire les deux en même temps (Cameron, 2002; Gonzalez et Cameron 2009). Les fentes branchiales sont supportées par un squelette de collagène, les barres branchiales primaires et secondaires qui peuvent être reliées par des synapticulae (Cameron & Perez, 2012; Cameron & Ostiguy, 2013). Des

similitudes fonctionnelles, développementales et morphologiques combinées aux données paléontologiques ont prouvé que les branchies pharyngiennes sont une synapomorphie des deutérostomes et non une apomorphie des chordés (Ogasawara et al., 1999; Gerhart et al., 2005; Rychel et al., 2006; Rychel and Swalla, 2007; Gonzalez & Cameron, 2009; Gillis et al., 2012; Fritzenwanker et al., 2014; Nanglu et al., 2016). Chez les entéropneustes la région pharyngienne et la région suivante, la région génitale, se chevauchent souvent (Deland et al.,2010; Cameron & Perez, 2012; Cameron & Ostiguy, 2013; Jabr et al., 2018). Cette région génitale est formée de deux rangées de gonades (4 chez certains genres) qui forment souvent des crêtes ou peuvent se développer en « ailes génitales » chez certains membres des familles Ptychoderidae et Torquaratoridae (Deland et al., 2010; Lukinykh et al., 2018). Ensuite, vient la région hépatique qui peut porter des sacculations chez Spengelidae, Ptychoderidae et Torquaratoridae, mais est marquée par une coloration plus foncée chez tous les groupes (Benito et al., 1993; Bridges & Woodwick, 1994; Cedhagen & Hansson, 2012). Finalement, le tronc se termine avec la région digestive post-hépatique qui n'a aucune caractéristique particulière sinon de petites protubérances glandulaires dans lesquelles des osselets ont été trouvés chez deux espèces (Cameron & Bishop, 2012). Chez les Ptychoderidae, une autre structure peut être trouvée dans le mésentère ventral de la partie digestive postérieure du tronc, la pygochorde (Yoshimura et al., 2019). La pygochorde est une masse de cellules hautement vacuolées et riches en collagène fibrillaire qui a probablement une fonction de support squelettique (Yoshimura et al., 2019).

Quand les vers se nourrissent par filtration, des cils sur les barres branchiales produisent le courant d'eau qui aspire et transporte les particules (Cameron, 2002; Gonzalez & Cameron, 2009). Les particules trop petites passent entre les branchies et sont expulsées, mais les

plus grosses sont retenues et passent dans le tube digestif pour être digérées (Gonzalez & Cameron, 2009). L'organe cilié préoral en forme de U manipule et sélectionne les particules avant l'ingestion (Gonzalez et Cameron, 2009). Les vers produisent un abondant mucus qui aide à l'adhésion et au transport des particules chez les vers détritivores (Cameron, 2002). Les espèces des eaux profondes de la famille Torquaratoridae possèdent aussi des extensions latérales sur leur collet, appelées les lèvres du collet, qui aident à acheminer les sédiments jusqu'à la bouche (Jabr et al., 2018).

Certains entéropneustes sont à développement indirecte et passent par un stade larvaire appelé tornaria (Lowe *et al.*, 2015). Il s'agit du seul stade de vie connu de *Planctosphaera pelagica* (Hart *et al.*, 1994). Les tornarias sont des larves de type dipleurula avec trois cœlomes comme les larves des échinodermes (Fig. 1.3; Lowe et al., 2015). La première cavité, le protocoel, communique avec l'environnement extérieur via un hydropore dorsal qui forme un organe rénal (Fig. 1.3; Ruppert & Balser, 1986). La larve tornaria porte un anneau de cils postérieur spécialisé pour la propulsion (le telotroch), une touffe de cils apicaux qui agissent comme un gouvernail, et un organe apical sensoriel avec un ocelle pour détecter la lumière (Fig. 1.3; Strathmann & Bonar, 1976; Nezlin, 2000; Nakajima et al., 2004; Braun et al., 2015). Ces structures permettent aux larves de nager activement vers le haut ou le bas selon leur âge et la présence de lumière du jour; les jeunes larves montrent un phototaxisme positif et celles prêtes à se métamorphoser un phototaxisme négatif (Strathmann & Bonar, 1976 Braun et al., 2015). Une seconde bande de cils entoure la bouche et le corps de la larve et sert à l'alimentation par filtration (Fig. 1.3; Strathmann & Bonar, 1976).

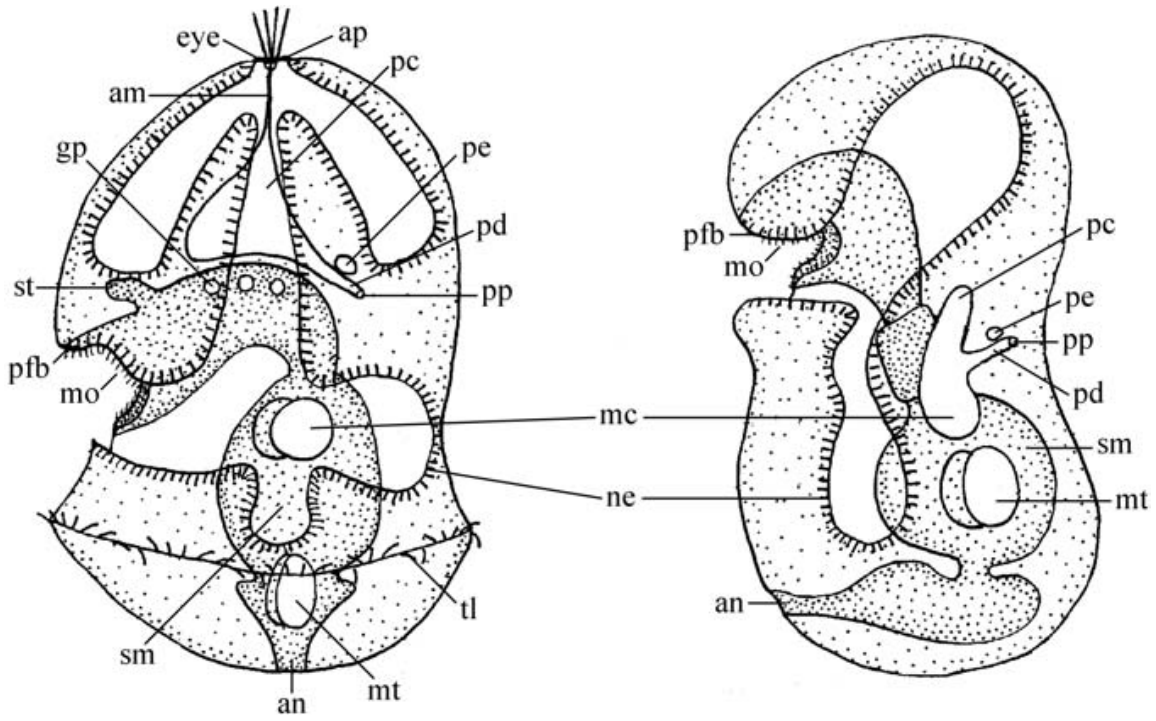

Figure 1.3 Schéma de larve de type dipleurula d'un Entéropneuste (gauche) et d'une étoile de mer (droite) (adapté de Cameron, 2005, fig. 3). **Ap,** plaque apicale; **am,** muscle retracteur de la plaque apicale; **eye,** ocelle; **ne,** neotroch; **pd,** canal du protocoel; **pfd**, bande d'alimentation péri-oral; **sm,** estomac; **tl,** telotroch. Voir la légende de la figure 1.2 pour les abréviations additionnelles.

Les différentes familles d'entéropneustes peuvent être distinguées selon les variations des caractères susnommés. Les Harrimaniidae sont à développement directe, n'ont pas de sac hépatique, d'aile génitale ou de muscle circulaire dans le tronc (Deland et al, 2010). Un genre (*Stereobalanus*) de cette famille a récemment été placé comme groupe frère à tous les autres entéropneustes par des analyses mitogénomiques (Li et al., 2018). *Stereobalanus* a une morphologie unique avec quatre crêtes génitales restreintes à la région pharyngienne, des barres branchiales visibles de l'extérieur, et les canaux du collet sont réduits ou absents (Deland et al, 2010; Ezhova & Malakhov, 2015). Son type de développement est encore inconnu et son placement au sein des Harrimaniidae est au minimum questionnable (Deland et al, 2010; Cannon et al., 2014; Li et al., 2018). Les Spengelidae sont caractérisés par leur possession d'un procès vermiforme antérieur sur leurs stomochordes, d'une couche

de muscles circulaire à l'intérieur de la couche longitudinale, et d'une larve tornaria (Cameron et al., 2010; Cameron & Perez, 2012). Certain Spengelidae possèdent également des sacs hépatiques et des synapticulae (Cameron et al., 2010; Cameron & Perez, 2012). Les Ptychoderidae sont aussi à développement indirect, ne possèdent pas de procès vermiforme, mais ont des septas latéraux dans le tronc, la couche de muscles circulaire du tronc est à l'extérieur de la longitudinale, ils ont normalement des sacs hépatiques et peuvent avoir des ailes génitales (Cameron & Ostiguy, 2013). Finalement, les Torquaratoridae sont des habitants des mers profondes épibenthiques avec un développement inconnu, à l'exception d'une espèce qui couvent leur descendance (Osborn et al., 2013). Cette famille a des ailes génitales, des lèvres du collet, des replies cutanés ventraux sur le tronc, des barres branchiales peu développées, une musculature peu développée, et une stomochorde et un squelette du proboscis réduits voir absents (Cameron et al., 2010, Jabr et al., 2018).

1.1.3. Pterobranchia

Chez les ptérobranches, le prosome est modifié en bouclier céphalique (Fig. 1.4). Cette structure est impliquée dans la sécrétion de leurs tubes, le « coenecium », et du déplacement en son sein (Lester, 1985; Dilly, 1986). Le squelette du proboscis est absent chez cette classe (Mayer & Bartolomaeus, 2003; Merker et al., 2014). Une stomochorde solide supporte un complexe cœur-glomérule moins développé que celui des entéropneustes, mais avec la même fonction (Fig. 1.4; Mayer & Bartolomaeus, 2003; Merker et al., 2014).

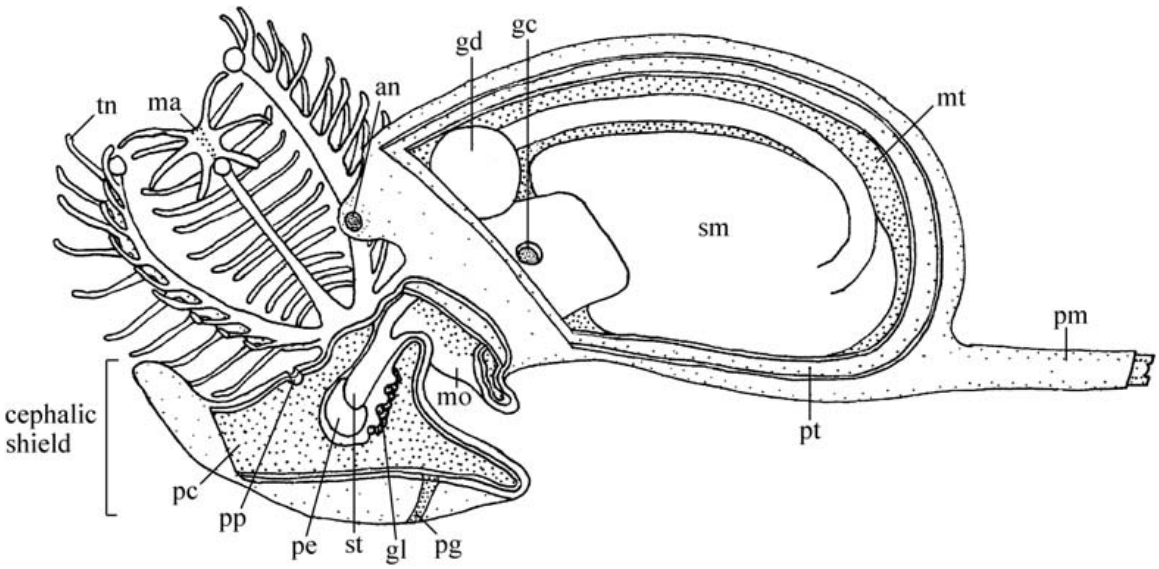

Figure 1.4 Illustration du ptérobranche *Cephalodiscus* (adapté de Cameron, 2005, fig. 4). **gc,** perforation branchiale; **ma,** bras mesosomal; **pg,** bande pigmentée; **tn,** tentacule mesosomal. Voir les légendes des figure 1.2 & 1.3 pour les abréviations additionnelles.

Le collet porte une (Rhabdopleuridae) ou cinq à neuf (Cephalodiscidae) paires de bras, chacun avec deux rangées de tentacules ciliés, qui servent à la nutrition suspensivore (Fig. 1.4; Halanych, 1993; Maletz, 2014). Il n'y a pas de tube neural dans le collet, mais un ganglion dorsal est présent et probablement homologue au tube neural des entéropneustes (Fig. 1.4; Rehkämper et al., 1987; Stach et al., 2012).

Le métasome est divisé en un tronc en forme de sac et un stolon (Fig. 1.4; Maletz, 2014). Le tube digestif est en U et l'anus est médiodorsal (Fig. 1.4; Maletz, 2014). Le métasome porte une seule paire (Cephalodiscidae) ou aucune paire (Rhabdopleuridae) de branchies et une (Rhabdopleuridae) ou deux (Cephalodiscidae) gonades (Sato & Holland, 2008; Dilly, 2014). Le corps se termine par un stolon qui lie le zoïde à la colonie (Rhabdopleuridae) ou pas (Cephalodiscidae) (Maletz, 2014).

Les zoïdes peuvent se reproduire par bourgeonnement (Maletz, 2014). Chez les Cephalodiscidae, les bourgeons se forment à l'extrémité distal du stolon et se détachent à

maturité (Dilly, 2014). Chez les Rhabdopleuridae, les bourgeons se forment sur la longueur du stolon et ne se détachent jamais, formant une véritable colonie (Strano et al., 2019).

Le coenecium abrite et protège les zoïdes. Chez les Rhabdopleuridae il montre une structure faite d'anneaux semicirculaires ou circulaires, des « fuselli », qui sont absents des Cephalodiscidae (Dilly, 1986; Gonzalez & Cameron, 2012; Maletz, 2014). Chez ces derniers, des corps étrangers, tels que des spicules d'éponges et des valves de diatomées, sont souvent intégrés au coenecium (Dilly 1986; Gonzalez & Cameron, 2012). La reproduction sexuée engendre des petites larves capables de nager et caractérisées par une dépression ventrale qui s'installe à un nouvel endroit propice et se métamorphose en zoïde, premier d'une nouvelle colonie (Stach, 2013; Dilly, 2014, Strano *et al.*, 2019).

1.2. Echinodermata

1.2.1 Échinodermes modernes

Les échinodermes sont les plus proches parents vivants des hémichordés et incluent cinq classes modernes (Cannon *et al.*, 2014). Même si la monophylie du clade Ambulacraria est fortement supportée par les données moléculaires et la morphologie larvaire, la morphologie des adultes des deux phylums est très différente (Lowe *et al.*, 2015). Pour commencer, les échinodermes ont perdu la symétrie bilatérale au profit d'une symétrie radiaire d'ordre cinq, même si leurs larves sont encore bilatérales (Byrne *et al.*, 2016). Cette symétrie penta-radiaire a cependant été perdue et une symétrie bilatérale secondaire est apparue chez plusieurs ordres comme Cyrtocrinida, Irregularia et plusieurs Holothuroidea (Kerr & Kim, 1999; Roux *et al.*, 2002; Saucède *et al.*, 2003). Une famille de ces derniers,

les Rhopalodinidae, a même reperdu la symétrie bilatérale une seconde fois, et a acquis une symétrie radiaire d'ordre dix (Kerr & Kim, 1999). Les échinodermes sont aussi caractérisés par leur squelette, formé de spicules de calcite à haut taux de magnésium, qui donne le nom à l'embranchement (Cannon *et al.*, 2014). Leur squelette est unique par sa structure hautement poreuse appelée un stéréome (Bottjer *et al.*, 2006; Cannon *et al.*, 2014). Ils possèdent aussi un système aquifère dérivé de l'axocoel et de l'hydrocoel gauche de la larve qui correspondent aux protocoel et mesocoel des hémichordés respectivement (Lowe *et al.*, 2015).

Dans les larves d'échinodermes, l'axocoel (protocoel) gauche porte, comme chez les hémichordés, un canal qui mène à un hydropore ayant une fonction excrétrice (Ruppert & Balser, 1986). Cet hydropore est incorporé au madrépore chez l'adulte (McEdward & Miner, 2001). L'axocoel gauche devient le sinus axial avec des affinités et homologies incertaines avec les autres deutérostomes (McEdward & Miner, 2001; Ezhova *et al.,* 2013; Ezhova & Malakhov, 2020). Le complexe axial semble être impliqué dans la circulation du système hémal (Ezhova *et al*., 2013). L'hydrocoel (mesocoel) gauche devient le système aquifère chez l'adulte (Eshova *et al.,* 2013). L'axocoel droit et l'hydrocoel droit sont globalement perdus ou deviennent la vésicule du madrépore respectivement (McEdward & Miner, 2001). Les derniers deux cœlomes, les somatocoels (métacoel), forment les cavités cœlomiques du corps de l'adultes (McEdward & Miner, 2001). La plupart des larves d'échinoderme forment un squelette larvaire. Le plus étudié étant celui des echinopluteus (Morino *et al.*, 2016).

1.2.2 Échinodermes fossiles

Les plus vieux fossiles d'échinodermes, les homalozoaires, peuvent être retracés jusqu'au Cambrien (Zamora *et al.*, 2012; Smith *et al.*, 2013). Même si leur plan de corps est très différent des échinodermes récents, leur squelette de calcite avec un stéréome démontre fortement leur appartenance au groupe-tronc des échinodermes (Zamora & Rahman, 2014). Les plus basaux des homalozoaires, les Ctenocystoidea, étaient bilatéraux comme le dernier ancêtre commun putatif des Ambulacraria. (Zamora *et al.*, 2012). Ces derniers n'ont apparemment pas de système aquifère (Zamora *et al.*, 2012). Le reste des homalozoaires montrent des degrés variés d'asymétrie directionnelle et de torsion (Smith, 2008). Ils possèdent aussi des branchies comme les chordés et les hémichordés et sont présumés avoir été des animaux filtreurs (Zamora *et al.*, 2012; Rahman *et al.*, 2015). Cette tendance à la torsion est rendue encore plus évidente dans un autre groupe, les Helicoplacoidea, qui montrent une organisation spiralée du système ambulacraire (Zamora *et al.*, 2012). La torsion comme origine évolutive de la symétrie radiaire est encore visible lors de la métamorphose des échinodermes modernes (Zamora *et al.*, 2012).

1.3. Biominéralisation

1.3.1 La diversité des partie dures chez les animaux

Les animaux ont acquis, au cours de l'évolution, un véritable florilège de structures qui peuvent être regroupées sous le terme de « parties dures » pour des fonctions tout aussi variées. Certains animaux mous comme les placozoaires, les cténophores, les schiphozoaires et les xenacoelomorphes n'ont que de petits statolithes calcifiés comme

seules « parties dures » qui leur confèrent une capacité de graviception (Tamm, 2014; Nakano *et al.*, 2017; Mayorova *et al.*, 2018). Plusieurs autres phylums d'animaux utilisent les « parties dures » pour des fonctions de support et de protection comme les arthropodes, les éponges, les coraux, les échinodermes, les chordés, les mollusques et plus encore (Kingsley, 1989). Certains stades larvaires, comme les larves d'échinodermes, utilisent aussi leur squelette comme un poids qui assure que la larve reste dans la même orientation en gardant son centre de gravité à l'extrémité postérieur (Pennington & Strathmann, 1990).

Ces « parties dures » peuvent être faites de protéines (comme le collagène, la spongine et la kératine), de polysaccharides (comme la chitine et la cellulose), de minéraux (le carbonate de calcium, le phosphate de calcium et les silices sont les plus communs) ou d'une combinaison de plusieurs d'entre eux (Donoghue *et al.*, 2006; Murdock & Donoghue, 2011; Sato *et al.*, 2011; Zhao & Li, 2014; Luo *et al.*, 2015).

Au sein d'un même taxon, la nature des « parties dures » peut varier même dans les structures homologues. Par exemple, le squelette des vertébrés peut être fait de cartilage ou de $CaPO_4$ (Donoghue *et al.*, 2006); Les soies des vers polychètes peuvent être faits de chitine ou de $CaCO_3$ (Fauchald, 1977); La coquille des brachiopodes peut être faite de $CaPO_4$ ou de $CaCO_3$ (Luo *et al.*, 2015); L'opercule des gastéropodes peut être corné, calcifié et parfois supplémenté d'écailles de FeS_2 ou de Fe_3S_4 (Chen *et al.*, 2015; Heller, 2015). La liste pourrait continuer sur des pages et des pages, mais les prochaines sections se concentreront sur les lignées deutérostomes.

1.3.2 Le squelette des échinodermes

Les membres du phylum Echinodermata possèdent un endosquelette très développé qui fournit structure, support et protection à ces animaux (O'Donnell *et al.*, 2010). Ce squelette est fait exclusivement de calcite à haut taux de magnésium; une forme de carbonate de calcium plus soluble que l'aragonite, mais moins que la vatérite ou le $CaCO_3$ amorphe (Falini *et al.*, 1996; O'Donnell *et al.*, 2010; Woosley *et al.*, 2012). Les spicules sont formés d'un unique cristal de calcite beaucoup plus résistant aux fractures que leurs équivalents synthétiques et très riche en glycoprotéine acide (Berman *et al.*, 1990).

Le squelette des échinodermes est caractérisé par sa structure très poreuse connue sous le nom de stéréome. Cette porosité permet aux osselets de prendre des formes variées et d'avoir une grande résistance aux stress physiques (Stock, 2014). La complexité des formes qui peut être atteinte est telle que, comme chez certaines ophiures phototaxiques, le stéréome peut adopter la forme d'un réseau de microlentilles qui agissent potentiellement comme un œil composé de la taille de l'animal (Aizenberg *et al.*, 2001; Vinogradova, 2016). La taille du squelette varie aussi énormément dans ce phylum, mais même chez les membres où il est réduit à des éléments isolés d'à peine quelques dizaines de microns, comme plusieurs Holothuroidea, leur forme est toujours celle d'un stéréome poreux (Massin et Lane, 1991).

Le squelette apparait très tôt chez les larves de type pluteus et est remplacé à la métamorphose (Wilt *et al.,* 2003). Les cellules responsables de la formation du squelette se nomment sclérocytes (Wilt *et al.,* 2003). Chez les oursins, le squelette larvaire est sécrété par une unique lignée de cellules : les cellules du mésenchyme primaire (Wilt *et al.,* 2003). Les sclérocytes sécrètent les ions nécessaires à la minéralisation dans des vacuoles

intracellulaires dans lesquelles la cristallisation débute (Kingsley, 1990; Cameron et Bishop, 2012). Ensuite, une fusion entre les vacuoles de plusieurs sclérocytes forme un espace occlus où le squelette se développera (Kingsley, 1990; Cameron et Bishop, 2012). L'organisation de ces espaces en tubes qui donne la forme au squelette est assurée par le facteur de croissance endothélial vasculaire (VEGF) qui contrôle la croissance des sclérocytes (Morgulis *et al.*, 2019). Ce même facteur de croissance est utilisé dans la plupart des autres phylums pour contrôler la croissance des différents vaisseaux (Morgulis *et al.*, 2019).

1.3.3 La minéralisation des chordés

Le phylum Chordata est divisé en trois sous-phylum qui ont chacun des « parties dures » différentes. Les Cephalochordata ne minéralisent pas leur squelette qui est formé de collagène de type II (Rychel et al., 2006; Rychel and Swalla, 2007). Ce squelette est représenté par les barres branchiales et une notochorde non-vacuolée (Ogasawara et al., 1999; Rychel et al., 2006; Rychel and Swalla, 2007). Chez les Tunicata, plusieurs espèces produisent des spicules calcifiés et les intègrent à leur tunique (Lambert & Lambert, 1997; Monniot & Monniot, 2008). Les spicules sont faits soit de $CaCO_3$ amorphe, de calcite, d'aragonite ou de vatérite selon les espèces et le type de spicule (Lambert, 1992; Lambert & Lambert, 1997; Aizenberg *et al.*, 2002; Monniot & Monniot, 2008). Leur tunique, elle, est faite de tunicine, un polysaccharide semblable à la cellulose des plantes (Belton *et al.*, 1989; Zhao & Li, 2014). Finalement, les vertébrés peuvent minéraliser leurs os avec de l'hydroxyapatite de calcium et leur otolithe avec du carbonate de calcium, ou conserver l'état ancestral cartilagineux de leur squelette (Ren *et al.*, 2013).

1.3.4 La biominéralisation des hémichordés

La découverte récente d'osselets en carbonate de calcium dans les vers *Saccoglossus bromophenolosus* et *Ptychodera flava* (Enteropneusta, Hemichordata) suggère que la biominéralisation du $CaCO_3$ pourrait être un trait ancestral du clade Ambulacraria (Hemichordata & Echinodermata) (Cameron and Bishop, 2012). Les osselets des hémichordés sont microscopiques, d'une taille de 10 à 30 microns, faits de carbonate de calcium sous la forme d'aragonite et situés juste sous l'épithélium du tronc (Cameron and Bishop, 2012). Les osselets de *S. bromophenolosus* ont une forme de brocoli à deux bouts. Les extrémités sont faites de plusieurs trabécules formés d'empilements de cristaux, et de pores qui rappellent le stéréome des échinodermes. Ils se forment dans un espace extracellulaire occlus par des cellules semblables aux sclérocytes des échinodermes. Ceux de *P. flava* sont des sphères avec une couche laminaire externe et un intérieur poreux (Cameron and Bishop, 2012). Rien n'est connu de la composition protéique des osselets d'hémichordé, mais des gènes homologues aux gènes de biominéralisation de l'oursin, comme Sp-Msp130L, Sp-Msp130, Sp-Msp130r1, Sp-Msp130r2, Sp-Msp130r3, Sp-Mt1-4/MmpL7 et Sp-Clara7LA (Glean3_entries 06387; 02088; 13822; 16506; 13823, 28748 et 12518 respectivement), sont présents dans le génome de *Saccoglossus kowalevskii* (Cameron and Bishop, 2012).

Nous sommes encore au tout début de notre compréhension des osselets d'hémichordé et plusieurs questions sont encore en suspens : Y a-t-il une matrice protéique qui contrôle la croissance des osselets et quelles sont les protéines qui s'y retrouvent? Quand apparaissent-ils au cours du développement? Comment sont-ils répartis dans le corps des vers? À quoi servent-ils? Ils ont été retrouvés dans deux familles distantes (Ptychoderidae et

Harrimaniidae), ce qui suggère qu'ils sont probablement communs et présents dans d'autres espèces; lesquelles? Partagent-ils une histoire évolutive avec le squelette des échinodermes comme le suggèrent plusieurs similitudes?

1.3.5 MSP

La famille de gène MSP, mentionnée plus haut, est connue comme un élément essentiel du réseau de régulation génétique de la biominéralisation des échinodermes et comme une protéine abondante dans la matrice de leurs osselets (Mann *et al*, 2008). Des gènes homologues à cette famille de gènes ont été trouvés dans trois autre taxons : Mollusca, Cephalochordata et Hemichordata (Cameron & Bishop, 2012; Ettensohn, 2014). Chez les mollusques, ces gènes sont exprimés dans les régions du manteau qui sécrètent la coquille (Ettensohn, 2014). Ces gènes sont probablement arrivés dans leurs génomes par des évènements de transfert horizontal, depuis une algue ou une bactérie, une fois chez les mollusques et une ou deux fois chez les deutérostomes (Ettensohn, 2014). Tous ces taxons sauf Cephalochordata biominéralisent le carbonate de calcium (Mann *et al.*, 2008; Cameron & Bishop, 2012; Ettensohn, 2014). On ne sait pas encore s'ils sont impliqués dans la minéralisation des hémichordés (Cameron & Bishop, 2012).

1.4 Hypothèses et Objectifs

Les hémichordés ont très peu de structures solides, mais il y a des ressemblances fascinantes entre leurs parties dures et celles des autres deutérostomes tel que décrit plus haut (Cameron, 2018). Avec les échinodermes, ils semblent partager des osselets

dermiques de carbonate de calcium, mais de tels osselets n'ont été décrits que chez deux espèces d'hémichordés (Cameron & Bishop, 2012). Avec les chordés, ils partagent des barres branchiales pharyngiennes cartilagineuses. L'homologie entre ces dernières est solidement démontrée (Ruppert, 2005; Gillis *et al.*, 2012; Ou *et al.*, 2012; Lowe *et al.*, 2015; Simakov *et al.*, 2015). Cependant, même si on considère que l'ancêtre commun des deutérostomes avait des branchies, plusieurs auteurs considèrent qu'il doivent être asymétrique (Jefferies *et al.*, 1996; Sato & Holland, 2008). Les entéropneustes ont peu changé morphologiquement depuis 500 millions d'années. Ils sont donc un groupe clé qu'il faut étudier pour bien comprendre l'évolution des deutérostomes.

Avant de pouvoir inférer une homologie entre les osselets des hémichordés et des échinodermes, il faut d'abord confirmer que les osselets sont vraiment une caractéristique répandue chez les hémichordés. Ensuite, il faut déterminer si les ressemblances sont seulement superficielles ou s'il est plus parcimonieux de croire qu'elles sont le résultat d'une origine commune. Pour ce faire, j'ai déterminé la forme et la structure cristalline des osselets chez huit espèces supplémentaires d'entéropneustes dans le chapitre 2. J'ai également tenté de séquencer les protéines matricielles des osselets et d'identifier les fonctions possibles de ceux-ci à l'aide de l'immunohistochimie, mais ces deux expériences se sont révélées non-concluantes. Je les aborde plus en détail dans le chapitre 5.

Afin de déterminer à quoi servaient les branchies chez le deutérostome ancestral et si elles étaient symétriques, il faut d'abord bien savoir comment elles sont chez les deutérostomes vivant aujourd'hui. J'ai quantifié pour la première fois le niveau de symétrie pharyngienne chez des deutérostomes invertébrés. Comme personne n'avait encore fait ce genre d'étude sur ces groupes, ces nouvelles données permettent de solidifier l'hypothèse d'un

deutérostome ancestral ayant des branchies pharyngiennes symétriques utilisées pour l'alimentation par filtration.

Tangentiellement à l'étude des osselets d'entéropneustes, j'ai testé la viabilité de la microtomographie computationnel aux rayons-X pour visualiser l'anatomie interne des entéropneustes et notamment de leur parties dures. Initialement je désirais utiliser cette technique pour visualiser les osselets sans détruire le ver, mais cela s'est révélé impossible. Le chapitre 4 est donc une étude de l'efficacité de cette technique en taxonomie afin de rentabiliser les spécimens et données déjà récoltés pour tenter de visualiser les osselets.

En somme, l'embranchement Hemichordata est un exemple de groupe négligé qui mérite d'être plus étudier, car il nous reste encore beaucoup à apprendre sur eux et même sur d'autres taxa grâce à eux.

2 Acorn worm ossicle ultrastructure and composition, and the origin of the echinoderm skeleton

Charles Larouche-Bilodeau and Christopher B. Cameron

2.1 Author contribution

CLB and CBC created the ossicle isolation protocol and collected the animals on the field. CLB isolated the ossicle samples. CLB took the SEM micrographs and Raman spectra. CLB lead the data analysis and the writing of the chapter.

2.2 Abstract

Here, we expand our knowledge of hemichordate biomineralization by describing the shape and mineral composition of ossicles from eight acorn worm species, bringing the total known biomineralizing enteropneusts to ten and confirming that ossicles are widespread in Enteropneusta. Three general forms were identified with scanning electron microscopy, including a globular form that was found in the three major enteropneust families. The mineral composition of the ossicles was characterized with confocal spectroscopy analysis. The three polymorphs of calcium carbonate, calcite, aragonite and vaterite, were found and are species dependant. Calcite is the most common polymorph in enteropneusts and the only one known for echinoderms. Based on these findings we hypothesize that an enteropneust like ancestor to the Ambulacraria possessed microscopic, monotypic globular shaped, calcite ossicles, with stereom, low Mg content, and MSP130 proteins. These ossicles lacked intercalation with other ossicles. The function of acorn worm ossicles is unknown, but the position of ossicles in the trunk epithelia and near to the surface suggests predator deterrence, to provide grip on the walls of a burrow or tube, or as storage of metabolic waste, rather than as an endoskeleton function seen in fossil and crown group Echinodermata.

2.2.1 Keywords

biomineralization, Ambulacraria, acorn worm, Enteropneusta, evolution, Deuterostomia

2.3 Background

Biominerals in the animal kingdom range from the simple statoliths found in xenacoelomorphs, ctenophores and placozoans, to the extensive shells of molluscs, the reef forming skeleton of sponges and corals, and the vertebrate skeleton (Addadi & Weiner, 1997; Donoghue *et al*., 2006; Tamm, 2014; Nakano *et al.*, 2017; Mayorova *et al*., 2018). Most biomineralizing phyla use a form of calcium crystals including calcium carbonate or calcium phosphate (Murdock & Donoghue, 2011). In animals, mineralized tissue appeared during the Ediacarian-Cambrian transition, most likely via convergent or parallel evolution, though the number of independent origins is unclear (Kirschvink & Hagadorn, 2000; Murdock & Donoghue, 2011; Le Roy *et al.*, 2014; Murdock, 2020).

Hemichordata is a small phylum of exclusively marine animals that can be found at all latitudes and depths comprising two major classes: the tubicolous colonial pterobranchs and the benthic vermiform enteropneusts which were recently discovered to form biomineralized ossicles (Cameron, 2005; Osborn *et al.*, 2011; Cameron & Bishop, 2012; Mitchell *et al*, 2012). The class Enteropneusta is composed of four families that are differentiated based on soft body morphological characteristics including the genital wings, hepatic sacs, collar lips and the presence or absence of a tornaria larva (Cameron 2005, Deland *et al.*, 2010; Osborn *et al.*, 2011; Cameron and Ostiguy, 2013; Cannon *et al.*, 2014). The two enteropneusts currently known to form biominerals are members of distantly-

related families: the direct developing harrimaniid *Saccoglossus bromophenolosus* and the indirect developing ptychoderid *Ptychodera flava,* which suggest that biomineralization may be widespread among Enteropneusta or alternatively that ossicles evolved more than once from the same "toolkit" (Cameron and Bishop, 2012, Murdock, 2020). Cameron and Bishop (2012) also provided some evidence that hemichordate ossicles share with echinoderms calcium carbonate ossicles with stereom and MPS130 genes.

Hemichordates are united with the highly mineralized echinoderms in a clade called Ambulacraria (Cannon *et al*, 2009; Cameron & Bishop, 2012). This clade shares a dipleurula larva, an axial complex and a tripartite coelom organisation (Ruppert & Balser, 1986; McEdward & Miner, 2001; Cameron, 2005; Ezhova *et al.,* 2013). The main synapomorphy of echinoderms is an extensive, structurally complex skeleton with ossicles that intercalate, except in Holothuroidea (Aizenberg, 2001). This skeleton is formed of many ossicles that grow in extracellular occluded spaces and act optically like a single crystal (Berman *et al.*, 1990). Those ossicles are composed of high magnesium calcite, a polymorph of calcium carbonate, organized into a porous microstructure called stereom (Smith, 2005; Mann *et al.*, 2008). In echinoderms, biomineralization involves many proteins like the SM30, SM50 and MSP130 protein families, metalloproteases and carbonic anhydrases (Mann *et al.*, 2008; Khor *et al.*, 2019). Hemichordate ossicles form in an extracellular occluded space formed by the sheath of sclerocyte cells. They are found in the epithelia and are composed of calcium carbonate in the form of aragonite in *Saccoglossus bromophenolosus* (Cameron & Bishop, 2012). Ossicles of *Saccoglossus bromophenolosus* have a mesh-like microstructure on their surface that is reminiscent of stereom, but they are apparently solid internally (Cameron & Bishop 2012). The

Saccoglossus kowalevskii genome includes genes homologous to the echinoderm Sp-Msp130L, Sp-Msp130, Sp-Msp130r1, Sp-Msp130r2, Sp-Msp130r3, Sp-Mt1-4/MmpL7 (matrix metalloproteases) and Sp-Clara7LA (carbonic anhydrases) (Glean3_entries 06387; 02088; 13822; 16506; 13823, 28748, 12518, respectively). There is no direct proteomic sequence data from acorn worm ossicles, but this data provides tantalizing evidence that hemichordates and echinoderms ossicles may be homologous structures, although we need deeper knowledge of hemichordates biomineralisation before the homology can be inferred or not (Cameron and Bishop, 2012; Ettensohn, 2014).

Here we described the ultrastructure and biomineral composition of ossicles from eight additional acorn worm species, from three families, quintupling the number of known biomineralizing acorn worms(Fig. 2.1). This study provides a broad sampling and characterization of enteropneusts ossicles, allowing a deeper understanding of the origin and evolution of echinoderm and enteropneust ossicles.

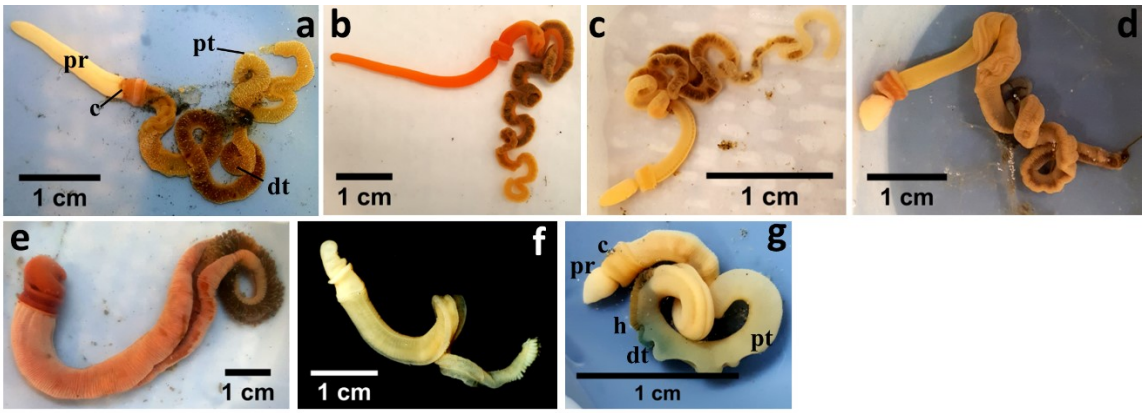

Figure 2.1. Photographs of acorn worms analysed in this study. **a**. *Saccoglossus kowalevskii*. **b.** *Saccoglossus pusillus*. **c**. *Harrimania planktophilus*. **d**. *Protoglossus graveolens*. **e**. *Schizocardium californicum*. **f.** *Glossobalanus berkeleyi*. **g.** *Balanoglossus occidentalis*. (c. collar; dt. dark trunk; h. hepatic sacs; pt. pale trunk; pr. proboscis) **a, b, c, d, e & g** were alive, and **f** was fixed and stored in ethanol.

2.4 Materials and Methods

2.4.1 Acorn worm collection and fixation

Four acorn worm species from the family Harrimaniidae were collected. *Saccoglossus kowalevskii* (Agassiz, 1873, Fig. 2.1 a) were collected in Waquoit Bay National Research Reserve, Cape Cod, Massachusetts, from September 1 to 30, 2017, during the low tides. *Saccoglossus pussilus* (Ritter, 1902, Fig. 2.1 b) and *Harrimania planktophilus* (Cameron, 2002, Fig. 2.1 c) were collected in the intertidal zone of Cape Beale, British Columbia, Canada. *Protoglossus graveolens* (Giray & King, 1996, Fig. 2.1 d) was collected in Lowe's Cove adjacent to the Darling Marine Center, Walpole, Maine, in May 2017 during the low tides. One species from the family Spengelidae, *Schizocardium californicum* (Cameron & Perez, 2012, Fig. 2.1 e), was collected in Morro Bay State Park, Morro Bay, California, USA in June 2018, during the low tides. Three species of the family Ptychoderidae were collected. *Glossobalanus berkeleyi* (Willey, 1931, Fig. 2.1 f) on May 5th, 2007, and *Balanoglossus occidentalis* (Chapter 4, Fig. 2.1 g) on June 16th, 2018, both in Penrose Point

State Park, Washington, during the monthly low tides. *Balanoglossus aurantiacus* (Girard, 1853) were collected adjacent to the Duke University Marine Laboratory, North Carolina on March 8th, 1996. Those species were chosen to provide a broad sampling of the enteropneust families and because they are easy to acquire. No Torquaratoridae were sampled because of their rarity and the destructive nature of our experiments.

All worms were transported from the collection site to a laboratory or incubator in bottles filled with seawater. Individual worms were then transferred to weigh boats that were submerged in flow-through seawater tables without sediment and allowed to vacate their guts for 12 hours, at temperatures close to or colder than that of the seawater at the collection site. Once a worm gut was evacuated, it was cleaned using forceps, relaxed in a 7% $MgCl_2$ seawater solution and fixed in a 4% formalin solution in Borax saturated water overnight. The solution was then changed to Borax saturated 70% ethanol solution for storage.

A culture of embryos from *S. kowalevskii* was started and kept for 4 months to describe when ossicles appeared and what they looked like in the first stages. The culture was provided by Christopher Lowe's lab from Waquoit Bay National Research Reserve, Cape Cod, Massachusetts on September 22, 2019. The embryos were cared for following Lowe *et al.* (2004).

2.4.2 Ossicle isolation and observation

To determine the presence of ossicles from different body regions of a worm, large worms were cut into longitudinal segments corresponding to different body regions and small

worms (less than about 40 mm) were kept whole. Those regions were, from anterior to posterior, the proboscis, the collar, the pharyngeal region, post pharyngeal gonadal region, the dark mid-trunk, the hepatic region (if it was present in the species), and the post-hepatic trunk. The epidermis of each sample was dissected from the gut and digested overnight in an Eppendorf tube with 7% NaClO (Javex bleach). If organic material was still visible, the bleach was replaced, and the digestion step repeated. Once the soft tissue was digested, the bleach was replaced with distilled water, and the Eppendorf tube was left on a rack to allow the ossicles to settle.

To observe the ossicles, 50 µL of the ossicle precipitate was put on a glass slide with a cover slip and viewed with an Olympus BX51 compound light microscope with polarised filters and photographed with a Retiga 2000R camera using QCapture Pro 6.0 software. The samples were washed four times in distilled water and dehydrated through a graded series of ethanol. Changes were made by adding solutions to one side of the slide with a glass pipette while removing solution from the opposite edge using the capillary force of a Kimwipe. After two changes of 100% ethanol the cover slip was removed and the ossicles air dried. The areas of each slide with ossicles were then identified under a microscope and marked using a fine sharpie to facilitate observation under SEM. Using a diamond pen, the glass slides were trimmed and then glued to an SEM stub using double sided tape and coated with gold. Electron micrographs were taken with either a Hitachi TM3030Plus environmental tabletop SEM, at the Integrated Quantitative Biology Initiative (IQBI), or a JEOL JSM-7600TFE Field Emission Scanning Electron Microscope at Polytechnique Montreal department of Mathematical and Industrial Engineering centre for characterization and microscopy of materials (CM)2. The later provided the best resolution

and had a Lower Secondary electron detector, the working distance was between 11.9 and 13.6 mm, the acceleration voltage was 5.0kV and the magnification was between 3K and 25K.

2.4.3 Ossicle biomineral composition

The mineral composition and crystalline polymorph of the calcium carbonate ossicles were determined with Raman confocal spectroscopy at University of Montreal department of chemistry Laboratoire de caractérisation des matériaux (LCM). Ossicles from the sea star *Pisaster ochraceus* and a valve fragment from the chiton *Katarina tunicata* were tested as controls for calcite and aragonite, respectively. Following the method by Cameron & Bishop (2012), the spectra were acquired using a Renishaw InVia Raman microspectrometer with a deep depletion CCD detector, 1800 lmm–1 grating and a holographic notch filter. Excitation was provided by a Spectra Physics argon ion 514.5 nm laser with 28 mW output and 5 mW at the sample. The spectrometer was mounted onto a Leica microscope with a 50X objective in an 1808 backscatter collection configuration. Using the formulae developed by Borromeo *et al.* (2017), the concentration of magnesium (Mg) was calculated for each spectrum corresponding to calcite.

2.5 Results

2.5.1 Ossicle microstructure

Ossicle form and presence was noted from the proboscis, the collar, the pharyngeal region, the gonadal region, the dark mid-trunk and the pale hind-trunk of *Saccoglossus Kowalevskii* (Fig. 2.1). The proboscis, collar, pharyngeal region and the pale hind-trunk lacked ossicles. Ossicles were found in the gonadal region of 46% of the worms and in the darkest mid-trunk of 90%of the worms (N = 50). Ossicles of the harrimaniid *Saccoglossus kowalevskii* (Fig. 2.2 a) had a central shaft with two flared terminal lobes forming the so-called "doubled ended broccoli shape". The shaft was smooth and square in cross section (Fig. 2.2 a) The terminal ends of *S. kowalevskii* ossicles were made of single, columnal crystals square in cross-section, and pointed at the tip (Fig. 2.2 a & Supplementary Fig. 1 a & b). Surface view of those crystals did not show a mesh-like structure like those of *Saccoglossus bromophenolossus* (Supplementary Fig. 1 b; Cameron & Bishop, 2012). Broken ossicles showed that these terminal crystals (length 1.3 ± 0.2 μm, N=10) were arranged around a central porous lacuna reminiscent of echinoderm labyrinthic stereom (Supplementary Fig. 1 c; Smith, 1980). A second type of ossicle was found in *S. kowalevskii.* They did not have the flared lobes and instead appear as square prism shape with pyramidal ends (length = 14.5 ± 3.8 μm, n = 14, Fig. 2.2 b & Supplementary Fig. 1 d). The terminal ends of the *S. kowalevskii* ossicles are variable in size and ranged from, small swellings (Supplementary Fig. 1 e), to sufficiently large that they almost touch medially, resulting in a medial ridge (length = 20.6 ± 3.6 μm, n = 25, Supplementary Fig. 1f). When the terminal ends were lobed, the width was correlated with the ossicle length, with longer ossicles having larger terminal lobes (Supplementary Fig. 2, R^2=0.6327, N=25).

Pores with a maximum diameter of 1 μm were present on the surface of prism ossicles, reminescent of a microperforate stereom (Fig. 2.2 b). Each of these ossicle shapes were found in male and female worms. Ossicles were not found in early developmental stages up to the six gill-slit stage (the oldest worms that were cultured) suggesting that they first developed at a later stage, but each of the ossicle forms were found in worms as short as 40 mm with imature gonnads suggesting that biomineralization starts prior to sexual maturity.

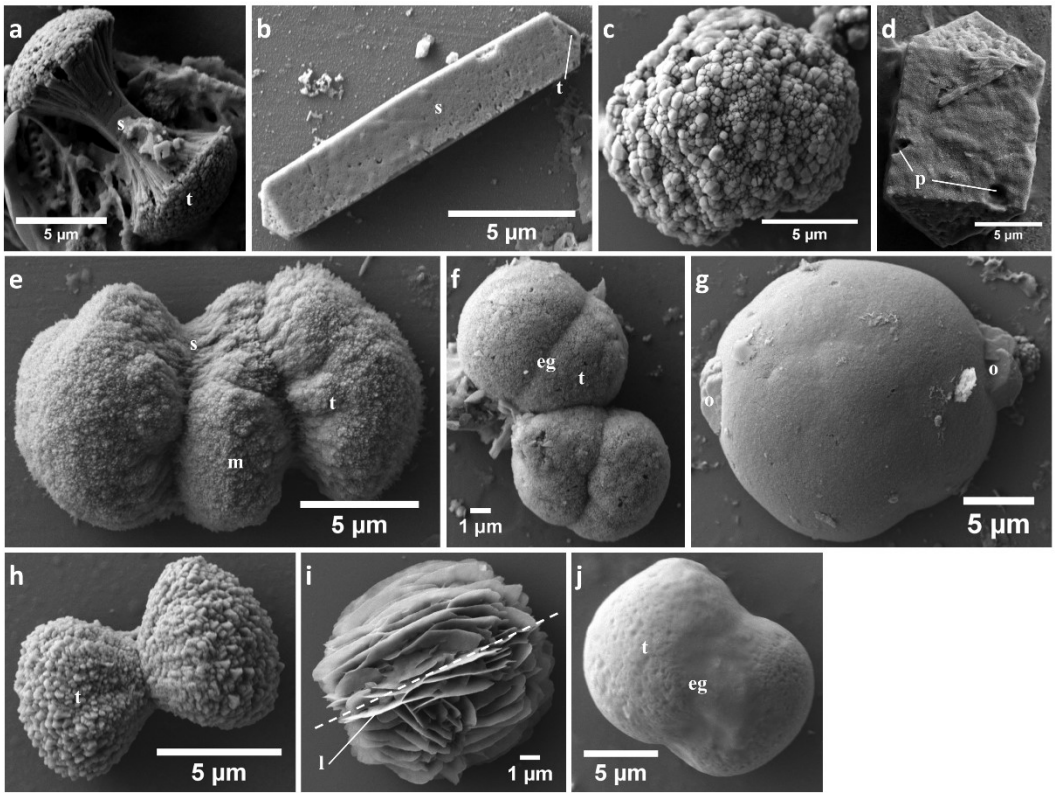

Figure 2.2 Scanning electron micrographs of enteropneusts ossicles. **a.** Broccoli-shaped ossicle of *Saccoglossus kowalevskii.* **b.** Prism-shaped ossicle of *S. kowalevskii.* **c.** Broccoli-shaped ossicle of *Saccoglossus pusillus* **d.** Prism-shaped ossicle of *S. pusillus.* **e.** Ossicle of *Harrimania planktophilus.* **f.** Ossicle of *Protoglossus graveolens.* **g.** Ossicle of *Schizocardium californicum.* **h.** Ossicle of *Balanoglossus occidentalis.* **i.** Ossicle of *Balanoglossus aurantiacus.* **j.** Ossicle of *Glossobalanus berkeleyi.* **abbreviations:** eg, equatorial groove; l, laminae; m, median lobe; o, outgrowth; p, pores; s, shaft; t, tip

Twenty-five *Saccoglossus pusillus* were subjected to dissection and epithelial digestion. Ossicles were found in the pharyngeal and dark trunk regions of the worm body. Only six broccoli-shaped ossicles were found (Fig. 2.2 c), whereas prism-shaped ossicles, resembling ossicles without terminal lobe from *S. kowalevskii,* were common (Fig. 2.2 d). All but one of the six broccoli-shaped ossicles were lost in the rinsing steps, and the one examined with SEM consisted of an isolated terminal lobe (Fig. 2.2 c), so the shaft morphology is unkown. The terminal fragment was formed of an aggregate of polyhedral crystals resembling those of *S. kowalevskii*. Trabeculae of *S. pusillus* were columnar with

an obtuse point at the tip and no visible mesh-like structure between the trabeculae in the same fashion as in *S. kowalevskii* (diameter = 0.4 ± 0.2 µm, N=15). The trabeculae cross-sections were rounded (Supplementary Fig. 3 a & b) rather than angular like those of *S. kowalevskii* (Supplementary Fig. 1 b). The prism ossicles had transverse wrinkles on the rectangular faces and a rough texture on the triangular faces (Supplementary Fig. 3 c). Some ossicles had one or two isolated pores on their surface (diameter < 1µm; Supplementary Fig. 3 d). In a broken ossicle, a porous medula could be seen inside the cavity and a dense cortex at its margin (Supplementary Fig. 3 e). Ossicles ranged from 10 to 20 µm (14.6 ± 2.5 µm) in length and 6 to 11 µm (8.7 ± 1.4 µm) in width (n = 14).

Other members of the Harrimaniidae, including *Harrimania planktophilus* and *Protoglossus graveolens* had ossicles with a double ended broccoli shape (Fig. 2.2 e & f). The terminal lobes were composed of trabeculae. *H. planktophilus* specimens were less than 40 mm in total length, so they were digested whole. Twelve ossicles were obtained from a whole animal, but the body region that bared the ossicles was not determined. Ossicles of *P. graveolens* were located throughout the length of the trunk and forty ossicles were isolated from two worms, but most were lost in the rinsing steps. Ossicles of *H. planktophilus* had a mean length of 12.4 ± 2.9 µm and a width of 9.1 ± 4.3 µm (n = 4), and those of *P. graveolens* had a mean length of 9.5 ± 2.8 µm and width of 7.7 ± 2.3 µm (n = 4). In both species the lobe trabeculae were numerous, compact and too small to image individually. The result was coarsely textured ossicles (Supplementary Fig. 4 & 5). The ossicles of *H. planktophilus* had, in addition to the terminal lobes, medial ones (Fig. 2.2 e). The grooves between lobes were formed of trabeculae that were continuous with trabeculae of the lobes (Supplementary Fig. 4 b). No shaft region was visible. The structure of the

medial lobes was indistinguishable from the terminal lobes (Supplementary Fig. 4 d). The inside of the ossicle was solid, without pores (Supplementary Fig. 4 e). Like in *P. graveolens* the ossicles of *P. graveolens* did not have a shaft (Fig. 2.2 f). These ossicles were spherical with an equatorial groove where the terminal lobes were in contact and had a few isolated surface pores (diameter < 0.1µm; Supplementary Fig. 5).

Ossicles were isolated from *Schizocardium californicum* of the family Spengelidae. Seven ossicles were found in an approximately 5 mm long section of the post-hepatic trunk. These ossicles were formed of one or more irregular smooth to rugose lobes (Fig. 2.2 g). The ossicles had polyhedral outgrowths at the ends (Fig. 2.2 g & Supplementary Fig. 6 a, b & d). The surface texture had a coarse appearance with pores reminiscent of a microperforate stereom (diameter <0.1 µm; Smith, 1980; Supplementary Fig. 6 c). The inside of the ossicle is porous akin to a labyrinthic stereom (diameter <0.3 µm; Smith, 1980; Supplementary Fig. 6 d). These ossicles were the largest observed in this study, with a mean length of 26.0 ± 4.6 µm (n = 7) and a max length of 31.3 µm.

Ossicles were isolated from three species of the family Ptychoderidae and showed the full range of ossicle morphology. Those of *Balanoglossus occidentalis* were smaller than saccoglossids (9.2 ± 1.2 µm, n = 12) and hourglass or hyperboloid shaped with convex terminal lobes (Fig. 2.2 h). The ossicles were uncommon. Twelve were isolated and recovered from the hepatic and dark post-hepatic trunk sections of three worms. The shape was of two opposing cones that were wide distally and narrow at the mid-region. The ossicles lacked a central shaft. Trabeculae were difficult to define in the largest ossicles of about 10 µm (Supplementary Fig. 7 a) but were apparent in the smallest (around 7 µm), where they formed rugose columns, longer than wide, arranged in a bouquet

(Supplementary Fig. 7 b). A trabecula was composed of an aggregate of small polyhedral crystals (Supplementary Fig. 7 c). Ossicle without trabeculae were also form of an aggregation of polyhedral crystals (Supplementary Fig. 7 a). One ossicle showed a hollow distal end (Supplementary Fig. 7 d). A single specimen of *B. aurantiacus* and a single specimen of *G. berkeleyi* were sectioned, and over 50 ossicles were isolated from the trunk section posterior to the hepathic sacs of each worm. The ossicles of *Balanoglossus aurantiacus* were shaped akin to desert rose crystals. They were spherical or ellipsoid shaped clusters of lamellae with a mean length of 13.0 ± 1.6 µm (n = 20) (Fig. 2.2 i). The lamellae were arranged around a common axis in eighty percent of the ossicles, otherwise they were arraged haphazardly (Supplementary Fig. 8 a & b). The lamellae surfaces were smooth (Supplementary Fig. 8 c). The core of the ossicle was forme by a network of pores reminescent of a labyrinthic stereom (Smith, 1980; Supplementary Fig. 8 d). Ossicles of *Glossobalanus berkeleyi* were composed of a pair of conjoined, solid, spheres (mean length of 18.1 ± 3.3 µm; n = 20) that had a smooth to rugose surface without trabeculae (Fig. 2.2 j). The surfaces had minute pores and canals akin to a microperforate stereom (from less than 0.1 µm to 0.3 µm; Smith, 1980; Supplementary Fig. 9).

2.5.2 Ossicle biomineral composition

To confirm that ossicles were composed of calcium carbonate in acorn worms, and to determine what polymorphs of calcium carbonate are present, Raman spectra were collected from at least 2 ossicles from each of the acorn worm species and compared to those of the control samples and to figure 3 of Nehrke *et al.* (2012). All species displayed a single polymorph. The controls were a calcite ossicle from the echinoderm *Pisaster*

ochraceus and an aragonite plate from the mollusk *Katarina tunicata*. Ossicles of *S. kowalevskii*, *S. pusillus, P. graveolens, G. berkeleyi* and *B. occidentalis* were calcite. Those of *H. planktophilus* and *B. aurantiacus* were aragonite, and those of the spengelid *S. californicum* were vaterite (Fig. 2.3), demonstrating that all three calcium carbonate polymorphs are present in acorn worms.

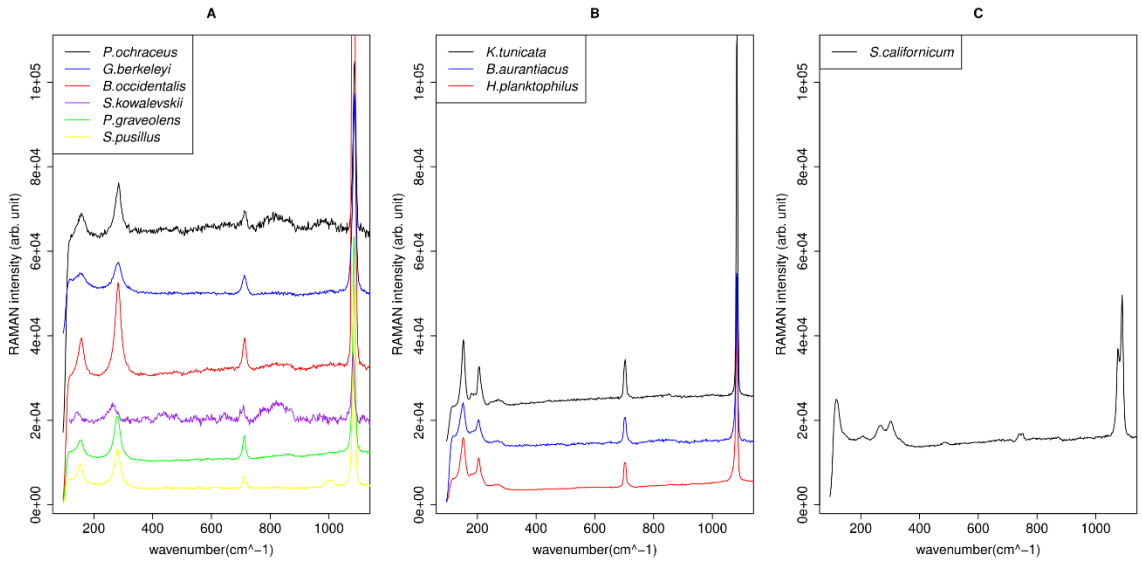

Figure 2.3. Raman spectra of enteropneusts ossicles. The peak pattern is characteristic of each polymorph. **a**. The spectra of *G. berkeleyi, B. occidentalis, S. kowalevskii, P. graveolens* and *S. pusillus* all show the same peak pattern as *Pisaster ochraceus* an animal known to make calcite ossicles. **b**. The ossicles of *B. aurantiacus* and *H. planktophilus* show the same peaks as the shell of *Katharina tunicata,* an animal known to mineralize aragonite. **c**. The ossicles of *S. californicum* are the only one to show peaks corresponding to vaterite (see Figure 3 from Nehrke *et al.* (2012)). The background noise was removed by subtracting a simple polynomial function to the spectra which does not alter the positioning or relative amplitude of the peaks. An arbitrary value was also added to each spectrum to prevent them from overlapping when plotted.

The calculation of magnesium concentration from Borromeo *et al.* (2017) confirmed high-Mg calcite for the sea star *Pisaster ochraceus.* The calculations determined ossicles from *S. kowalevskii*, *S. pusillus, P. graveolens, G. berkeleyi* and *B. occidentalis* were low-Mg calcite (Table 2.1).

Table 2.1. Calculated magnesium concentration in calcite samples. L, ν4 and ν1 are three major peaks of the calcite spectra. The lateral shift of those peaks is associated with magnesium concentration. The equations used to calculate the magnesium concentration are: L = 280.7 + 0.29 [% mol MgCO3], ν4 = 711.9 + 0.19 [% mol MgCO3] and ν1 = 1086.1 + 0.18 [% mol MgCO3].

Vibrational mode	*P. ochraceus*	*S. kowalevskii*	*S. pusillus*	*P. graveolens*	*G. berkeleyi*	*B. occidentalis*
L (cm^{-1})	284	263	282	280.1	284.3	282
(mol%)	11.37	<0.1	4.48	<0.1	12.4	4.48
ν_4 (cm^{-1})	717	709.5	711.3	711.3	711.5	713
(mol%)	26.8	<0.1	<0.1	<0.1	-2.11	5.79
ν_1 (cm^{-1})	1088	1082	1084	1086.4	1086.4	1082
(mol%)	10.5	<0.1	<0.1	1.67	1.67	<0.1
Average (mol%)	16.22	<0.1	<0.1	<0.1	4	<0.1

2.5.3 Ossicle trends among the Ambulacraria tree

Here we describe ossicles from eight species of acorn worm, adding to the two already known (Cameron & Bishop, 2012). Ossicles occur in all three major families. The size ranges from 3 to 30 microns, with most between 10 and 20 microns, and the largest found in *Schizocardium californicum* (30.8 microns) and *Saccoglossus bromophenolosus* (30.0 microns) (Cameron & Bishop, 2012). A double ended broccoli shape was conserved among

species of *Saccoglossus*. *Saccoglossus kowalevskii* bilobed ossicles were similar to those of *S. bromophenolossus* but the shaft was columnar with a square cross section (Fig. 2.2 a) whereas that of *S. bromophenolossus* is composed of laminar layer, and round in cross section (Cameron & Bishop, 2012). The trabeculae that form the terminal lobes of *S. kowalevskii* were columnar with a square cross section and pointed tip (Supplementary Fig. 1 b & c), whereas those of *S. bromophenolosus* are composed of stacked, laminar crystals (Cameron & Bishop, 2012). *S. kowalevskii* had a second prismatic shaped ossicle that may be a novel ossicle type, or an early developmental stage of a double broccoli-shaped ossicle, which have a prism-shaped shaft (Supplementary Fig. 1 d). If this is true, then the prism shape precedes the development of the bulbus termini. The width of the terminal lobes is directly correlated with the ossicle total length (Supplementary Fig. 2). Ossicles without terminal lobes also have a smaller mean length compared to ossicles with lobes, which suggest that prism ossicles are at an earlier developmental period. Prism ossicles could also be bilobed-ossicles with lobes broken by the preparation method, but both bilobed and prism ossicle were found within the same sample and no half-bilobed half-prism were ever found. Prism ossicles were found in both *S. kowalevskii* and *S. pusillus* but not in *S. bromophenolosus* (Cameron and Bishop, 2012). We lack data to know if the conservation of ossicle form in *Saccoglossus* is due to phyletic heritage or shared function. The ossicles are abundant in the protuberances of the trunk (Cameron & Bishop 2012) and so may provide some purchase onto the burrow walls. *Saccoglossus* feeds by extending its long proboscis out of the spiral-shaped burrow, to the surface, where it deposit-feeds. When disturbed, *Saccoglossus* rapidly withdraws into the safety of the burrow, and the ossicles may function to grip the walls.

Globular shaped ossicles that had a smooth to rugose texture were found in all three families including the harrimaniid *Protoglossus graveolens* (Fig. 2.2 f), the spengelid *Schizocardium californicum* (Fig. 2.2 g), and the ptychoderids *Glossobalanus berkeleyi* (Fig. 2.2 j) and *Ptychodera flava* (Cameron & Bishop, 2012), and appears to be plesiomorphic. Ossicles from *P. graveolens* and *S. californicum* were both globose with a rough texture. Those of *P. graveolens* and *G. berkeleyi* show some evidence of two lobes, suggestive of the distinct bi-lobed ossicles of *Saccoglossus*. *S. californicum* ossicles are unique with their polyhedral outgrowth, and both ptychoderids are more alike, although ossicles from *G. berkeleyi* are bilobed with a solid core, whereas those of *P. flava* are spherical and composed of an outer layer around a porous interior (Cameron and Bishop 2012). Transmission electron micrographs of sections through the epithelium of *S. bromophenolosus* showed that early-stage broccoli shaped ossicles begin development as amorphous liquid entrapped inside of an extracellular sheath formed by sclerocyte cells (Cameron and Bishop 2012). Simple globular, or spherical biominerals may be the default shape; a shape that lacks genetic influence.

Ossicle shape was variable within the ptychoderids and between the two *Balanoglossus* species. A globular shape characterized the ossicles of *Glossobalanus berkeleyi* (Fig. 2.2 j) and *Ptychodera flava*. Unique desert rose-shaped ossicles were found in *B. aurantiacus* (Fig. 2.2 i), whereas the ossicles of *B. occidentalis* (Fig. 2.2 h) were a double-ended broccoli shape, like those of saccoglossids, though the trabeculae had a different ultrastructure. The trabeculae were an aggregation of polyhedral crystals in *B. occidentalis* whereas they are individual columnar crystals in *S. kowalevskii,* or stacks of lamellar crystals in *S. bromophenolosus*. This shape variability within the family, and between the

two *Balanoglossus* species suggest that the development of ossicles in ptychoderids is unconstrained, and perhaps without function. In tunicates, biominerals are composed of stored waste products from metabolism (Lambert *et al.*, 1989). It may also be the case in enteropneusts. This morphological variation may hint that a wider sampling of acorn worm ossicles could reveal more forms. Variability then, may be the rule, and the uniform shape observed in *Saccoglossus* may be unusual.

A characteristic of all echinoderm ossicles is stereom. This is the three-dimensional organisation of calcitic trabeculae into an anastomosing mesh-like structure (see Smith, 1980 for the different stereom forms). The oldest fossils exhibiting stereom are dated to approximately 525 million years ago, during the early Cambrian (Smith *et al.*, 2013; Zamora & Rahman, 2014). Stereom is present in most extant representative of the phylum except in some holothuroids in which the skeleton is absent, and in larval forms that can have a unique skeleton or no skeleton at all (Pennington & Strathmann, 1990; Massin *et al.*, 1991). In pluteus larvae, the skeleton shape is the consequence of the vascular endothelial growth factor (VEGF) co-opted for biomineralization (Morgulis *et al.*, 2019). This growth factor controls vessel formation in vertebrates and the formation of the tubular spaces in which ossicles form in pluteus larvae (Morgulis *et al.*, 2019). VEGF is also involved in the formation of the adult skeleton. A clear porous structure, a cavity or minute pores were observed in ossicles of all species studied here and by Cameron & Bishop (2012), except *H. planktophilus*. The best evidence for stereom in the Enteropneusta are the bi-lobed broccoli shape ossicles of *Saccoglossus* (Supplementary Fig. 1 & 3, see also Fig. 2 from Cameron & Bishop, 2012), and the porous inside of broken ossicle from *Schizocardium californicum* (Supplementary Fig. 6) and *Balanoglossus aurantiacus*

(Supplementary Fig. 8). Such porosity can also be seen in some tunicate ossicles (Monniot & Monniot, 2008). These results support the hypothesis that the echinoderm stereom, or at least the biomineralization toolkit, may have its origins in the common ancestor to the Ambulacraria or even the Deuterostomia. Although, in enteropneusts, the pores and trabeculae are much smaller and more irregular, the mineralogy is more variable, and some ossicles appear made from multiple crystals (*Saccoglossus* and *Balanoglossus*). Without further data, we can not exclude the possibility that all those similarities could be the result of independent parallel evolution.

2.6 Discussion

Here we show for the first time that the calcium carbonate ossicles of acorn worms are calcite, aragonite and vaterite, and that calcite and aragonite are widespread. This is significant because echinoderm ossicles are also made of calcite (Zamora & Rahman, 2014). Calcite ossicles were found in *S. kowalevskii, S. pusillus, P. graveolens, G. berkeleyi* and *B. occidentalis*. Aragonite was found in *S. bromophenolosus* (Cameron & Bishop, 2012), *H. planktophilus* and *B. aurantiacus* and vaterite was found in *S. californicum* (Fig. 3). These three calcium carbonate polymorphs are found simultaneously in the shell of the bivalve species *Laternula elliptica*, and among different species of tunicates (Lambert, 1992; Lambert & Lambert, 1996; Aizenberg *et al.*, 2001; Nehrke *et al.*, 2012), suggesting that the crystal polymorph is a highly evolvable character. An extreme example is the brachiopod shell, which is $CaPO_4$ in linguliforms and $CaCO_3$ in other brachiopods, yet widely regarded as homologous (Nehrke *et al.*, 2012; Luo *et al.*, 2015). Mapped onto a phylogenetic tree for the Ambulacraria (Fig. 2.4), calcite is the most parsimonious ancestral

polymorph, replaced for aragonite three times and vaterite one time in the Enteropneusta clade. This suggest that the hypothetical enteropneust-like ancestor of ambulacraria possessed calcitic ossicles.

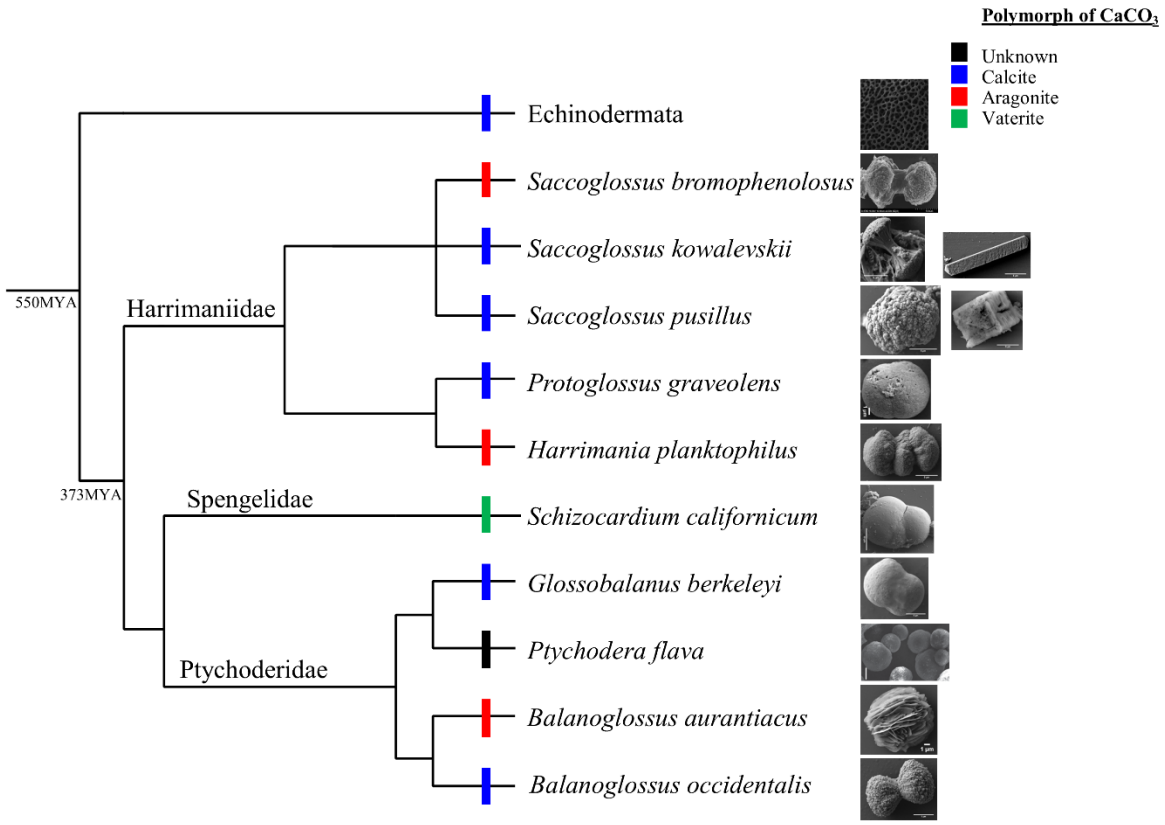

Figure 2.4. Phylogenetic tree of biomineralization in Ambulacraria. The phylogenetic tree is based on (Cannon *et al.*, 2009; Cannon *et al.*, 2014; Cameron, 2018; Li *et al.*, 2018). The mineral polymorph of each species is represented by a coloured line on the tree. The shortest tree suggest calcite as the ancestral state (L=5). Aragonite has a minimum length of 7.

The echinoderm skeleton is composed of high magnesium calcite, but its phylogenetic precursor may have been more variable in polymorph like the ossicles of hemichordates (Fig 2.3, table 2.1). $CaCO_3$ mineralizing phyla may select a polymorph depending on the water chemistry of the geological period when they acquired the biomineral (Porter, 2010; Ries, 2010). Echinoderm fossils first appear in early Cambrian calcite seas (Porter, 2010) and by 510 mya had diversified rapidly into four diversified body plans (Zamora *et al.*, 2012; Smith *et al.*, 2013; Zamora *et al.,* 2014). The skeleton probably evolved just 10-15 million years earlier (Smith *et al.*, 2013), but molecular clock data suggests that the

Ambulacrarian phyla diverged 559 million years ago during late Ediacaran (Simakov *et al.*, 2015), when water chemistry favored aragonite rather than calcite (Wood *et al.*, 2017). This contradicts the ancestral state inferred from our results which could mean that we are missing information on a possible earlier aragonitic stage in the ambulacrarian fossil record or that the evolutive scenario is more complex than a simple single origin of ambulacrarian ossicles. This might be explained by the absence of an Ediacaran ambulacrarian fossil record. Taken together, our data suggest that the ancestor to the Ambulacraria was a worm that possessed microscopic, monotypic globular shaped, calcium carbonate ossicles, with stereome, low Mg content, and MSP130, matrix metalloproteases and carbonic anhydrases proteins. These ossicles lacked intercalation with other ossicles (Cameron & Bishop 2012; Ettensohn, 2014) and were acquired in the Ediacaran. From those microscopic precursors, the echinoderms would later evolve the complex, intercalated, high-Mg calcite skeleton in early Cambrian calcite seas. In enteropneusts the ossicles are variable in mineralogy and microstructure, and small like the putative ancestral state. This would suggest that there is little to no selective pressure on the polymorph and no pressure for bigger ossicles. Their small size would, in turn, explain why they were never detected in the fossil record. It is still unknown if pterobranchs have ossicles and in enteropneusts the function of the ossicles is still unknown, but given their location in the surface epidermis and minute size, they might serve in predator deterrence, to provide grip on the walls of a burrow or tube, or as storage of metabolic waste, rather than as an endoskeleton function seen in fossil and crown group Echinodermata.

2.7 Acknowledgements

We would like to thank the following facilities for their services: The Integrated Quantitative Biology Initiative (IQBI) funded by the Canadian Foundation of Innovation (CFI) project 33122 for their Hitachi M3030 plus; University of Montreal department of chemistry and their Laboratoire de caractérisation des matériaux (LCM) for their service of Raman spectroscopy; Polytechnique Montreal department of Mathematical and Industrial Engineering centre for characterization and microscopy of materials (CM)2 JEOL JSM-7600TFE Field Emission Scanning Electron Microscope; The Institute for Research in Immunology and Cancer of the University of Montreal. And, of course, their respective technicians and lab managers. Funding was provided by a Discovery Grant from Natural Sciences and Engineering Research Council of Canada (NSERC Grant 1283784)

2.8 Code and Data availability

The data file with ossicle size measurement used to get the mean sizes and supplementary Fig. 2 as well as the raw Raman data and R code used to determine the polymorph of enteropneusts ossicle are accessible at: https://doi.org/10.5281/zenodo.5103051

3 Filter feeding, deviations from bilateral symmetry, developmental noise and heterochrony of hemichordate and cephalochordate gills

Charles Larouche-Bilodeau, Xavier Guilbeault-Mayers and Christopher B. Cameron

3.1 foreword

This chapter has been published in the journal Ecology and Evolution, and is accessible in open access at: https://onlinelibrary.wiley.com/doi/full/10.1002/ece3.6962

3.1.1 Author contribution

Charles Larouche-Bilodeau: Data curation (equal); Formal analysis (equal); Investigation (lead); Methodology (supporting); Project administration (supporting); Resources (supporting); Software (supporting); Visualization (equal); Writing-original draft (lead); Writing-review & editing (lead). Xavier Guilbeault Mayers: Conceptualization (equal); Data curation (lead); Formal analysis (equal); Investigation (equal); Methodology (equal); Project administration (supporting); Software (lead); Visualization (lead); Writing-original draft (supporting); Writing-review & editing (supporting). Christopher B. Cameron: Conceptualization (lead); Data curation (supporting); Formal analysis (supporting); Funding acquisition (lead); Investigation (supporting); Methodology (supporting); Project administration (equal); Resources (lead); Supervision (lead); Validation (lead); Writing-original draft (equal); Writing-review & editing (supporting).

3.2 Abstract

We measured gill slit fluctuating asymmetry (FA), a measure of developmental noise, in adults of three invertebrate deuterostomes with different feeding modes: the cephalochordate *Branchiostoma floridae* (an obligate filter feeder), and the enteropneusts

Protoglossus graveolens (a facultative filter feeder / deposit feeder) and *Saccoglossus bromophenolosus* (a deposit feeder). FA was substantially and significantly low in *B. floridae* and *P. graveolens,* and high in *S. bromophenolosus*. Our results suggest that the gills of species that have experienced a relaxation of the filter feeding trait exhibit elevated FA. We found that the timing of development of the secondary collagenous gill bars, compared to the primary gill bars, was highly variable in *P. graveolens* but not the other two species, demonstrating an independence of gill FA from gill bar heterochrony. We also discovered the occasional ectopic expression of a second set of paired gills posterior to the first set of gills in the enteropneusts, and that these were more common in *S. bromophenolosus*. Moreover, our finding that gill slits in enteropneusts exhibit bilateral symmetry suggests that the left-sidedness of larval cephalochordate gills, and the directional asymmetry of Cambrian stylophoran echinoderm fossil gills, evolved independently from a bilaterally symmetrical ancestor.

3.2.1 Keywords

Filter-feeding, gill slits, fluctuating asymmetry, ectopic expression, Hemichordata, Cephalochordata, Deuterostomia.

3.3 Introduction

In bilaterian organisms, structures can be symmetrical or asymmetrical, the latter being subdivided into three forms: antisymmetry, directional asymmetry, and fluctuating asymmetry (Endler, 1986; Lahti et al., 2009). Fluctuating asymmetry (FA) consists of

random deviations from perfect bilateral symmetry on a population of organism (Graham et al., 2010). This variation around the perfect symmetric distribution represents a measure of development noise or developmental instability (Rott, 2003). As both sides of a bilateral trait develop under the control of the same genome, the developmental phenotypic target of a population should be perfect symmetry (De Coster et al., 2013), but developmental noise results in deviations from perfect bilateral symmetry, or an increase in FA (Emlen et al., 1993; Møller & Swaddle, 1997).

A high level of fluctuating asymmetry and high variability in size and number of a phenotype are signs of reduced functionality and relaxed selective pressure where drift predominates. This is conspicuous when homologous structures are compared that show high functionality versus a relaxation in that function (Guthrie, 1965; Tague, 1997). In those cases where function is lost, the relaxed selective pressure may result in many paths or scenarios (Lahti et al., 2009). A trait that has lost its function may be lost, become vestigial, persist or experience exaptation. Vestigialisation is expected when the trait bears a cost without benefits and may lead to the loss of the trait. Persistence is when a trait remains, when the relation between cost and benefits is the other way around or null (Lahti et al., 2009). Exaptation is when a phenotypic trait remains for a function than is different than its original role (Tague, 1997; Dorken et al., 2004; Lahti et al*.,* 2009).

Here we investigate the interspecific gill symmetry and intraspecific gill fluctuating asymmetry in the cephalochordate *Branchiostoma floridae* Hubbs, 1922, and two enteropneusts; *Protoglossus graveolens* Giray & King, 1996, and *Saccoglossus bromophenolosus* King, et al., 1994 (Fig 3.1). These species are ideal to investigate gill fluctuating asymmetry for the following reasons. *B. floridae* is an obligate filter feeder

(Ruppert et al., 2000), *P. graveolens* is a facultative filter feeder (Gonzalez & Cameron, 2009), and *S. bromophenolosus* is a deposit feeder that does not filter food particulates (Knight-Jones, 1953; Cameron, 2016), which allows us to relate gill function to gill fluctuating asymmetry. Gills are a discrete, rather than a continuous trait and therefore less prone to measurement error (Palmer & Strobeck, 1986). The three species are in the same adult size range, and their gills show high repeatability. These gills show no evidence of wear that can complicate left-right comparisons (Rott, 2003), and finally, the acorn worms live in the same habitat, so differences in gill symmetry are not due to different environments.

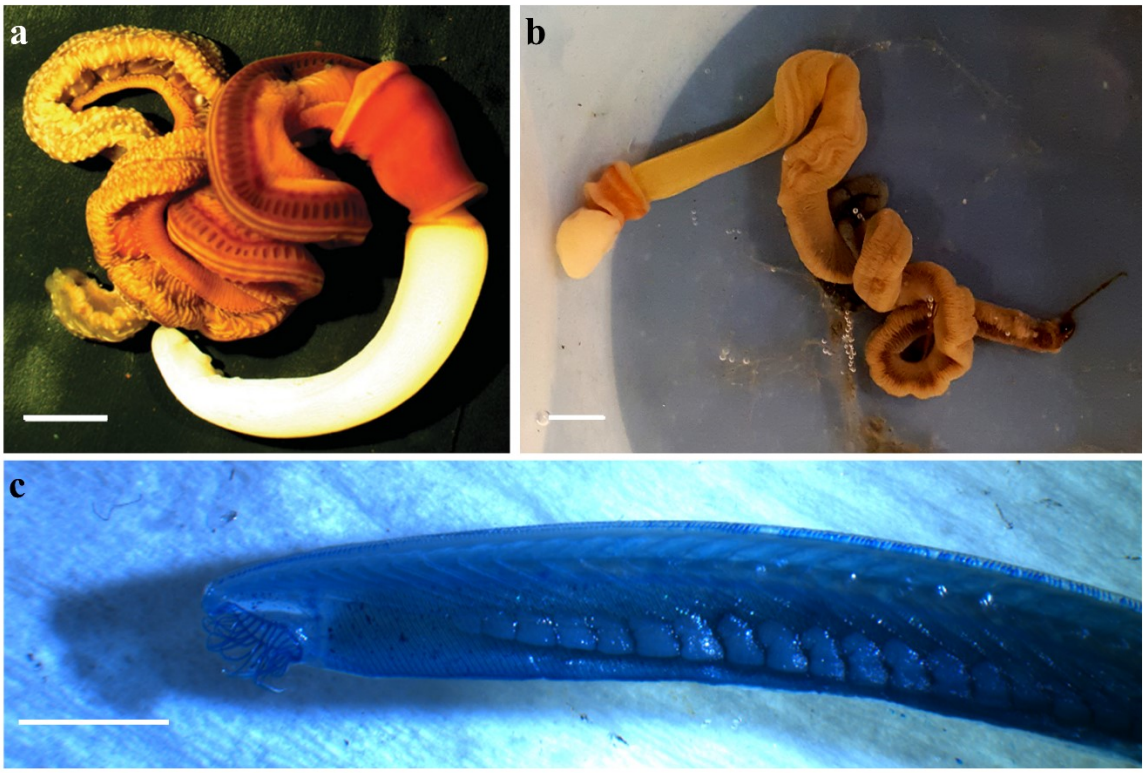

Figure 3.1: Photographs of a) *Saccoglossus bromophenolosus*, b) *Protoglossus graveolens* and c) *Branchiostoma floridae.* a) and b) were live specimens. c) was stained and cleared. Scale bars equal 4mm.

Gills are a shared, plesiomorphic feature of the deuterostomes. This homology has been established from comparative morphology, molecular development, comparative genomics, and the fossil record (Ruppert, 2005; Gillis *et al.*, 2012; Ou *et al.*, 2012; Lowe *et al.*, 2015; Simakov *et al.*, 2015). Hemichordate and cephalochordate gills are dorsolaterally located, frequently paired, and connect the inner pharyngeal cavity to the environment (Ruppert et al., 2000; Cameron, 2002; Gonzalez & Cameron, 2009). Gills begin development as a simple pore, which is then elongated dorsal to ventral by extension of collagenous gill bars, creating a primary gill slit. This slit is then divided into two secondary gill slits by the downward projection of a secondary gill bar (or tongue bar) resulting in a series of M-shaped collagenous gill bars. As worms grow, gills are added posteriorly first as pores, then as primary gill slits bordered by primary gill bars, and finally as secondary gill slits when

the primary gill slit is divided by the downward growth of secondary gill bars (Ezhova & Malakov, 2020; Fig. 3.2). The gill bars are endodermal collagenous (type II) skeleton (Ogasawara et al., 1999; Cameron, 2005; Rychel et al., 2006; Rychel & Swalla, 2007; Satoh, 2008; Sato & Holland, 2008; Philippe et al., 2011; Röttinger & Lowe, 2012). Genes expressed during the development of gills of hemichordates and chordates include Pax1/9, Nkx2.1, Nkx2.2, Fox A, FoxC, FoxL1, FoxI, Eya, and Six1 (Ogasawara et al., 1999; Okai et al., 2000; Gerhart et al., 2005; Gillis et al., 2012; Fritzenwanker et al., 2014). The first four genes are transcription factors that are arranged in a synteny unique to the deuterostomes, including echinoderms (Simakov et al., 2015).

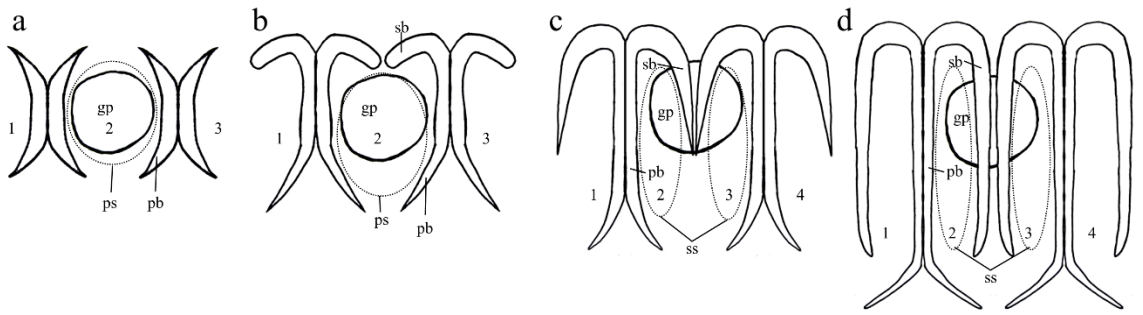

Figure 3.2: Line drawing of the developmental stages of the gill slits and bars based on my observation of developing gills. See also Ezhova & Malakov (2020). Note that gill pores are ectodermal and drawn as solid lines, whereas gill slits and bars are endodermal and the slits are drawn as dotted lines. a) Early gill slits are round in circumference and bordered by small lateral primary gill bars. b) The primary gill bars develop around the gill slit elongating it and forming the early stage secondary gill bars. c) The secondary gill bars elongate ventrally, dividing the primary gill slit into two elongated secondary gill slits. d) The secondary gill bars are fully developed and the same length as the primary gill bars. Gill slits were numbered in each drawing representing how we counted them gp, gill pore; pb, primary gill bar; ps, primary gill slit; sb, secondary gill bar; ss, secondary gill slit.

The symmetry of the ancestral deuterostome is a subject of debate because living and fossil species may be bilateral or directionally asymmetric (Jefferies, 2001; Sato & Holland, 2008; Zamora & Rahman, 2014; Cameron, 2016). Deuterostomes are comprised of two major branches, and the acorn worms are thought to most closely resemble the ancestral Ambulacraria (including echinoderms) whereas the cephalochordates the ancestral Chordata (including tunicates and vertebrates) (Peterson & Eernisse, 2016). Gills of Cambrian fossil (Caron et al., 2013; Nanglu et al., 2016) and living acorn worms have not been quantified but are assumed to be symmetric. Gills of many stem echinoderms (Jefferies et al., 1996; Jefferies, 2001; Smith, 2008; Zamora et al., 2012; Smith et al., 2013; Zamora & Rahman, 2014; Rahman et al., 2015) and larval cephalochordates (Willey, 1891; Boorman & Shimeld, 2002; Dominguez et al., 2002) exhibit directional asymmetry. Here we quantify the symmetry of the gills of an adult cephalochordate and two acorn worms. We also count the number of posterior gill slit pairs that have primary gill bars but lack

secondary gill bars, as a measure of heterochrony. Finally, we show that some acorn worms develop a second gill complex, which we interpret as previously unknown form of gill developmental error.

3.3 Materials and Methods

3.3.1 Specimen collection and treatment

The enteropneust *Saccoglossus bromophenolosus* (n=65), and *Protoglossus graveolens* (n=50) were dug at low tide, near to the old brickyard in Lowe's Cove, adjacent to the Darling Marine Center, University of Maine. The enteropneusts live in sediment composed of clay, mixed with organic calcium carbonate debris and sand. These two acorn worm species are sympatric and often collected from the same shovel of sediment, and thus differences in their FA is more likely due to differences in function rather than the environment. The cephalochordate *Branchiostoma floridae* (n=50) were collected in Tampa Bay in the 1980's, fixed in formalin and stored in 70% alcohol in the department of biological sciences, Université de Montréal. Adapting the methods from Inouye (1976) and Dingerkus & Uhler (1977), the acorn worm specimens were relaxed in a 7% solution of magnesium chloride and fixed in a 10% formalin solution. All specimens were then dehydrated in a sequential series of ethanol (i.e., 30%, 50%, 70%, 95% and 99%) for an hour at each step. Subsequently, they were stained in a solution of 0.1 % Alcian blue 8GX, 5% acetic-acid and 70% ethanol for 24 hours, neutralized in a 1% solution of potassium hydroxide for a further 24 hours, cleared with a 1% pancreatic trypsin buffer solution, dissected, and then the left and right gill slits were counted.

3.3.2 Data collection

We counted only fully developed gill slits bordered by clear gill bars, either primary or secondary. We avoided counting pores because in the early stages, they are small, lack gill bars (and Alcian stain) and so difficult to quantify with confidence. We also avoided counting very early stages of gill bar development, when they can be confused with folds in the epithelium, where Alcian blue was sometimes found. Special attention was given to the posterior gill slits. From posterior to anterior, the gills are in the earliest to latest stages of development. We counted the number of undivided primary gill slits that were bordered by primary gill bars, but not divided into secondary gill slits by the downward extension of secondary gill bars. The difference in relative number, or timing, of the primary slits compared to the secondary gill slits allowed us to compare gill slit developmental heterochrony between these three organisms. Finally, we noted a few exceptional cases where a second gill complex developed in the intestine of some acorn worms. These gills were not counted as part of our other analysis.

3.3.3 Statistical analysis

Fluctuating asymmetry of gill slits were assessed by calculating a symmetry index (R-L) and generating a relative density of this index by species, where relative density was log transformed to avoid negative values and retro-transformed for visualisation. To assess departure from a perfect symmetrical distribution four mode of distribution were calculated: the mean, the standard deviation, the skewness and the kurtosis using the

function mean() and sd() from the package ‘stat’ (R Core Team, 2018) and the function kurtosis() and skewness() from the package ‘moments’ (Komsta and Novomestky, 2015). Subsequently, the kurtosis and skewness were compared to the 5 % and 95 % quantile of the distribution of those mode calculated from 100 000 rounded normal distributions (μ = -0.01, σ = 1.50). The average mean and standard deviation of the distribution of the symmetry index were used to generate the normal distributions to account for the nature of our data. As kurtosis is independent of the variance of the distribution it served to quantify the movement of mass toward the tail of the distribution (Westfall, 2014) and the skewness served as a measure of a horizontal stretch of the distribution. Due to the lack of replication of the symmetry index (R-L) dispersion descriptors (i.e. kurtosis and standard deviation), linear model (lm) from the package 'stats' and generalized least squares (gls) from the package 'nlme' (Pinheiro et al., 2018; R Core Team, 2018) were used to perform a direct assessment of the differential level of FA among species by comparing the squared residuals of the symmetry index. Linear and generalized least squares model were also used to assess difference between the overall number of gill slits among species. Variance analysis of the symmetry index was not carried out to evaluate differences in the symmetry aspect of the gill pores, as the putative absence of differences among species would be an artefact of the greater variance observed in *S. bromophenolosus* and would not be informative regarding differences in symmetry among species. Considering the experimental design of our study and the structure of the data, a Student's t-test by permutation (n= 9999) for paired sample, function t.paired.perm() (Legendre & Legendre, 2012), were used to assess the difference between the both side of the bilateral trait for each species. For all linear models, the assumptions of homogeneity of variance and

normally distributed residuals were ascertained by visual inspection. The models were modified as needed with an appropriate variance function to effectively deal with heteroscedasticity, when present (Zuur, 2009). If the residual structure showed little difference between several models, the selection was made by comparing the AICs. In figures, letters used to denote differences among groups were based on Tukey HSD and were generated using the function emmeans() and CLD() from the 'emmeans' packages (Lenth, 2019).

Heterochrony in the sequential development of the gill slits was assessed by calculating the mean and the standard deviation of the number of gills lacking secondary gill bar for each species.

3.4 Result

3.4.1 Variance and fluctuating asymmetry

The acorn worms *Saccoglossus bromophenolosus* (N= 65), *Protoglossus graveolens* (N= 50) and the cephalochordate *Branchiostoma floridae* (N= 50) gill slits are bilaterally symmetric and exhibit fluctuating asymmetry (Fig. 3.3; Table 3.1). The standard deviation of gill pair number is greater in *Saccoglossus,* a genus that does not use the gills for filter feeding (Table 3.1). Similarly, the differences in symmetry index (R-L) squared residuals among species show that only *Saccoglossus* has a significantly higher FA (*S. bromophenolus* - *P. graveolens*: $P < 0.05$, *S. bromophenolus* - *B. floridae* : $P < 0.05$ and *P. graveolens* - *B. floridae* : $P > 0.05$) (Fig. 3.4 b). The number of gill slits of *S. bromophenolosus* was significantly less than *P. graveolens* and *B. floridae* (Fig. 3.4 a; P <

0.0001), and no difference was detected between the latter two species (Fig. 3.4 a; $P > 0.05$). Similar to the standard deviation, the kurtosis decreased as the functionality of the gill slits increased; the highest kurtosis was the deposit feeder *S. bromophenolosus*, then the facultative filter feeder *P. graveolens*, and the lowest was the obligate filter feeding cephalochordate *B. floridae* (Fig. 3.5; Table 1). High kurtosis reveals a movement of mass towards the tail of the distribution, and therefore an increase of FA (Fig. 3.3). The greatest difference of left vs. right number of gills in *S. bromophenolosus* was ten, whereas a maximum of three was observed in the other species.

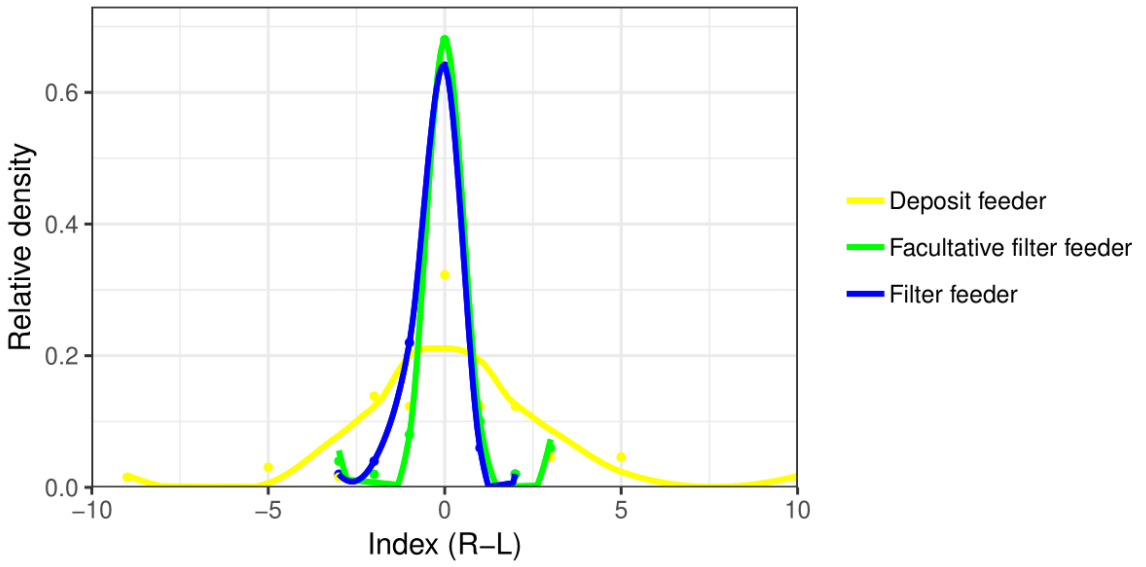

Figure 3.3: Graphical representation of the distribution of the symmetry index (R-L) for each species. *Saccoglossus bromophenolosus* (Hemichordata) is a deposit feeder, *Protoglossus graveolens* (Hemichordata) is a facultative filter feeder, and *Branchiostoma floridae* (Cephalochordata) is an obligate filter feeder. *S. bromophenolosus, P. graveolens* and *B. floridae* have symmetry index distribution means of 0.15, 0.08 and -0.26 and symmetry index distribution standard deviations of 2.57, 1.12 and 0.80, respectively.

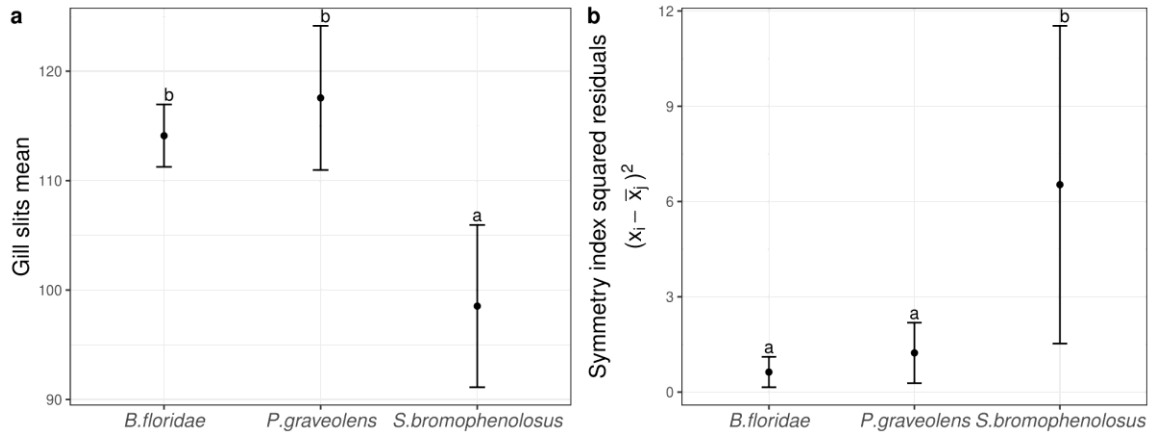

Figure 3.4: Differences a) in number of gill slits and b) symmetry index (R-L) squared residuals among species. Error bars represent the 95% confidence intervals; letters above each mean represent Tukey honest significant difference (HSD) groupings ($P \leq 0.05$).

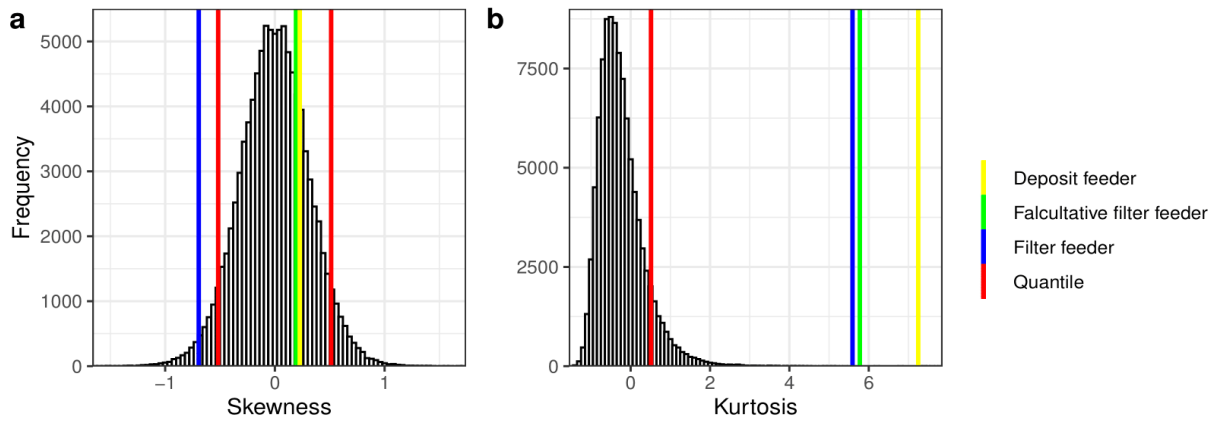

Figure 3.5: Representation of the two modes of the distribution of the symmetry index (R-L) for each species a) in the skewness, and b) the kurtosis. S. bromophenolosus, P. graveolens and B. floridae have a kurtosis of 7.25, 5.78 and 5.59, and a skewness of 0.23, 0.19 and -0.69, respectively. The distribution of the skewness and the kurtosis were calculated from 10 000 rounded normal distribution (μ= -0.01, σ = 1.50). In panel a) the vertical lines beginning from the left represents the 5% quantile and the 95% quantile respectively and in panel b) the vertical line represents the 95% quantile. The deposit feeder is *S. bromophenolosus,* the facultative filter feeder is *P. graveolens*, and the obligate filter feeder is the cephalochordate *B. floridae*.

Table 3.1: Four of the distribution modes, squared residuals of the symmetry index (R-L) and p-value of the paired Student-t test for each species. Letters above each mean represent Tukey's honestly significant difference (HSD) groupings ($P \leq 0.05$).

	Species	*S. bromophenolosus*	*P. graveolens*	*B. floridae*
	Nutritional behavior	Deposit feeder	Falcultative filter feeder	Filter feeder
Standard deviation	Symmetry index	2.57	1.12	0.80
	Right and left gill slits	24.41	18.84	8.16
Squared residuals	Symmetry index	1.68^{b}	0.61^{a}	0.57^{a}
Mean	Symmetry index	0.15	0.08	-0.26
	Right and left gill slits	98.54^{a}	117.56^{b}	114.11^{b}
Third mode	Kurtosis	7.25	5.78	5.59
Fourth mode	Skewness	0.23	0.19	-0.69
Paired Student-t test	P-values	0.67	0.71	0.04

3.4.2 Asymmetrical aspect of fluctuating asymmetry

Each of the three species exhibited fluctuating asymmetry. No left or right biases were detected for *P. graveolens* or *S. bromophenolosus* ($P > 0.05$), and a significant left bias (i.e. more gills were on the left side in 14 of the 18 asymmetric individuals) was detected in the gill slits of *B. floridae* (paired Student-t test: $P = 0.04$). This latter finding did not demonstrate directional asymmetry (DA) because most specimens were perfectly symmetric (32 out of 50) and asymmetries were small deviations (up to 3 gill slits) on both sides of the symmetrical state. Skewness confirms these results: the skewness of the symmetry index of *B. floridae* was higher than expected if it was part of a perfectly symmetrical distribution (Fig. 3.5). The paired Student's-t test and the skewness of the

symmetry index of *S. bromophenolosus* and *P. graveolens* were within what was expected for a symmetrical distribution (Table 3.1; Fig. 3.5).

3.4.3 Sequential development of the gill slit complex

New gills are added sequentially to the posterior pharynx. The posterior pairs then, are the youngest and least developed. They begin as simple pores, which are elongated into slits by the downward growth of the primary gill bars. Each slit is then divided into two by the downward projection of the secondary gill bars (Fig. 3.6a, b, c & d). We found one exception to this developmental sequence. A single *S. bromophenolosus* specimen had a gill slit with a short series of under-developed secondary gill slits and bars between fully developed gills (Fig. 3.6e). The number of gills that lacked secondary gill bars in the posterior pairs of gills varied between species, and thus the comparison of absence to presence of secondary gill bars is a measure of heterochrony. The number of gills that lacked secondary gill bars was similar in *S. bromophenolosus* and *B. floridae* with an average 1 ± 0.6 (N=65) and 0.6 ± 0.5 (N=50) respectively on each side (Fig. 3.6a & c), whereas up to 29 pairs of gills lacked secondary gill bars in *P. graveolens* with a mean of 17 ± 5 (N=50) (Fig. 3.6b).

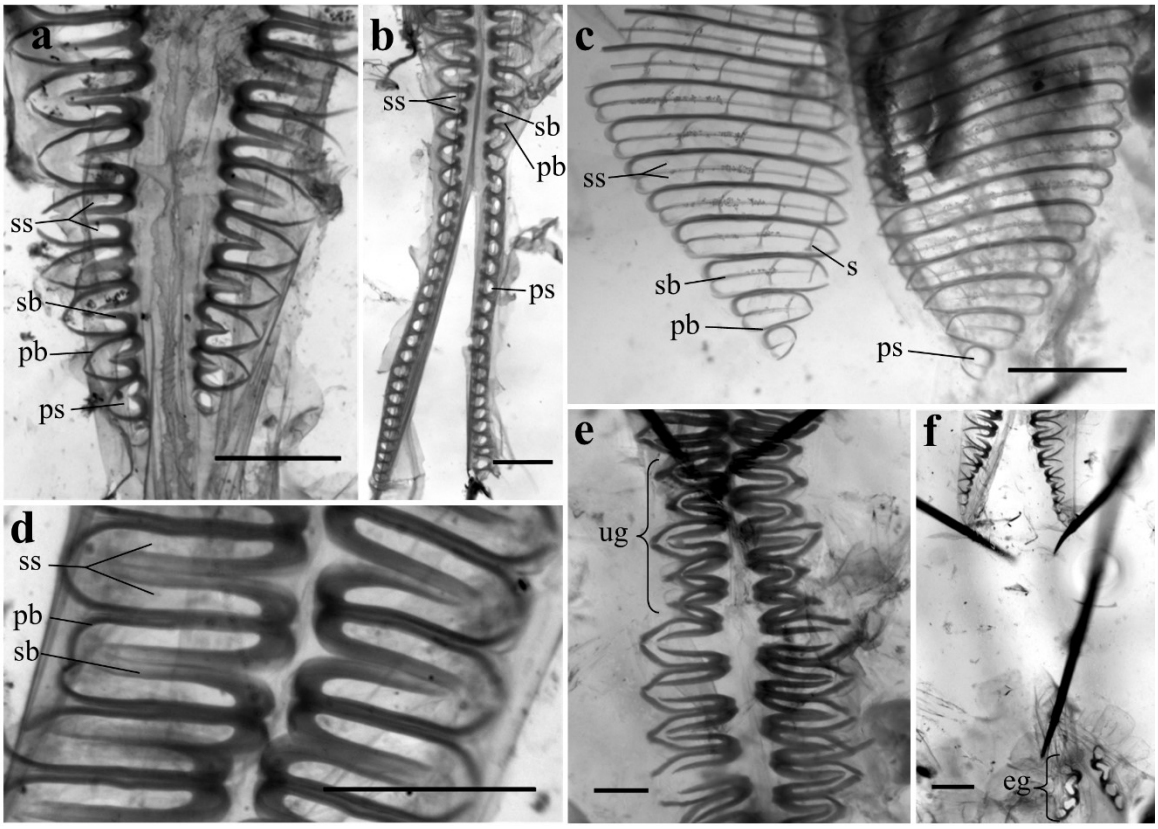

Figure 3.6: Photographs of the gill slit complexes of a) *Saccoglossus bromophenolosus*, b) *Protoglossus graveolens* and c) *Branchiostoma floridae*. d) *S. bromophenolosus* gill slits complex in higher magnification, and e) under-developed secondary gill slits following damage, and f) a second ectopic gill complex posterior to the normal complex. Anterior is at the top with a section of cleared intestine in between. All scale bars equal 500 µm except for b) were the scale bars equal 1000 µm. In all photograph the pharynx midline is dorsal except c) where it is ventral. eg, ectopic gills; pb, primary gill bar; ps, primary gill slit; s, synapticula; sb, secondary gill bar; ss, secondary gill slit; ug, under-developed gill bar.

3.4.4 Ectopic expression of a second gill complex in Enteropneusta

An unexpected finding of this study was that 8 of the 65 *S. bromophenolosus* specimens dissected (or 12.3%) had an additional pharyngeal complex (Fig. 3.6f) located posterior to the end of the normal complex, and separated by a length of intestine. It was typical in that it consisted of paired gill slits bordered by gill bars, and the posterior gills were less developed than the anterior gills (Fig. 3.6f). The secondary gill bars were never fully

developed. By comparison, an additional pharyngeal complex was found in one of the 50 *P. graveolens* specimens. A second ectopic gill complex and higher FA in *S. bromophenolosus* are both examples of developmental error.

3.5 Discussion

Fluctuating asymmetry of the pharyngeal gill is relatively low in the obligate filter feeder *Branchiostoma floridae* and the facultative filter feeder *Protoglossus graveolens* and is higher in the gills of the deposit feeder *Saccoglossus bromophenolosus*. This finding supports the idea that as the functional selection is relaxed, developmental noise augments. *S. bromophenolosus* has significantly fewer gill slit than the other species, but they have not completely disappeared, and therefore may be regarded as a trait that exhibits persistence, where there is no cost in maintaining the trait, rather than vestigial. Further evidence for persistence is that gills are found in all eighteen-described species of *Saccoglossu*s (Cameron et al., 2010). Another explanation for the persistence of the gills may be that they serve to eliminate water that is squeezed from sediment collected via deposit feeding (Burdon-Jones, 1962; Gonzalez & Cameron, 2009). The collagenous bars may provide some skeletal support to these frangible worms or keeps the pharynx from collapsing in on itself. We refrain from comparing the functions of the cephalochordate gills because the animals reside in a different environment, the larva exhibits a left-handed directional asymmetry, and they do not deposit feed.

We found that the gills of *S. bromophenolosus* and *P. graveolens* show fluctuating asymmetry in the number of gill slits in the pharynx without any side bias. These results were not consistent with the expression pattern of *Nodal* and *Pitx* genes in deuterostomes

(Wlizla, 2011). The *Nodal* and *Pitx* pathway that control left-right asymmetries in Chordata is expressed on the left side of the body (Boorman & Shimeld, 2002; Yu et al., 2002). In echinoderm larvae, both genes are expressed on the right side and they control the asymmetrical growth of the adult rudiment (Duboc et al., 2005; Luo & Su, 2012). In Hemichordata, *Nodal* and *Pitx* are expressed either symmetrically or on the right side and their role in controlling asymmetries is not clearly established (Wlizla, 2011; Röttinger et al., 2015). Asymmetries in hemichordates are restricted to the gonad of the pterobranch *Rhabdopleura* (Satoh & Holland, 2008), the proboscis pore (Grande et al., 2015; Röttinger et al., 2015) and the coiling direction of *Saccoglossus* (Wlizla, 2011). The single gonad of *Rhabdopleura* is an antisymmetry that is likely related to packaging a large egg inside of a small zooid. An asymmetric expression of *Nodal* may be linked to the left position of the proboscis pore (Wlizla, 2011; Röttinger et al., 2015). This pore is on the left of most hemichordate species, but may be located on the midline, on the right, and in the acorn worm *Stereobalanus* it is paired and symmetric (Cameron et al., 2010; Deland et al., 2010; Cameron & Ostiguy, 2013).

We found that the gills of the adult cephalochordate *B. floridae* exhibit FA, with a significant difference between left and right in favour of the left side. This adult stage left-side bias was likely inherited from the larval stage. *Branchiostoma* larvae exhibit a left-handed directional asymmetry, that is mostly lost in the adult stage. The larval gills develop as a single row of gill slit, the future left slits, on the right side of the body (Lankester & Willey, 1890; Willey, 1891; Boorman & Shimeld, 2002; Holland & Onai, 2012). A second row of gills then develops above in an inferior number. While the second row assumes some maturity, the first row begins to migrate to the left side and gills begin to atrophy.

When the migration of the first row of slit has arrived on the left side of the animal, Willey (1891) states that the numbers of left to right gills are equal. Our results do not reject this idea, but instead demonstrate that within a population of *B. floridae*, the left-sided bias is maintained in some individuals. The gonads of the cephalochordate genera *Epigonichthys* and *Asymmetron* are only on the right side (Nishikawa, 2004), and the gill asymmetry of larval *Asymmetron* is less conspicuous than *Branchiostoma* (Holland & Holland, 2010; Igawa et al., 2017). Cephalochordates gills are presumed to become symmetrical at metamorphosis but they maintain a trace of left-sided asymmetry as adults in the neural innervation of the pharyngeal complex, in the offset between opposing gills (in *Branchiostoma lanceolatum*) and now in the bias of their FA (Willey, 1891; Willey, 1894; Jefferies, 2001). This study underlines the importance of quantifying asymmetric variation in a population to detect a subtle left-sided asymmetry bias in adult cephalochordates.

The development of the secondary gill bars of *Protoglossus graveolens* with respect to the primary gill bars was highly variable demonstrating heterochrony. The posterior most gills of acorn worms are the youngest and exhibit early stages of development. Initially they are simple pores that then elongate into a slit by the downward extension of the primary gill bars. This gill slit is then divided into two by the downward extension of the secondary gill bar. The number of primary gill slits lacking secondary gill bars in *B. floridae* and *S. bromophenolosus* was invariably zero, one or two, whereas those of *P. graveolens* had an average of 17 ± 5 and up to 29 primary gill slits. This delay in the timing of development of secondary gill bars, with respect to primary gill bars, is an example of heterochrony where the development of secondary gill bars was delayed in *P. graveolens* with respect to the ancestral state presumed to be still present in *S. bromophenolosus* and *B. floridae*.

Functionally, *P. graveolens* is both a filter feeder (like *Branchiostoma*) and a deposit feeder (like *Saccoglossus*) so we found no relationship between the gill bars heterochrony, gill function and fluctuating asymmetry.

We discovered one *S. bromophenolosus* specimen with gills at an earlier stage of development than the gills just posterior to them, suggesting regeneration following damage (Fig. 3.6 e). More surprising was the finding of an entirely new second pharyngeal complex in 12.3% of the *S. bromophenolosus* specimens. The developmental mechanism for this was likely an ectopic expression of pharyngeal developmental genes, perhaps induced from a population of cells that were passed posteriorly through the gut. This is a previously unknown form of regeneration for acorn worms, though regeneration in the group is well document. Acorn worms are susceptible to breakage, and the posterior fragments of experimentally bisected animals will regenerate new individuals, including a new pharynx, from both anterior and posterior fragments (Willey, 1899; Dawydoff, 1909; Rao, 1955; Tweedell, 1961; Rychel & Swalla, 2008; Rychel & Swalla, 2009; Humphreys et al., 2010; Miyamoto & Saito, 2010). A duplicate pharynx complex was found in one *P. graveolens,* and none were found in the *B. floridae* specimens. Like the higher FA, a second pharynx complex buttresses the hypothesis that the gills of the deposit feeder *S. bromophenolosus* are more prone to developmental error than those of the filter feeders. Drift may predominate over selection in *Saccoglossus* gill development, though adaptive hypotheses cannot be ruled out. A second set of collagenous gill bars, for example, may resist breakage of the trunk, or maintain an open gut that in turn facilitates the passage of sediment or the absorption of nutrients. The instability seen in *S. bromophenolosus* is not reflected in the only other asymmetrical structure of Enteropneusta, the proboscis pore.

Some enteropneusts are known to have the pore on one side or the other (Deland et.al 2010), but none from the genus *Saccoglossus* (Cameron et al., 2010).

The hypothesis that gill used in filter-feeding evolved before the divergence of the hemichordate-echinoderm clade from the chordates (Cameron, 2002) has gained support from comparative morphology (Gonzalez & Cameron, 2009), molecular development (Ogasawara et al., 1999; Okai et al., 2000; Lowe et al., 2003), comparative genomics (Simakov et al., 2015), biomechanics (Vo et al., 2018), and the discovery of Cambrian acorn worm fossils and cambroernids (putative stem ambulacrarian) with pharyngeal openings (Caron et al., 2010; Caron et al., 2013; Nanglu et al., 2016). Here we append to this hypothesis, that the last common ancestor of Hemichordata and Cephalochordata was bilaterally symmetric. Our finding is limited by the number of species analysed, but in the context of the hypothesis above, our results provide a robust tendency within the study groups and bring evidence that gills of species that have experienced a relaxation of the filter feeding trait exhibit elevated FA. This finding is significant because it rejects hypotheses that the deuterostome ancestor was asymmetric (Jeffries et al., 1996; Sato & Holland, 2008). Instead, the directional asymmetry of many stem group fossil echinoderms (Smith, 2008; Zamora et al., 2012; Zamora & Rahman, 2014) and cephalochordates evolved independently (Kaji et al., 2016; Igawa et al., 2017). This study also cautious the use of single specimens to determine symmetry of nearly symmetric fossil or extant body plans. A 3D-reconstruction of a juvenile *Saccoglossus kowalevskii* found left side first asymmetric development of the gills (Kaul-Strehlow et al., 2013). We interpret this small asymmetry as a spandrel of the preferential right-handed coiling in pre-hatching embryos, rather than as an indication of directional or antisymmetry (Wlizla, 2011). The symmetry

of a species cannot be determined from an individual specimen because populations of bilateral species are comprised of individuals that exhibit variations around that mean, or FA, due to developmental noise. The deposit feeder *Saccoglossus* exhibits the highest noise, demonstrating that a loss in filter function relaxes selection on this trait. Likewise, pterobranchs use tentacles to filter-feed instead of the pharynx which is vestigial or lost in extant pterobranchs (Dilly, 1985; Lester 1985). The enteropneust family Torquaratoridae is a family of deep-sea deposit feeder who also show signs of vestigialisation of their gills (Holland et al., 2009; Jabr et al., 2018). Filter-feeding then, appears to be the original selective role of invertebrate deuterostome gills, and the sorting or transport of sediment (Knight-Jones, 1953), or respiration, or excretion are of little importance.

3.6 Acknowledgements

We thank the Darling Marine Center for their hospitality while collecting acorn worms. Funding was provided by a Discovery Grant from Natural Sciences and Engineering Research Council of Canada (NSERC Grant 1283784).

3.8 Conflict of interest

All authors declare no conflict of interest and that all experiments were done in an ethical manner.

3.9 Code and data availability

The code and data used for the statistical analysis has been deposited in Dryad and is accessible at https://doi.org/10.5061/dryad.ksn02v72r. The code used to perform the Student's t-test by permutation for paired sample is available at http://adn.biol.umontreal.ca/~numericalecology/Rcode/.

4 The efficacy of X-ray micro-computed tomography for acorn worm taxonomy: *Balanoglossus occidentalis* (manuscript species) from Puget Sound, Washington

Charles Larouche-Bilodeau, Noura Jabr, William E. Ritter and

Christopher B. Cameron

4.1 foreword

This chapter lacks a clear diagnosis of the described species and is not yet published. In its current state this chapter is not valid for the purposes of zoological nomenclature.

4.1.1 author contribution

WER provided the original manuscript, drawings, holotypes and paratypes. CBC & CLB collected new specimens. CLB did everything related to micro-CT scans. NJ made the new histological slides to compare them with WER original material. CLB lead the writing of the final manuscript.

4.2 Abstract

Enteropneust taxonomy has relied on histology for over a century, and this is still the main tool used in describing new species. This technique has many drawbacks like the amount of time and expertise needed to obtain reliable results. Even when the section is made perfectly the specimen is still destroyed. This is particularly an issue with unique specimens like animals collected from the deep sea that are hard and expensive to acquire. New technologies could help us alleviate these problems. Here we describe an enteropneust species that was heretofore a *nomen nudum, Balanoglossus occidentalis*. We describe it using the original unpublished observations from Ritter (1902), histology on a fresh specimen and X-ray micro-computed tomography (micro-CT) to attest the usefulness of micro-CT in enteropneust taxonomy. We show that micro-CT is a viable tool to identify

known species of enteropneusts quickly and reliably, but it can not totally replace histology for formal taxonomic description yet.

4.3 Introduction

Enteropneusts, or acorn worms, are soft bodied, benthic marine worms belonging to the deuterostome phylum Hemichordata (Horst, 1939; Cameron, 2018; Li *et al*., 2018). Enteropneusts are found at all latitudes, from the intertidal zone to the deep sea. They typically reside in the sediment and live in burrows or under rocks (Cameron, 2005). There are currently 114 extant species described, divided into the families Harrimaniidae (Spengel, 1901), Spengelidae (Willey, 1899), Ptychoderidae (Spengel, 1893), and Torquaratoridae (Holland et al., 2005) (Cameron, 2016).

Enteropneusts range from less than a millimeter (Worsaae *et al.*, 2012) to 2.5 meters in length (Spengel, 1893). The body is divided into three regions each housing different organs: the anterior proboscis, the mid collar and the posterior trunk (Cameron, 2005). The muscular proboscis functions in burrowing and feeding (Holland *et al.*, 2012a) and contains the heart-kidney stomochord complex, responsible for circulation and excretion, and the proboscis skeleton which supports the complex (Balser & Ruppert, 1990; Cameron et al., 2010; Cameron & Perez, 2012; Cameron & Ostiguy, 2013; Cameron, 2018). The proboscis bifurcates and extends posteriorly into the collar, ventro-lateral to a dorsal neural cord, dorsal vessel and perihaemal coeloms, and forms the mouth and buccal cavity. The trunk has an anterior branchiogenital region that includes the gills and gonads, a hepatic region, and a posterior elongate intestine that terminates in an anus (Cameron et al., 2010; Cameron

& Perez, 2012; Cameron & Ostiguy, 2013; Cameron, 2018). These structures, except for the collagenous proboscis skeleton and gill bars, are soft, small and prone to damage, especially if the digestive tube contains sediment, making histology and taxonomic description a challenge reserved for specialists. Here we compare the efficacy of X-ray micro-computed tomography to traditional taxonomic methods in the description of *Balanoglossus occidentalis* from Puget Sound, Washington.

Acorn worm taxonomy involves histological sectioning of fixed and wax embedded specimens (Spengel, 1893; Belichov, 1971; Woodwick & Sensenbaugh, 1985; Horst, 1939; Cameron *et al.*, 2010; Cameron & Perez, 2012; Cameron & Ostiguy, 2013; Holland *et al.*, 2005, 2009, 2012a, 2012b; Osborn *et al.*, 2012, 2013; and Priede *et al.*, 2012; Jabr *et al.*, 2018). To avoid damage to the specimens, or the sagittal sections, this process requires time, taxon specific expertise including working with tightly coiled specimens, and a steady hand. Mistakes made during the process can result in the total loss of anatomical details, and any species-specific evidence when working with unique, or hard to acquire specimens. Acorn worms are deposit feeders and specimens that are fixed with sediment in the gut cannot be sectioned, contributing to the taxonomic impediment (Spengel, 1893; Horst, 1939). Even when done well, the whole specimen is lost. Acorn worm holotypes consist of a series of serial sections on glass slides, organized from anterior to posterior. Further studies on their whole anatomy, or genomic data are therefore impossible.

Emerging solutions to these common problems with taxonomic histology include the use of modern computational and microscopic techniques that permit a detailed analysis of whole specimen anatomy in 3D (Baeumler *et al.,* 2008; Brenzinger *et al.*, 2013; Hawe & Haszprunar, 2013) without destroying the specimen. Confocal laser scanning microscopy

captures multiple two-dimensional optical sections at different depths in a sample that are subsequently stacked to create a digital 3D reconstruction. It is an effective technique to image all kinds of marine organisms such as diatoms, copepods and dinoflagellates (Michels, 2013). This has proven useful and popular in the study of micro-gastropods including members of the family Orbitestellidae (Baeumler *et al.*, 2008; Brenzinger *et al.*, 2013; Hawe & Haszprunar, 2013), allowing the observation of soft tissues (Baeumler *et al.*, 2008; Brenzinger *et al.*, 2013; Hawe & Haszprunar, 2013) and a clearer understanding of the complex morphogenesis of gastropods torsion. Confocal microscopy has drastically reduced the time and eliminated the histological training needed to analyse gastropod metamorphosis. A major limitation of confocal microscopy is that it is limited to small, translucent specimens (Baeumler *et al.*, 2008; Brenzinger *et al*., 2013; Hawe & Haszprunar, 2013).

X-ray micro-computed tomography (micro-CT) is a still emerging technology that can be used to non-destructively create 3D reconstructions of specimens with less work than confocal microscopy (Faulwetter *et al.*, 2013). It has been widely used in biological and paleontological studies and more recently to describe the anatomy of a fragile, soft bodied xenoturbellid worm, as well as the internal anatomy of fossils such as *Jaekelocarpus* but is still not a routine tool for formal taxonomic studies, especially for many invertebrates (Dominguez *et al.*, 2002; Metscher, 2009; Ziegler *et al.*, 2010; Legg *et al.*, 2012; Davies *et al.*, 2017; Nakano *et al.*, 2017). Compared to histology, Micro-CT is time efficient, it does not destroy the specimens and the digital data is easily stored and can be used to create a publicly accessible library of "cyber types'' (Faulwetter *et al.*, 2013) that are easily retrievable including if specimens are lost.

Here, we formally describe the acorn worm *Balanoglossus occidentalis* (Ritter, 1902; Ricketts *et al.*, 1985) based on a holotype of serially sectioned slides made by Ritter in 1899, from San Pedro, California, a paratype and a cybertype collected in Penrose Point State Park, Washington. The holotype and paratype are used to confirm the species identity and range of *Balanoglossus occidentalis* using traditional histology, and the cybertype was developed from sections and a 3D reconstruction developed using a micro-CT scanner. This was done to assess the efficacy of CT-scanning technology in Enteropneusta taxonomy.

4.4 Materials and Methods

4.4.1 Histological specimen preparations

Two sets of histological sections were used for the traditional taxonomic description. The first set were those of William E. Ritter, based on specimens that were collected in the nineteenth century. Ritter gave these slides to Theodore H. Bullock, with the hope that he would complete the formal description of the species (Deland *et al.*, 2010). Bullock, in turn, asked Christopher B. Cameron to provide a taxonomic description and deposited the Ritter material in the Smithsonian Institution National Museum of Natural History, Washington, DC, from where we loaned the material. A second worm was sectioned from a specimen collected on June 16, 2018, in Penrose Point State Park, Washington, during the monthly low tides. The worm was left in clean sea water for 12 hours to evacuate its gut of sediment. Worms were then relaxed in 7% magnesium chloride, fixed in Bouin's solution and stored in 70% ethanol.

The fresh specimen was paraffin embedded, trimmed and sectioned on a microtome and the sections mounted on a serial collection of glass slides. Mounted sections were then dehydrated to 100% ethanol and dewaxed in Xylene before being rehydrated and stained with Masson's trichrome. The Ritter specimen was fixed in Bouin's solution and appears to be stained with a Hematoxylin solution. All slides were photographed on an Olympus SZX16 stereomicroscope or an Olympus BX51 compound microscope with a Q Imaging Retiga-2000R digital camera using Q Capture Pro software by Q Imaging.

4.4.2 Micro-CT scanning

Of the many worms that were collected fresh, one of the smallest (21.3 mm in total length) complete specimens was selected for micro-CT scanning to maximize the resolution on a full body scan. The worm was stained in 1% phospho-tungstic acid in 70% ethanol for 3 days to enhance soft-tissue contrast. Phospho-tungstic acid was used because it provides clearer differentiation of small structure than iodine and is less toxic than osmium (Metscher, 2009). The specimen was brought to the Integrated Quantitative Biology Initiative facility, McGill University, and scanned with a Zeiss Xradia Versa 520. A first scan was made of the whole specimen with AMC drift correction, 0 beam hardening, voltage of 60 kV, currant of 82 µA, exposure time of 1.7 sec, LE2 source filter, LE6 secondary filter, 1601 Projection numbers, single FOV, vertical stitching and a resolution of 9,0373 µm. Then, a second scan was made focusing on the collar and the base of the proboscis because these regions are particularly informative to taxonomic descriptions of acorn worms. This second scan had a Projection number of 2401 and a resolution of 4.5075 µm. Each scan took 3 hours. The image files were then stacked to create the 3D virtual

specimens using the Dragonfly software from Object Research Systems. The 2D view angle was adjusted to be perpendicular to the worm axis with the dorsal side on top. Light and contrast were adjusted within Dragonfly. Tomograms were acquired from the 2D view. To create the 3D reconstruction of isolated organs, each region of interest was manually painted using the region of interest painter on the 2D view on every slice where they appeared. This last step took 2 days.

4.5 Ritter's original description (1902) of *Balanoglossus occidentalis* n. sp.

The following is Ritter's original unpublished description (1902) of *B. occidentalis* edited to update anatomical names so that they conform with Cameron (2005), Deland et al (2010), and Cameron and Perez (2012). This was done to avoid confusion of multiple terms used, in the classic literature, for the same structures. Some examples of terms that were replaced include genital wings rather than alae, and hepatic sacs rather than liver lobes. Other terms not commonly in use during Ritter's time have been included, for example, perihaemal and peribuccal muscles. These muscles develop from paired forward diverticula of the trunk coeloms into the collar. The perihaemal coeloms are located to each side of the dorsal blood vessel and in *B. occidentalis* innervate the collar cord, and the peribuccal muscles are located to either side of the buccal cavity.

4.5.1 External Characteristics

A large individual with a total length of 500 mm. Body thickest in mid-genital region, abdomen of nearly uniform diameter throughout with a slight enlargement at the extremity.

Proboscis in medium state of distention, a little longer than collar; collar with a pronounced anterior rim. Proboscis pore single slightly to the left of the median line, at the summit of a low mound. Genital wings (alae) are highly developed, dorsally inserted, reaching their greatest depth in the middle region from where they become gradually lower in their course backward, but posterior termination rather abrupt, this slightly behind the anterior end of the hepatic lobes. Anteriorly the wings are also considerably lower than in the middle part. Genital pores in distinct, close rows near the border of the wings. Wings extending far, though a variable distance, behind the pharynx (Fig. 4.1).

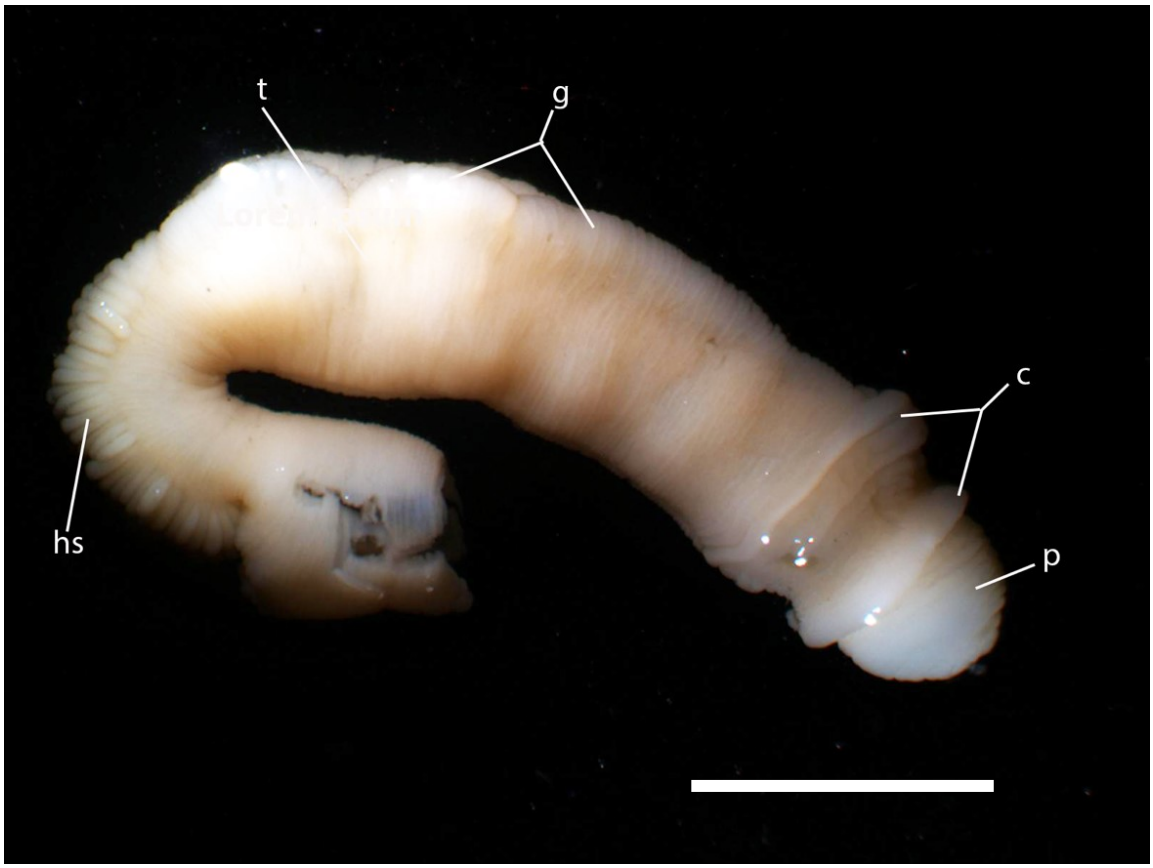

Figure 4.1. Photograph of the paratype of *Balanoglossus occidentalis* n. sp. Specimen will be put in the Smithsonian NMNH. **Abbreviations**: **c**, collar; **g**, genital wings; **p**, proboscis; **t,** trunk, **hs**, hepatic sacs. Scale bar is equal to 5 mm.

Branchial orifices (gill pores) about 200 in each series, though the number is very variable; each orifice opening externally at the bottom of the distinct pit (gill pores). A mid-dorsal band present in branchio-genital region which is distinctly metameric, the metameres being approximately though, with considerable variation, one for each two and a half pairs of branchial pores. Hepatic sacs large, more or less foliate, distinctly set off from the body from which they spring; from 40 to 60, depending on the size of the individual, on each side; several of the small anterior lobes situated between the posterior extremities of the genital wings. The colour of the proboscis is naples yellow, collar same excepting the

posterior rim which is light orange. Genital wings orange with a brick red band along the ventral side of the body in genital region. Hepatic sacs prevailingly green, some parts brownish, abdomen proper much the color of proboscis and collar.

4.5.2 Anatomical Characters

Ectoderm of the proboscis and to some extent of the collar containing a great number of irregular, round, or more frequently, elongated pits produced by excavations in its surface. Longitudinal muscle fibers of proboscis arranged in well-defined radial plates, from 40 to 50 in number. A highly developed connective tissue network nearly fills the proboscis cavity and penetrates in between the radial muscle plates for nearly half their width. (Fig. 4. 2 A & B).

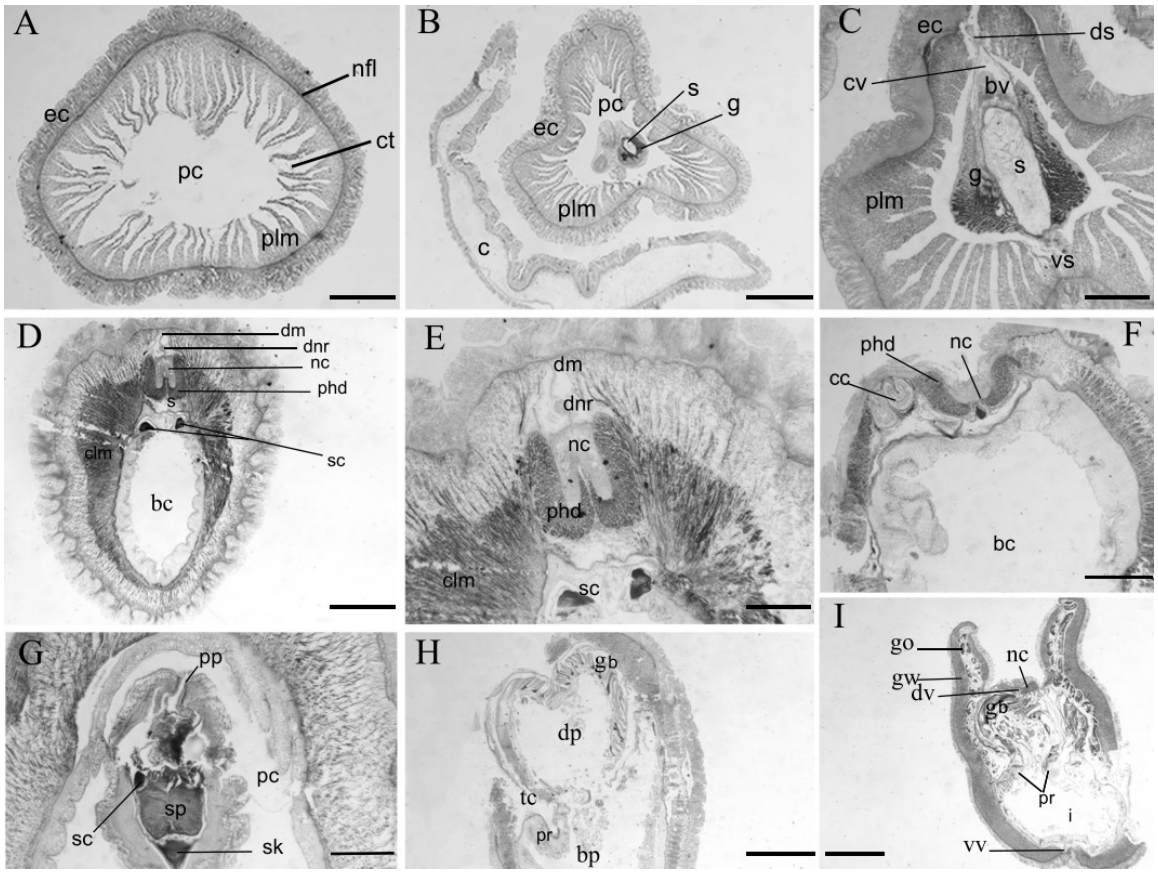

Figure 4.2. Light micrographs of transverse sections of *Balanoglossus occidentalis* n. sp. The sections are from Ritter's Holotype. Specimen will be put in the Smithsonian NMNH. (A) Cross section of the anterior of the proboscis showing longitudinal muscles and proboscis coelom. (B) Proboscis showing the conjunction point between the proboscis and the collar and the beginning of forming the proboscis complex. (C) Proboscis complex showing the stomochord, glomerulus, and dorsal and ventral septum; (D)Anterior region of the collar with dorsal roots, very well-developed collar longitudinal muscles and the skeletal cornua; (E) Anterior region of the collar showing the dorsal nerve root of the collar, and perihaemal diverticula. (F) Collar canal and buccal cavity; (G) skeletal keel and skeletal plate; (H) branchial region of the trunk shows gills; (I) Genital region of the trunk showing gonads and intestine. **Abbreviations**: **bc**, buccal cavity; **bp**, branchial pharynx; **bv**, blood vessel; **c**, coelom; **cc**, collar canal; **clm**, collar longitudinal muscle; **ct**, connective tissue; **cv**, cardiac vesicle; **dm**, dorsal mesentery; **dnr**, dorsal nerve root; **dp**, digestive pharynx; **ds**, dorsal septum; **ec**, ectoderm; **i**, intestine; **g**, glomerulus; **gb**, gill bars; **go**, gonads; **gw**, gonad wings; **nc**, nerve chord; **nfl**, nerve fiber layer; **pc**, proboscis coelom, **plm**, proboscis longitudinal muscles; **phd**, perihaemal diverticula; **pp**, proboscis pore; **s**, stomochord; **sc**, skeletal cornua; **sk**, skeletal keel; **sp**, skeletal plate; **tc**, trunk coelom; **vs**, ventral septum. Scale bars: (A, F) = 500µm; (B) = 400; µm (C) = 1000µm; (D, H and I) = 600µm; (E) = 450 µm; (G) = 150 µm.

Both dorsal and ventral proboscis septa extend fully to the base of the proboscis; ventral nearly coextensive in length with the stomochord, dorsal not reaching to its anterior end.

Glomerulus highly developed, bilobed in front of the tip of the stomochord (Fig. 4.2 B & C). Heart when gorged with blood has a sac much wider than the mouth by which it communicates with the blood sinuses of the glomerulus, it being in such conditions a deep invaginated sac into the pericardial cavity.

Right proboscis pore and terminal vesicle entirely wanting; left present in full development the stomochord of the thick-walled, small lumened type (Fig. 4.2 C); ventral coeca of varying form and size always present. Connection of the stomochord with the esophagus always maintained. Dorsal nerve cord of collar with from one to five dorsal roots (Fig. 4.2 D & E). Lumen of the cord never continues as a single cavity from end to end; nor on the other hand never wholly suppressed in any part; hence in a medium condition of development as compared with other species of the family. Collar canals well developed (Fig. 4.2 F). Nuchal skeleton is very variable in development, but crura are always short (Fig. 4.2 D & E), and large quantities of chondroid tissue are always present.

Form of the cord is sometimes nearly round, sometimes much depressed (apparently changeable) by action of depressor muscles. Circulatory system, gills and gonads (Fig. 4.2 H & I), branchial apparatus, hepatic sacs, and post thoracic abdomen conforming closely to other well-known species of the genus.

4.5.3 Some details of external characters

Comparing some characters of *Balanoglossus occidentalis* with those given for other species shows that while *B. occidentalis* is not the largest known species of the family, it is yet entitled to be ranked among the largest. It is exceeded in size by *Balanoglossus gigas* Fr. Müller in Spengel, 1893 that reach a length of 2.5m and is thus by far the largest known species; by *Glossobalanus sarniensis* Köehler, 1886, which reaches a total length according to Spengel, of 90 cm, and probably by *B. jamaicensis* Willey, 1899, though we have no information as to the total length of this form, Wiley having had only fragments to work with.

In general, a constant proportion is maintained between the size of the proboscis, collar, hepatic region, and the abdominal-caudal region. For the pharyngeal and genital region, however, it is otherwise. The pharyngeal region in particular, is exceedingly variable in length. Although in two specimens were about equal in size, when judged by the proboscis and collar, the pharynx of the first individual was more than three times as long as that of the other one. The fact that all my specimens are from the same locality makes it appears that the brachy-branchiate and macro-branchiate forms cannot here have any significance in connection with geographical distribution as Willy suggests may be the case in *Ptychodera flava* Eschscholtz, 1825.

As is apparent, from measurements of the most instances shows that the proboscis is considerably longer than the collar. Except for one individual where the collar approaches the proboscis in length, and that is due to disproportionate contraction of it. In the normal condition the proboscis is a more pointed cone than is the case in the animal figured (Fig. 4.3), and it is wholly incapable of being contracted into a sphere as it may be in some

species of the family; or of being nearly hidden in the anterior cup of the collar, as it may be in *Balanoglossus carnosus* Willey, 1899. The collar is somewhat longer on its ventral than on its dorsal side and is slightly compressed laterally. The genital wings rarely stand out horizontally as they are represented as doing in some other species but on the other hand appear never to lap over each other at their free edges so as to produce a temporary peribranchial chamber, as, for example, Willey has described them as doing in *Balanoglossus carnosus* Willey, 1899. Standing as they do but little short of upright, it is frequently the case that their congestion in sexually mature specimens, whether male or female, almost wholly obliterates the inter-wings channel, so that the branchial region can hardly be seen without pushing the wings apart. The individual shown in Fig. 4.3 was the only one of my preserved specimens possessing well developed gonads in which a clear view of the branchial region could be obtained. Although there is but a short section at the anterior end of the wings that contains no gonads, these latter do not reach their maximum development for some distance, from one to two or more centimeters, and consequently it is here that the total depth of the animal becomes greatest. In sexually immature specimens the anterior converging ends of the wings are distinctly thicker than the portions farther back; in fact, except anteriorly they are very thin in such animals. With the development of the gonads, however, this disparity in thickness disappears almost entirely. The flouncing of the wings seen (Fig. 4.3) is even more pronounced in some of the larger animals with gonads highly developed. The wings terminate posteriorly in this species almost as abruptly as they do, according to Willey in *Balanoglossus carnosus* Willey, 1899. There is not, however, as in that species, an interval between their termination and the beginning of the hepatic region. The two regions always overlay somewhat. The foliate

hepatic sacs are bunched more or less distinctly into a few, two or three, large masses. The series of lobes is very definitely set off on each side from the body wall from which they spring. As a rule, each sac extends entirely across the series to which it belongs, and is much flattened antero-posteriorly; so that on the whole the hepatic region resembles considerably that of *Glossobalanus minutus* Kowalevsky, 1866. The form of the sacs is, however, subject to considerable individual variation, at least as they appear superficially. In some specimens they approach the form of cylindrical processes. This appears, however, to be due to crowding and displacement. In regions where this crowding and displacement has not occurred, the sacs are quite regularly in pairs. More so, it would appear, than is usually the case in other species.

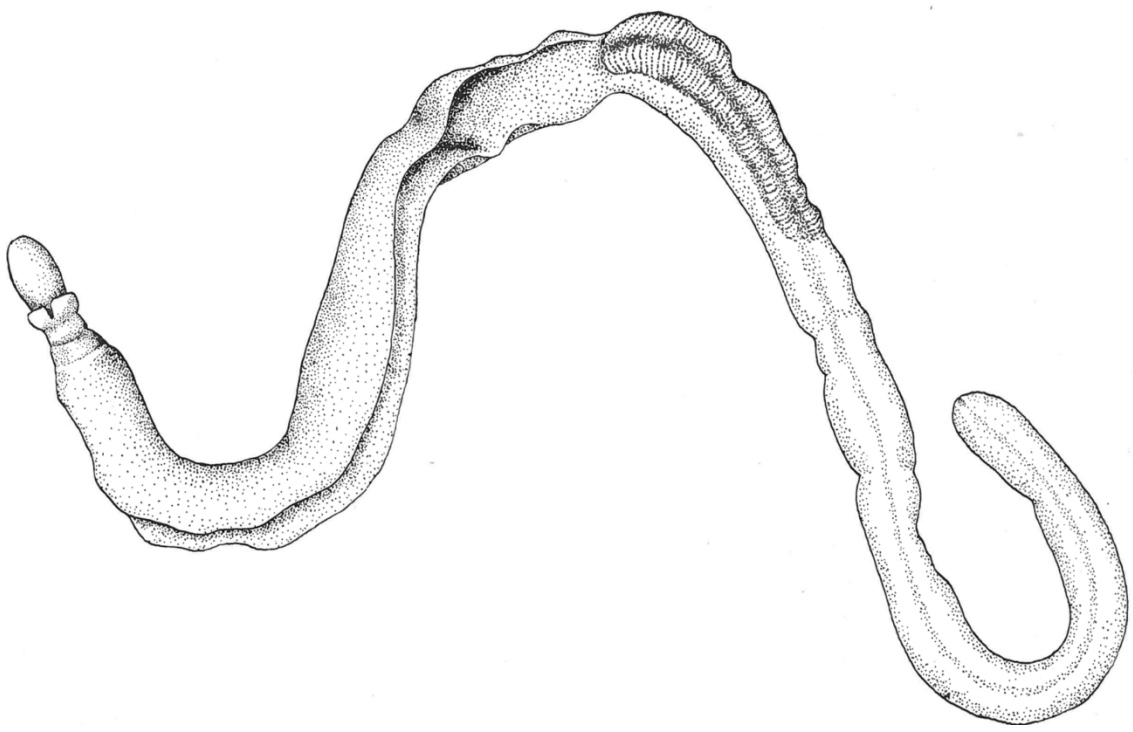

Figure 4.3. Ritter's original unpublished drawing of a full specimen on *Balanoglossus occidentalis.*

Furthermore, the pairs frequently correspond for considerable stretches to the "segmentation" of the median dorsal cord in this region, so that in such places the resemblance to a true metamerism is striking. The body wall immediately behind the hepatic region is usually depressed more than elsewhere, and is frailest at this point, and consequently severs here more easily than elsewhere. On account of the extreme delicacy of the body not only at this point, but also, though in less degree, at the junction of the genital and hepatic regions, whole specimens usually show a short close kink in the hepatic region. The median lines, both dorsal and ventral, are distinct throughout the length of the abdominal caudal region and are both single in preserved specimens as they are in the form of deep median furrows.

4.5.4 Internal Anatomy

Proboscis in no other species of the Enteropneusta is the epidermis known to possess the characters presented by it in this one. Throughout the proboscis this layer possesses a great number of deep, elongated, anastomosing pits, the elongation generally corresponding with the long axis of the animal. A surface preparation of the epidermis presents under a low power of the microscope appearance in Fig. 4.4 A. The shaded bands represent ridges and the intervening shaded areas the pits (the preparation is shown as seen by transmitted light, and the ridges being somewhat thicker and denser than the pits, appear darker). The narrow dark lines in the light area correspond to the slit like bottoms of the pits. Fig. 4.4 B is a drawing of a small portion of the epidermis. An examination of the sections shows that the structure above described is not due to a folding, but rather that the pits, or trenches, are deep cuts into the epidermis; so deep, in fact, as to frequently extend almost entirely through it.

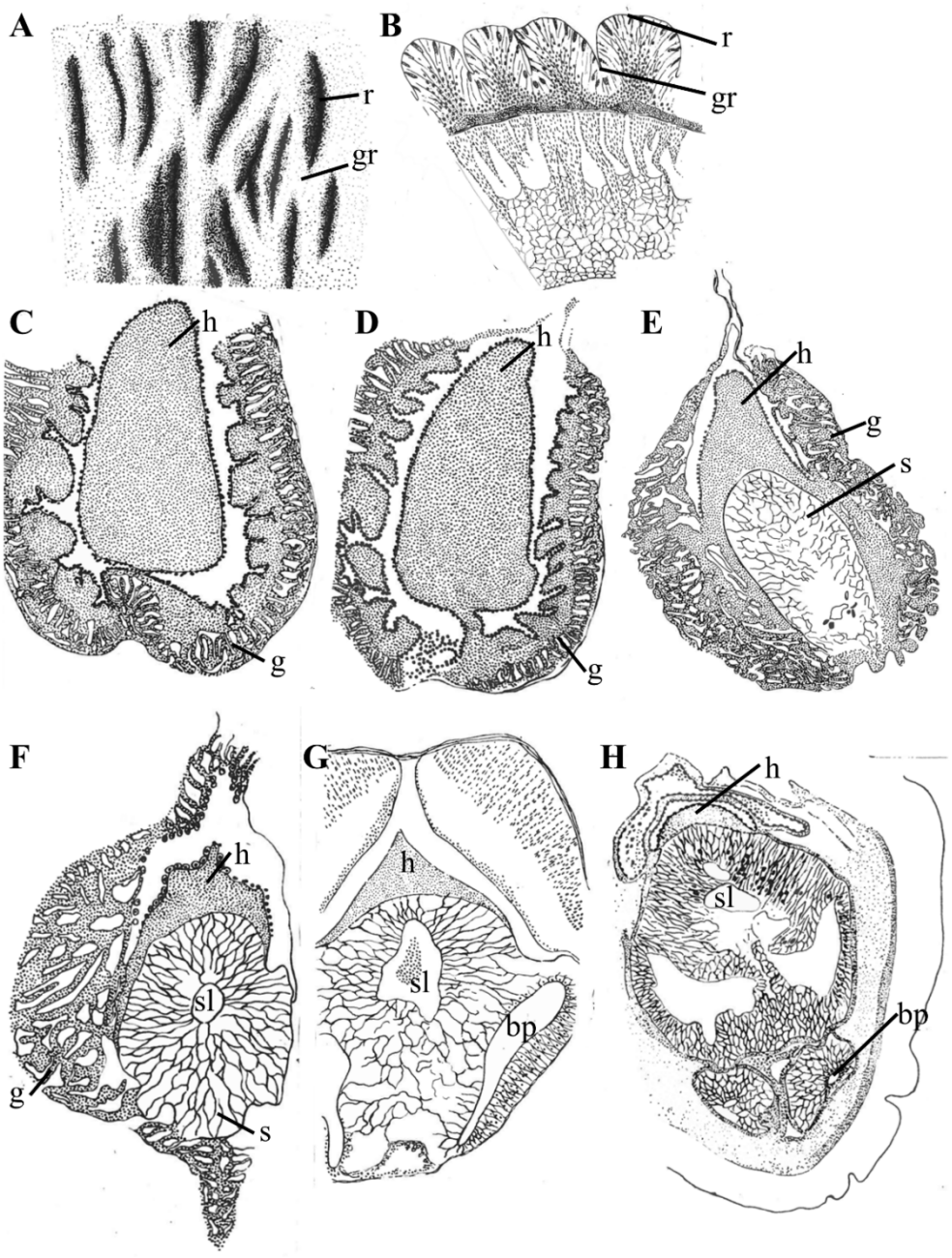

Figure 4.4. Ritter's original unpublished drawings of the epidermal grooves, heart-glomerulus complex and stomochord anatomy. A. surface preparation of the proboscis epidermis. Shaded bands represent ridges and the lighter area represent the anastomosing pits; B. transversal section of the proboscis epidermis showing that the pits are not folds but cuts in the epidermis; C. transversal section through the anterior part of the heart-glomerulus complex where the heart lies within the pericardium as a closed vesicle; D. Section through the anterior part of the complex where the heart connects with the blood sinus; E. Section of the complex in the anterior part of the stomochord; F. Section of the through the middle of the stomochord showing the usual relation of each organ; G. Section of the complex through the stomochord blind pouches; H. Section of the complex through the stomochord blind pouches with outside limitation. **Abbreviations**: **bp**, stomochord blind pouch; **g**, glomerulus; **gr**, epidermal groove; **h**, heart; **r**, epidermal ridge; **s**, stomochord; **sl**, stomochord lumen.

As with all other Enteropneusta, the nuclei of the epidermal cells, which reach entirely through the epidermis, are situated for the most part in the deeper portion of the layer. But here instead of being distributed in a uniform layer, as they are in other species, they are massed into dense columns, as they appear in the sections (Fig. 4.4 B), corresponding to the ridges and are reduced to a very thin layer under the ditches. I have spoken of the ditches as being cut into the epidermis. This, however, is not an adequate characterization of them when histologically considered. Such cuts would, of course, if conceived as made into an epidermis of typical structure, separate the cells concerned lengthwise in their outer portions. As a matter of fact, however, many of the cells in the ridges, the nuclei of which are in the nuclear columns above mentioned, fan out toward the sides of the ridges, so that the entire surface of the ditches is composed of the ends of cells. In other words, the whole surface of the epidermis, both on the ridges and the ditches, is made up in practically the same way that it would be where it is a plane surface, as in other species. Although the entire surface of the epithelium of the proboscis is ciliated, the cilia of the ditches are noticeably longer than those of the ridges. The gland cells are essentially alike both as to number and distribution, in the two regions.

As may be seen by Fig. 4.4 B the base of the epidermis does not conform except to a slight extent to the ridges and ditches but is very nearly uniform in thickness throughout. In some places it is somewhat thicker under the ridges; in fact, one may say that this is the rule, but it is by no means always so. It is clear from the description that these folds of the epidermis are not artifacts due to contraction as one might, perhaps at first conjecture. If evidence to this effect beyond what the epidermis itself furnishes, were needed, it may be found in the

fact that the layer of circular muscle fibres, the contraction of which would have to be supposed to produce the folding, is very thin, is uniform in thickness, and shows no evidence of any special contraction. These ditches and ridges are developed in the collar epithelium also to some extent, though less than in the proboscis.

There is no heavy band of circular fibers at the base of the proboscis like that described by Spengel in *Balanoglossus clavigerus* Delle Chiaje, 1829. In most, if not in all species of this genus a well-developed mesh work of connective tissue similar to that in *Glossobalanus minutus* Kowalevsky, 1866 and most other species, but lacking according to Willey in *Glossobalanus ruficollis* Willey, 1899 is here present and serves not only to bind together the inner edges of the muscle plates, but also to form the wall of the central proboscis cavity. Spengel is of the opinion that the absence of this connective tissue network from the interval between the radial muscle plates is apparent only, and it is due to treatment of the animals in preparing them for study. In *Balanoglossus occidentalis* I cannot believe this explanation will hold. The net work is closely adherent to the muscle plate wherever it is present and when it tears by contraction, its presence can be detected by the broken fragments that still cling to the muscles. But in most of the spaces the surfaces of the plate are entirely free from such shreds. I therefore conclude that there are numerous spaces between the muscle plates entirely devoid of connective tissue. In addition to the consideration just presented favoring this view, such a condition as that shown in Fig. 4.4 B, tends to the same end. Here the fine fibered uniform meshed connective tissue extends in between the plates for fully one third of the way toward their basses and is very clearly set off from the coarser muscle fibres which are embodied in it. The outer surface of the connective tissue mass, i.e. the surface looking toward the epidermis, is quite as clear cut

as is that bounding the central proboscis cavity. These are natural surfaces, I am convinced. Whether or not these inter-muscular cavities communicate with the central proboscis cavity otherwise than through the meshes of the connective tissue, I do not know. I have not found such communications that I could regard with certainty as being natural.

The stratum of connective tissue bordering the central proboscis cavity is considerably denser than elsewhere, and the nuclei are correspondingly more numerous. This condition produces an appearance considerably like a peritoneal lining for the cavity. No true endothelium is present; however, such as occurs in *Saccoglossus*. The central proboscis cavity narrows down greatly as it approaches the glomerulus, and finally disappears entirely as Willey, 1899, finds it to do in *Balanoglossus carnosus* Willey, 1899.

The portion of connective tissue intervening between it and that of the base of the proboscis in which the proboscis complex is situated is of considerable thickness and density. This basal cavity is divided, as usual, in the greater portion of its length, into two lateral halves by the proboscis complex (Fig. 4.2 C), and the ventral and dorsal septa. Dorsally, however, the division is not complete anteriorly, the septum not reaching to the extreme end here. Ventrally, on the other hand, the division is complete anteriorly, but not quite posteriorly, the septum terminating here a little short of the extreme end of the cavity.

The relation of the posterior proboscis cavity to the proboscis pores is the usual one for the genus. The right half dwindles in size in its backwards course, and finally pinches out entirely. The left, on the contrary pushes over more and more toward the median dorsal line, until it reaches the terminal vesicle which in its turn opens to the exterior by the large single proboscis pore situated slightly to the left of the medial dorsal line (Fig. 4.2 G & 5D). The differentiation of the exit conduit of the proboscis cavity into different portions,

as first clearly pointed out by Willey, 1899, is so well shown here that I have thought it best to present some figures illustrating it. Fig. 4.5 A shows a section passing through the posterior end of the dorsal coelomic canal (the transition from this to the connecting duct is very gradual, and hence no definite point of passage from the one to the other can be located). Fig. 4.5 B nine sections farther back, cuts the connecting duct in about its smallest part; while Fig. 4.5 C twenty sections still farther back, passes through the terminal vesicle in its largest part, and is very near the proboscis pore. The striking difference not only in size but also in the character of the wall of the connecting duct and the terminal vesicle are brought out with sufficient clearness by the figures.

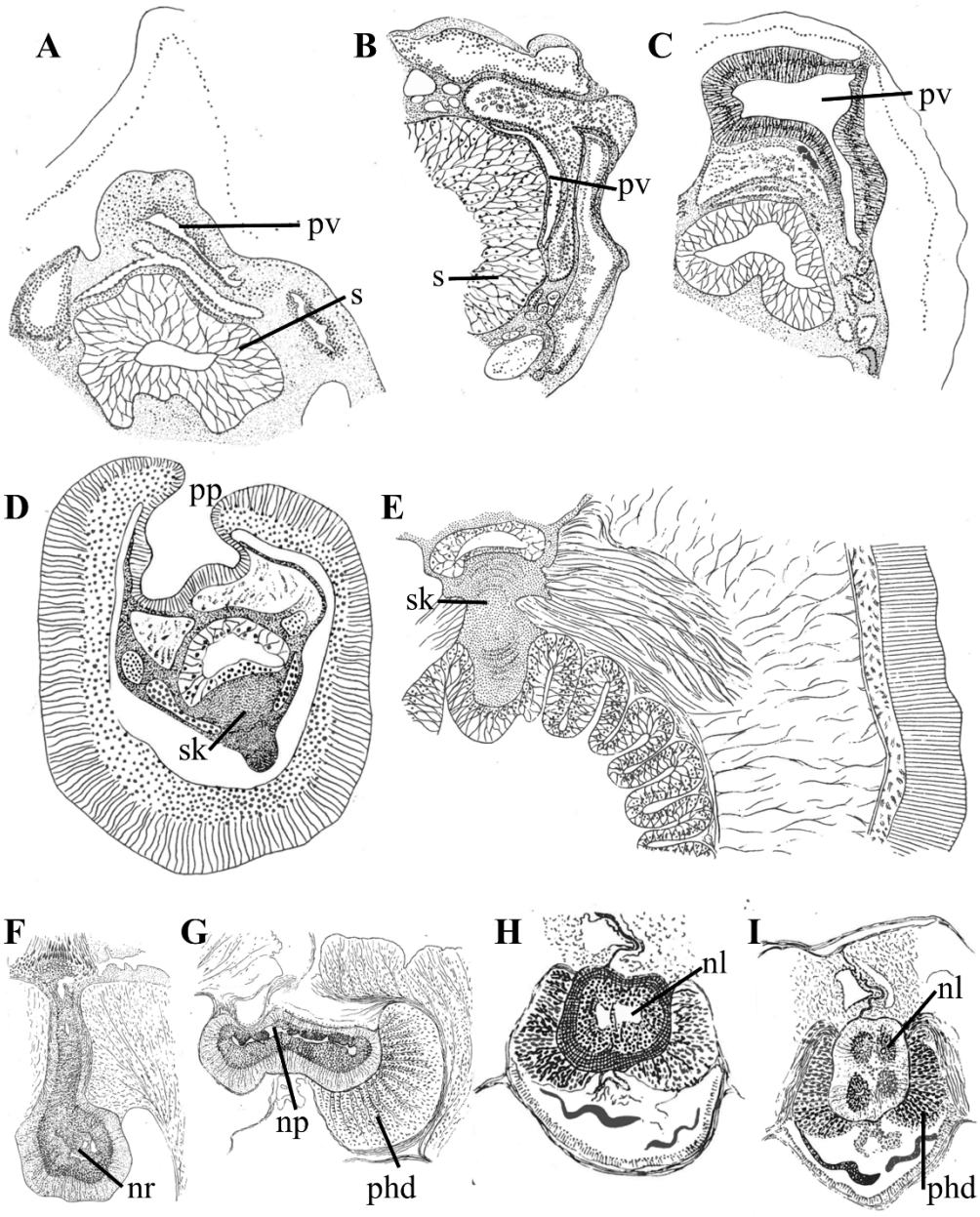

Figure 4.5. Ritter's original unpublished drawings of the proboscis skeleton, the proboscis pore and vesicle, and the neural chord anatomy. A. Section through the posterior end of the coelomic canal; B. Section through the narrowest part of the proboscis duct; C. Section through the proboscis terminal vesicle largest part. D, Section through the opening of the proboscis pore; E, Section through the skeletal keel; F, Section through the first nerve root; G, Section through the anterior neuropore; H. Section through the middle of the nerve chord; I. Section through the posterior part of the neurochord. **Abbreviations**: **nl**, neurochord lumen; **np**, neuropore; **nr**, nerve root; **phd**, perihaemal diverticulum; **pp**, proboscis pore; **pv**, proboscis vesicle; **s**, stomochord; **sk**, proboscis skeleton.

From Fig. 4.4 C to F it will be seen that the glomerulus not only spreads widely over the surface of the pericardium, but also that it reaches down over the lateral and ventral portions of the stomochord extensively. In no other species of the genus, so far as I can gather from the accounts of other observers, does the organ reach quite so wide an expansion. In a somewhat modified form it extends onto the dorsal and ventral septa (Fig. 4.4 F). The modification of the tissue of these extensions relative to that of the glomerulus proper, consists in the presence of a larger quantity of the splanchnic epithelium to the blood capillaries. The capillaries are much finer, in fact, here than in the glomerulus. An approach to this condition is found on the dorsal septum in *Glossobalanus minutus*, according to Spengel, but appears to be wanted in all other species.

Willey has pointed out that the antero-posterior extent of the dorsal and ventral septa is a matter of some systematic importance *B. occidentalis* agrees with those species in which the ventral septum is very nearly coextensive with the length of the stomochord. The dorsal septum, on the other hand, falls short by considerably reaching to the anterior end. Both extend back to the very limit of the proboscis coelom; so that this cavity is separated into two lateral halves posteriorly.

The pericardial cavity contains some of the peculiar cells found in other species, but in no portion is it full of them, as it is in *Glossobalanus minutus* for example, according to Spengel.

The great development of the glomerular blood vessel or sinuses in the heart in this species is noteworthy. Fig. 4.4 C & D represent sections of the glomerulus far toward its anterior end. The size of the heart is so enormous that it is only by carefully tracing it back to find its relations to the other parts, at its posterior end that one can believe it to be this organ.

No doubt, however, remains when this is done. It is true that such a dilation of the structure as is shown here is exceptional, though it is unusually large in all individuals, as are also the number and size of the vessels entering into the composition of the whole glomerulus.

The relations of the heart in the specimen here figured deserve special attention. It will be observed that in Fig. 4.4 C just referred to, that the organ lies within the pericardium, as a wholly closed vesicle. Five sections farther back Fig. 4.4 D shows that a narrow communication with the great blood sinus here exists. In other words, the heart is a nearly closed sac formed by folding into its own cavity of the ventral wall of the pericardium. The very thin wall of the heart is readily traceable around into direct continuity with the wall of the pericardium. By following the series still farther back, with the increase in size of the stomochord, the usual relations of heart, pericardium, and stomochord come to view (Fig. 4.4 E & F). The heart, then, is here the ventral wall of the pericardium pocketed into the pericardial cavity, the mouth of the pocket remaining open in the backward and laterally thought narrowly to form the main vessels. In a word, the heart is constructed on the principle of the tunicate heart. Spengel has described an essentially similar arrangement in *Stereobalanus canadensis* Spengel, 1893. And the same thing in *Balanoglossus australiensis* Hill, 1894 at first sight it appears remarkable that different species of even the same genus have hearts constructed on quite different plans. As a matter of fact, however the difference is rather apparent that the real heart above described is only a slight modification of the prevailing style for the whole group and is readily derivable from it. That this is the interpretation to be placed upon what we see here becomes obvious when we find that in another individual of the present species the heart of the ordinary form appears. In fact, it is probable that the one or the other form may exist in one and the same

individual at different times. It would appear that when the heart becomes gorged with blood, as it obviously is in the individual here treated, it takes this form; while when it empties itself and becomes normal in size it assumes the usual form. The stomochord presents nothing of spacio-graphic importance, but from a general morphological point of view several facts in connection with it are of considerable interest. Its wall in the proboscis portion is everywhere thick, and its cavity rather small (Fig. 4.4 F), it agreeing in this particular with those species of which *Glossobalanus minutus* and *Saccoglossus* generally are types, rather than with those species of which *Balanoglossus biminiensis* Willey, 1899 and *Balanoglossus gigas* Fr. Müller in Spengel, 1893 are types, where the cavity becomes very large, and the wall relatively thick. At its anterior end the cavity is broken up into several secondary ones placed one above the other. In the middle region, in front, then, of the basal portion from which coeca are, as in most other species, given off, the cavity is simple.

Two lateral coeca are always present (Fig. 4.4 G) projecting forward, but variable in their extent in different individuals. These are coeca from the central cavity only. They are excavations in the substance of the organ like the central cavity itself. In some specimens, however, a pair of coeca differing from these in that each has an outside limitation as well, is given off on the ventral side of the chorda (Fig. 4.4 H). Here it will be observed that each coecum has a layer of stomochordal sheath around it as well as of chordal tissue proper. These coeca project forward as do most of the others. One of them communicates by a small opening with the central cavity, but the others appear to have become entirely severed from it. As these coeca are not present in all individuals the importance to be attached to them, so far as I see, is evidence of the variability of this portion of the stomochord.

The stomochord maintains its connection with the esophagus in this as in most other species. The isthmus presents nothing of specific interest. It is, however, deserving of note as a reinforcement of the truth so general for the whole group, that its narrowest portion is in the peduncle where the body of the nuchal skeleton reaches its maximum of size and strength, and that posterior to this, before the esophageal connection is reached, it expands again laterally. This is done in an unusual way in one specimen from San Pedro. Here at its smallest place the section is triangular with the dorsoventral diameter equal to that of the transverse. Suddenly, within the extent of three or four sections the whole makes an abrupt turn ventro-dorsally, the dorsoventral diameter becomes greatly reduced, and the transverse correspondingly expanded laterally.

The following facts are of interest in connection with the nuchal skeleton: In some individuals the crura diverge laterally so abruptly that their distal ends appear in the same transverse section with their proximal ends. In these individuals the structures are very short and thick. These individuals resemble more in this respect *Schizocardium brasiliense* Spengel, 1893 than any known species of Ptychodera. In other individuals again the length and course of the crura correspond more nearly with the more usual Ptychodera type. So far as my observations have gone the specimens from San Pedro possess crura of the first type, while those from Puget Sound have the second type. Should this difference be found to be constant it would furnish ground for separating them specifically. I cannot, however, believe from the evidence at hand that the difference will prove to be constant.

Another unusual, if not unique condition, is found in the relation of the keel to the body - again in the San Pedro specimens. In the first place the keel is nowhere, in the specimens examined deep and thin as it usually is, e.g., in the Puget Sound specimens of the species,

but is broadly triangular in section, and is not a single mass from side to side, but is composed of two slabs put together roof wise, with the apex ventral. Each slab is in close contact with the esophageal wall by which it was secreted. The interval between the slabs is in part vacant space in my preparations and in part is occupied by irregular masses, some small, some large, of a homogeneous wax-like substance, the real nature of which I do not understand. It is certainly debris of some sort and is probably the product of breaking down of the skeletal tissue that even yet is found to some extent between the lateral slabs, and between the base of the keel and the body proper. The same material is found to some extent in other portions of the skeleton. None has been observed in specimens from Puget Sound. It is to be noted, however, that all the San Pedro specimens thus far obtained have been large ones - fully grown, perhaps old ones; and this degenerative condition of the skeletal tissue may be correlated with this fact.

Spengel has described and figured a peculiar brown substance in the center of the skeletal body of *Harrimania kupfferi* von Willemoes-Suhm, 1871 which may be the same material as that occurring in *Balanoglossus occidentalis* though not yet broken up. He also figures a few bodies in the skeleton of *Balanoglossus apertus* Spengel, 1893 that are undoubtedly the same as what I find so abundant in the present species.

Spengel, expresses the view that in Ptychoderidae, with the exception of *Ptychodera erythraea* Spengel, 1893, the chondroid tissue does not reach a great development. This conclusion would certainly not hold for *Balanoglossus occidentalis*, as is evident from Fig. 4.4 H. This is a point of some interest for if Spengel is right, as I believe he is, in supposing Ptychodera to be the most highly specialized of the Enteropneusta, we should expect to

find all its essential parts, and particularly its framework, as is clearly the case with the branchial skeleton, more highly elaborated than in the less specialized species.

I would here call attention to the impossibility of making a sharp distinction between primary, or skeletal tissue proper; and secondary, or chondroid tissue. The distinction between the two, first made by Marion and later dwelt upon much more at length by Spengel, is certainly of importance because in general it is natural and readily recognizable. Skeletal tissue proper usually contains no cells and is entirely homogeneous except for the layers of deposit nearly always so obvious in sections of the body and keel (Fig. 4.5 E) and is secreted either by the esophageal epithelium or the stomochord. Chondroid tissue, on the other hand, always, probably, contains nests of cells and is usually the product, according to Spengel, directly or indirectly, of coelomic epithelium. Moreover, skeletal tissue proper usually has a rather denser appearance.

However, in such a section there is no morphological criterion for distinguishing absolutely, the one kind from the other. The stomochordal sheath is very thick here and the substance of it is identical with that of the skeletal body with which it is directly continuous so far as can be detected. In it, it will be observed, are numerous spaces containing clusters of cells (Fig. 4.5 D), but such spaces and cell clusters occur also, rarely to be sure, in the skeletal body itself. The body is undoubtedly, here, secreted by the ventral wall of the stomochord. The stomochordal sheath might be, so far at least as its outermost strata are concerned, secreted by either coelom or stomochord. As a matter of fact, I have no doubt that it is produced from both sources.

Collar nerve cord: With reference to the medullary canal *Balanoglossus occidentalis* occupies a mid-position between species like *Glossobalanus hedleyi* Hill, 1897,

Balanoglossus carnosus Willey, 1899. In which the lumen is uninterrupted from end to end, and those of which *Glossobalanus minutus* Kowalevsky, 1866, or still better *Balanoglossus biminiensis* Willey, 1899 are types where it is broken up into fragments and wholly obliterated for longer or shorter intervals.

The anterior neuropore is broad and narrow, the cord here being much depressed (Fig. 4.5 G). Toward the middle, however, its dorsoventral diameter increases while its transverse decreases until beyond the middle it becomes deeper than broad (Fig. 4.5 H & I). The lumen here is very irregular. It may be quite simple and large, though with a ragged outline from what appears to be a coagulum to its walls here and there; or in other parts again, still farther back, it may be almost completely divided into two lateral lumens by partitions reaching into it both dorsally and ventrally, the ventral one being most prominent (Fig. 4.5 H). In other places again one finds indications of division of each of these lateral lumens into two or more secondary ones (Fig. 4.5 I). Usually, though not everywhere, the lumen is limited by a distinct cuticulum on the inner surface of the cellular layer. The dorsal wall of the cord may be nearly as thick as the ventral, and the fiber layer, as in other species of this genus, extends entirely around. Throughout its length the cellular portion of the dorsal wall may contain a large quantity of a coarse, granular, yellow substance, not apparently in the cells but rather displacing them. Whether this is due to degeneration or not, I am unable to say. Many deeply staining cells, secretary cells, probably, are also found, more particularly, though not exclusively in the dorsal wall toward the anterior end. The description of the cord here given is as I find it in a large specimen from San Pedro. These fibers are interested dorsally into the basement membrane enveloping the cord and ventrally into the esophageal wall so that their contraction might pull the edges of the cord

ventral and thus produce the concavity of the ventral surface found in some specimens. This muscle gradually increases in volume in this specimen as we go farther back, and finally merges into the subneural, perihaemal muscles, which are very large, and reach around unusually far onto the lateral and dorsal side of the cord (Fig. 4.5 G).

In but one individual have I found this lateral depressor muscle of the nerve cord, as it may be called reaching such a development; and correspondingly, in but this one I have found the cord so flattened down dorsoventrally. The muscle does, however, exist in some other specimens, in others again it seems to be entirely wanting. There is nothing quite comparable to this relation of the cord and muscle in any other species, so far as I can make out, though *Balanoglossus clavigerus* Delle Chiaje, 1829 probably comes nearer to it than any other compare. Spengel, and Hill 1897, states that the cord of the *Glossobalanus hedleyi* Hill, 1897 is "dorsoventrally flattened and band-like in shape, convex above and concave in its mid-region below". His figures, however, do not indicate such a relation between the cord and muscles in that species. The same author, '94, says of *Balanoglossus australiensis* that the "collar nerve cord varies in shape in transverse sections in different individuals and in different parts of the same individual, from band-shape to almost circular". His figures also show that what are probably muscle fibers extend around the cord in this species: So, the interesting question arises here also of whether or not the shape of the cord is subject to change through muscular action. What purpose there can be in such an arrangement it is difficult to conceive. It may be not primarily to change the shape of the nerve cord but perhaps the nerve cord acts as origin for these fibers as a part of the great muscular system of the collar, and that it is only incidentally that the cord is changed in form when the muscle contracts.

The number of dorsal nerve roots is variable in this as in so many other species. The maximum number observed thus far is four; the minimum, one. As is usual also, they vary in size and direction as well. Some run out at nearly a right angle from the cord, while others form a very acute angle with it, and some of them arise to one side or the other of the median line of the cord. Fig. 5 F shows the roots in a specimen in which the single one is present. The following points concerning it are of interest: Its large size; the considerable thickness of the fibrous layer extending over its whole surface; and the presence of a cavity within it. The cavity is confined to the distal end of the root and extends through something less than half its length. It does not communicate with the central cavity of the cord as is the case in *Glossobalanus sarniensis* Köehler, 1886 and some other species. The peculiar bunch of irregular granules in which the root terminates (Fig. 4.5 F) is very sharply set off from both the root itself on the one hand, and the overlying ectoderm on the other. The granules, or bodies of which it is in the main composed, are variable in size, irregular in form, though generally approaching globular, mainly homogeneous in structure and readily stainable with hematoxylin. They are probably of the same nature as the material constituting the body described by Willey 1894, p. 271, as terminating the single dorsal root in, *Spengelia porosa* Willey, 1898, and regarded by him as mucoid substance. This terminal knob itself appears to be rather a foreign body thrust into the collar ectoderm, than any constituent part of it. The long ectodermal cells are crowded off to each side of its outer convex surface where they come in contact with it. Attention may be profitably called to the termination of the axial cavity of this root beneath the end knob. The cavity is rather wider here than at any other point; so that we may regard the terminal knob as the distal thickened wall of a terminal vesicle, thus making another point of resemblance between

this and the single root of *Spengelia porosa* Willey, 1898. The layer of "Punctsubstanc" of the root is obviously directly continuous over into the corresponding layer of the collar ectoderm (Fig. 4.5 F). Spengel describes a similar continuity in *Glossobalanus sarniensis* Köehler, 1886, and probably this is the rule.

4.6 Comparison of the Puget Sound, WA paratype to Ritter's San Pedro, CA holotype

Ritter speculated that the *Balanoglossus* in Puget Sound, WA was the same as that found in San Pedro, CA, and so we collected specimens from this northern known location of its range and sectioned it as a paratype for comparison with Ritter's original material, prepared in 1899, and text (provided above). The paratype was prepared for histology and sectioned in 2019. The two specimens appear to be the same though some differences were noted between them, which we will summarise here.

The paratype specimen had a total length of 21.1 mm, much shorter than the 500 mm holotype specimen. This size difference can be explained by a difference in maturity, the new material being of smaller, less mature worms. The main differences between the paratype and Ritter's material were in the proboscis anatomy. The holotype's longitudinal muscles filling the proboscis coelom were shorter, thicker and arranged in well-defined radial plates, compared to those of the paratype that numbered near to 50 and tended to take a long thin shape (Fig. 4.2 A). In the holotype, the ectoderm of the proboscis was twice the size of the proboscis ectoderm of the paratype, and the holotype's elongated pits were not as defined in the paratype specimen (Fig. 4.2 A & 4.4 A & B). The general view of paratype proboscis complex (stomochord, heart, and glomerulus) had a smooth rounded appearance, while that of the holotype had a sharp, longitudinal appearance (Fig. 4.2 B &

C). The holotype proboscis pore and blind pouches of the stomochord were wider and well-formed in contrast to the paratype (Fig. 4.2 G). The paratype proboscis skeletal keel was smaller and lacked the sharp ventral keel of the holotype (Fig. 4.2 G). All other proboscis characteristics were identical in the holotype and the paratype.

The collar of the paratype was identical to the holotype with one notable exception; its nerve root was well formed and ran longer through the collar, whereas the holotype root appeared intermittently (Fig. 4.2 E). Also, the collar longitudinal muscles were less well developed in the paratype (Fig. 4.2 D). The trunk regions were comparable and showed no notable differences. The few differences that we did find are most probably due to differences in size and sexual maturity,

4.7 Description of Micro-CT scanned specimen (cybertype).

A third whole specimen that was collected at the same time and location as the paratype was prepared as a cybertype using micro-CT scanning. This procedure was done to determine the taxonomic utility of CT scans for acorn worms. The following text then, is not to determine the differences from the holotype and paratype, but to provide details of what morphological details are observable with current CT-scan technology.

The cybertype total length was 21.3 mm, with a proboscis 3.5 mm in length, and a collar a little more than half the length of the proboscis at 2.2 mm (Fig. 4.6). The pharyngeal region was 5 mm long and the gonads 6.5 mm long (Fig. 4.6 C). The pharyngeal region immediately followed the collar, whereas the gonads began 0.4 mm posterior to the collar (Fig. 4.6 C). Hepatic sacculations are on a 6.8 mm long portion of trunk and the post-hepatic region was 4 mm (Fig. 4.6 C). Like the paratype, in life, the proboscis was creamy

white, the collar an orangish tan, the anterior trunk a light tan, the hepatic sacculation brown but the posterior ones teal, with the trunk supporting the sacculation following the same pattern, and the post-hepatic trunk was a transparent tan (Fig 4.6 B).

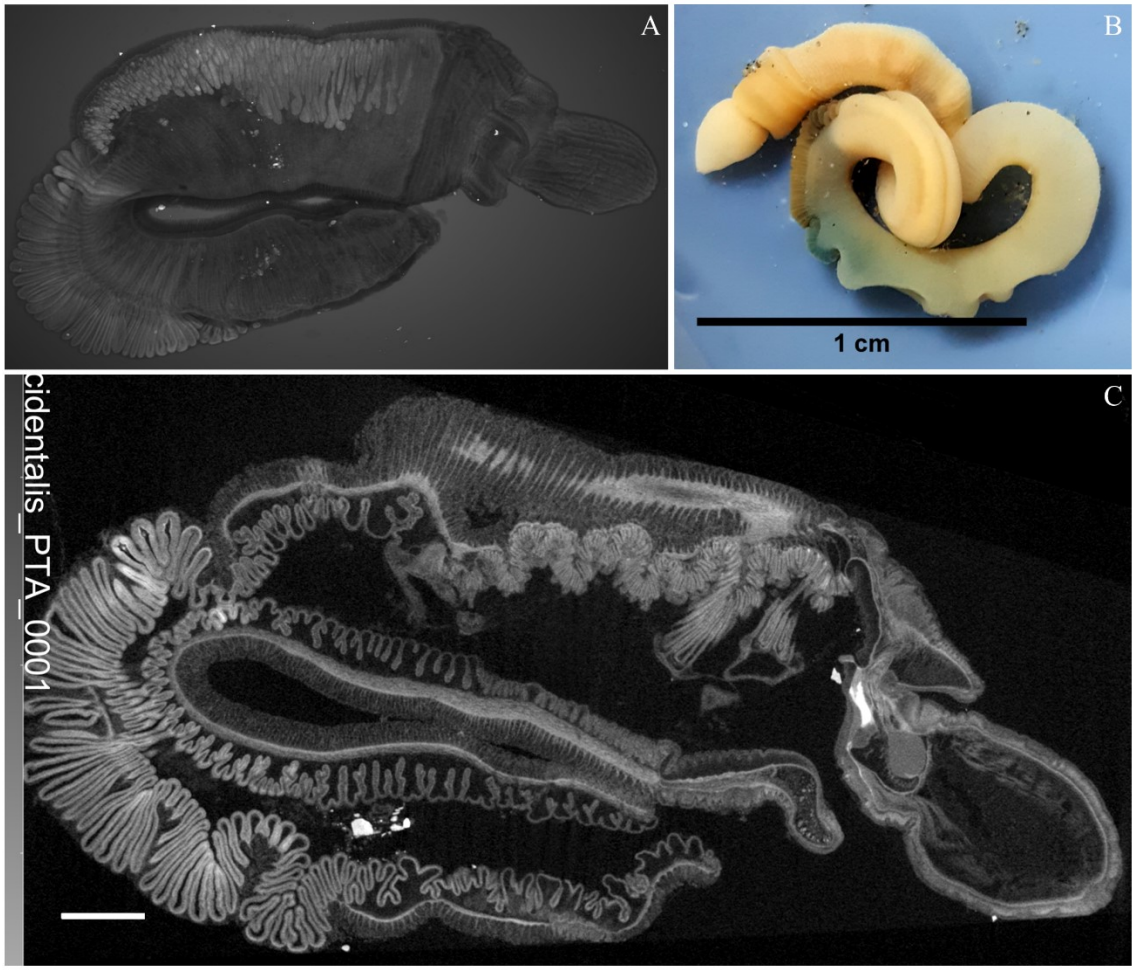

Figure 4.6. *Balanoglossus occidentalis.* A. 3D reconstruction of the cyber type by X-ray micro-CT scan; B. live specimen showing the coloration of the species; C. X-ray tomogram of a sagittal section through the midline of the cybertype. Scale in C = 1 mm.

The proboscis was most similar to the Ritter holotype, with the development of a deep network of mostly longitudinal pits and grooves in the epidermis. Inside the proboscis, the longitudinal muscles were arranged in radial bundles (Fig. 4.7 A). The coelom extended to the tip of the proboscis, and circular muscles were absent. The thin nerve fiber layer and the basement membrane of the epidermis were of similar thickness (Fig. 4.7 A). Dorsal septum was present and reached the proboscis wall. Posteriorly this septum disappeared as

a fold in the proboscis contacts the cardiac vesicle (Fig. 4.7 A). The ventral septum did not extend the full length of the stomochord and reached the proboscis wall only where the dorsal fold of the proboscis contacts the cardiac vesicle (Fig. 4.7 A). The glomerulus is paired and well developed. The heart and glomerulus are bigger on the left side of the protocoelom (Fig. 4.7 A & 4.8). The stomochord is conical with an upward curvature at the tip, a small lumen that extends to the tip and a single dorsolateral outgrowth on the right side (Fig. 4.7 A, 7 B, 8 B, 8 C & 8 D). Two small blind pouches were located ventrally behind the outgrowth (Fig. 4.7 B). In the neck of the proboscis, the stomochord was reduced to a rod sitting on top of the skeleton (Fig. 4.7 B). Only the left proboscis pore was present, and it was mediodorsal in position (Fig. 4.7 B). The skeleton meets the stomochord anteriorly as a circular, vertical plate where it is continuous with the anterior basal lamina (Fig. 4.8 E). In the neck, it is hourglass shaped, and posteriorly it extends in two cornua at a right angle. The proboscis skeleton keel was prominent in the region of the dorsal buccal cavity (Fig. 4.7 C). The cornua reached the middle of the collar (Fig. 4.8 A).

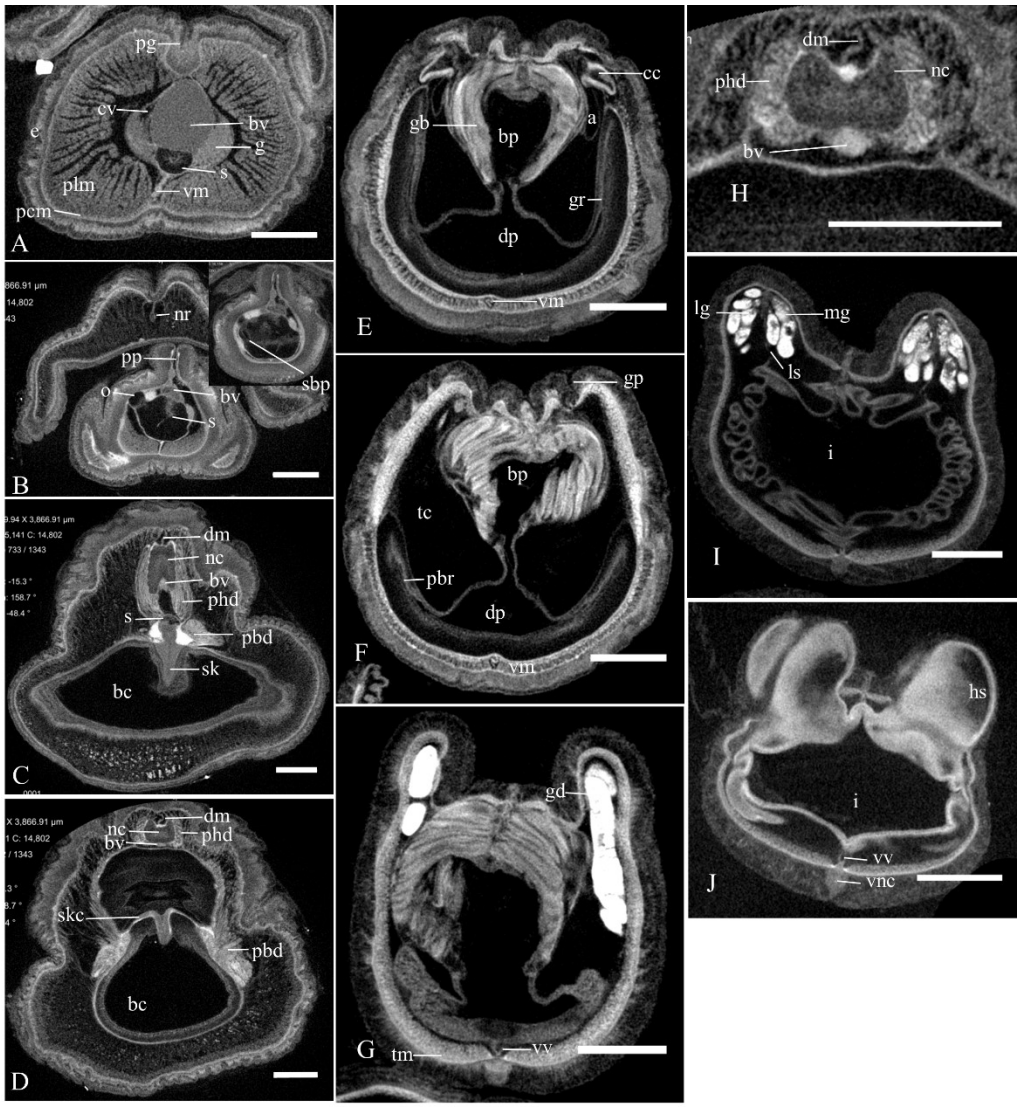

Figure 4.7. X-ray tomograms of *Balanoglossus occidentalis* cybertype. A. Proboscis with longitudinal and circular muscles, heart-glomerulus complex and ventral mesentery; B. Proboscis neck showing the stomochord outgrowth and blind pouch, the proboscis pore and the first nerve root; C. Anterior collar with skeleton keel and the beginning of the left peribuccal diverticulum; D. Mid-collar region showing the division of the skeleton cornua; E. Posterior collar showing collar canals and lateral groves of the digestive track; F. Junction between collar and trunk regions showing a gill pore; G. Pharyngeal region with a single row of gonads on each side; H. Zoom on the dorsal nerve chord complex of D; I. Post pharyngeal genital region with two rows of gonads on each side; J. Hepatic region with a single row of sacculation on each side; All scale bars = 0.5 mm; **Abbreviations**: **a**, atrium; **bc**, buccal cavity; **bp**, branchial pharynx; **bv**, blood vessel; **cc**, collar canal; **cv**, cardiac vesicle; **dm**, dorsal mesentery; **dp**, digestive pharynx; **g**, glomerulus; **gb**, gill bars; **gd**, gonad; **gp**, gill pores; **gr**, lateral groove; **hs**, hepatic sacculation; **i**, intestine; **lg**, lateral gonad; **ls**, lateral septum; **mg**, medial gonad; **nc**, nerve chord; **nr**, nerve root; **o**, stomochord outgrowth; **pbd**, peribuccal diverticulum; **pbr**, parabranchial ridge; **pg**, proboscis groove; **phd**, perihaemal diverticulum; **pcm**, proboscis circular muscle; **plm**, proboscis longitudinal muscle; **pp**, proboscis pore; **s**, stomochord; **sbp**, stomochord blind pouch; **sk**, skeleton keel; **skc**. Skeleton cornua; **tc**, trunk coelom; **tm**, trunk muscle; **vm**, ventral mesentery; **vnc**, ventral nerve chord; **vv**, ventral vessel.

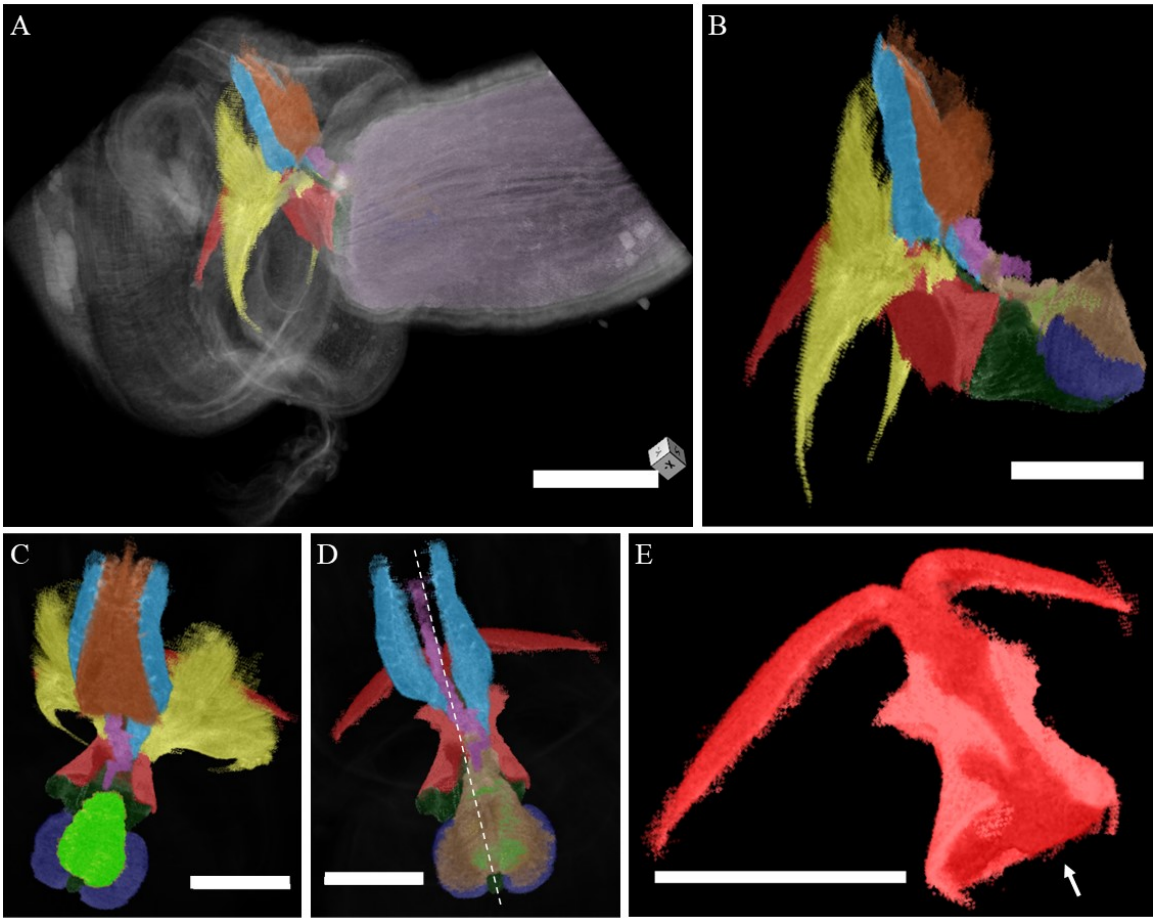

Figure 4.8. 3D reconstruction of X-ray micro-CT scans of *Balanoglossus occidentalis*. A. sideview of collar and posterior proboscis with transparent body wall and highlighted organs. The skeleton cornua reaches the mid-collar; B. sideview of proboscis skeleton, stomochord, heart-glomerulus complex, neural chord, perihaemal diverticulum and peribuccal diverticulum; C. dorsal view of the same organs without the pericardiac vesicle. Note the heart and glomerulus are bigger on the animal's left side, the single outgrowth of the stomochord is on its right and only the left perihaemal diverticulum follows the blood vessel into the proboscis neck; D. dorsal view of the same organs as B without peribuccal diverticulum and neural chord. Note how the heart, the blood vessel and the perihaemal diverticulum are skewed to the left side of the animal midline (dashed line); E. isolated proboscis skeleton. Note the flat surface where it meets the stomochord (arrow); Orange, neural chord; Light blue, Perihemal diverticulum; Dark blue, glomerulus; Yellow, peribucal diverticulum; Light green, hearth; Red, proboscis Skeleton; Dark Green, stomochord; Beige, cardiac vesicle; Violet, blood vessel

The dorsal septum of the collar began at the level of the proboscis pore and the stomochord outgrowth (Fig. 4.7 B). There, it links the first nerve root with the dorsal wall of the collar. Posteriorly, it is complete. A total of four nerve roots were found. The nerve cord lacked a lumen or lacunae (Fig. 4.7 C & H). The neuropore, neural lumen or lacunae were not

observed in the CT-scanned specimen. The left perihaemal diverticulum extended into the proboscis neck (Fig. 4.8 C & D). A ventral septum was present behind the tips of the skeletal cornua (Fig. 4.7 E). The gills start a little posterior to that point (Fig. 4.7 E & F). Collar canals were well developed (Fig. 4.7 E).

The digestive portion of the buccal cavity has a pair of long, flat parabranchial ridges separating the dorsal (or branchial) chamber from the ventral (or digestive) tube (Fig. 4.7 F). These should not be confused with the peribranchial chamber in Ritter's holotype text, which described the space enveloped between the mature gonadal wings, dorsal and external to the animal. Posteriorly, the parabranchial ridges are shorter where the gonads begin, and the digestive part occupies the ventral third of the pharynx (Fig. 4.7 G). The branchial pharynx occupies the remaining dorsal two thirds. Gonads start at the 9th gill bar. Gonads are in a single, dorsal row on each side in the pharyngeal region (Fig. 4.7 G). Lateral septa appear at the last gill bar. Posterior to the gill bars, two rows of gonads are located to each side (Fig. 4.7 I). The gonads form small genital wings anteriorly that enlarge posteriorly (Fig. 4.7 G & I). The post-pharyngeal gut is highly plicate (Fig. 4.7 I). The hepatic sacs are in a single row on each side and of the same size throughout the hepatic region (Fig. 4.7 J).

4.8 Remarks

We compared some structures of *Balanoglossus occidentalis* to the other three *Balanoglossus* species that have been collected from the same water (found throughout the Western Pacific). In *Balanoglossus occidentalis* the proboscis in a medium state of

distention is a little longer than the collar, in contrast to *Balanoglossus carnosus* Willey, 1899, in which the collar has an enormous size of 17.5 mm long and the proboscis length is 6 mm (Willey, 1899). Longitudinal muscle fibres are present in the proboscis with absent circular muscle, in contrast to *Balanoglossus misakiensis* Kuwano, 1902 that has a circular muscle in the proboscis and in the anal region (Kuwano, 1902). The pericardium does not arise into two horns as in *Balanoglossus misakiensis* Kuwano, 1902. In *Balanoglossus occidentalis* the stomochord is of the thick-walled and small lumened type, while in *Balanoglossus carnosus* Willey, 1899 there are both dorso-lateral and ventro-lateral subdivisions of the stomochord lumen, and the stomochord ends bluntly in front and disappears (Willey, 1899). What is also unique in *Balanoglossus occidentalis* is the glomerulus format, that not only spreads widely over the surface of the pericardium, but also reaches down over the lateral and ventral portions of the stomochord extensively. In no other species of the genus is this format observed. In *Balanoglossus occidentalis* the digestive portion of the trunk is smaller than the branchial portion (one third to two thirds, respectively), in contrast to *Balanoglossus misakiensis* Kuwano, 1902 where both parts have the same size (Kuwano, 1902). The genital wings in *Balanoglossus occidentalis* seldom stand out in a horizontal position, as they do in some other species. They also appear never to wrap over each other at their free edges to produce a temporary peribranchial chamber, as, for example, Willey has described them as doing in *Balanoglossus carnosus* Willey, 1899. The genital wings in *Balanoglossus occidentalis* are positioned little short of upright, it is considered that their congestion in sexually mature specimens almost wholly efface the inter wings channel, so that the branchial region can hardly be seen without pushing the wings apart. In *Balanoglossus occidentalis* the wings terminate

posteriorly almost as abruptly as they do in *Balanoglossus carnosus* Willey, 1899. There is not, however, as in that species, an interval between their termination and the beginning of the hepatic region. The two regions always overlay somewhat. The gonads of *Balanoglossus occidentalis* are in a good developmental situation, in contrast to *Balanoglossus proterogonius* Belichov, 1928 (Vserossijskij & Bjalynickij-Birulja, 1928).

4.9 The efficacy of CT-scans in Enteropneusta taxonomy

Morphological and anatomical studies based on histology have been at the heart of taxonomy for over two centuries, and can provide us with specific and wealthy details on the body organisation of species. However, histological techniques have several disadvantages: They are costly, the type specimens are destroyed, and they require specialized training and substantial time and effort to generate a serially sectioned and stained specimen. Fixed specimens with sediment in the gut, or coiled, or in a state of deterioration, as is often the case with acorn worms, may be collected by non-specialists, who render the material unusable for serial sectioning. Acorn worms must be allowed to evacuate their guts before preservation (see Materials and Methods in Deland et al. 2010 for details). Finally, histological sections are prone to artifacts from microtome sectioning, staining, and mounting. Most of these disadvantages can be overcome with CT-scan technology.

Computer tomography scans have the advantages of : not destroying valuable whole holotype specimens; the preparation of material is limited to a short staining proces; and it creates a virtual cybertype that can form an accessible database. In our study, the specimen was submerged in stain for three days and then was ready to scan. Each scan

then took three hours. Getting pictures of cross sections from the 3D model took an afternoon of work on the Dragonfly program from ORS, including learning how to work with the program. The most time intensive step was to colour the different organs to highlight their respective organisation in 3D which took two days (Fig. 4.8). This is a truncated time period compared to the histology, which including fixation, sectioning, staining and photography, took four weeks.

Despite these advantages, micro-CT scans cannot totally replace traditional acorn worm histological methods because the monochromatic images do not provide the contrast of histological stains. We chose a small cybertype specimen to reduce scan time to maximize resolution. Still, a quick scan at low resolution was first done to locate taxonomically informative regions for higher resolution scans. Even at high resolution, nuclei, vacuoles, fibres and cell membranes were not seen. Lacking these subcellular details, different cell types were difficult or impossible to identify. Distinct tissue layers, and the boundaries between them were not always apparent. In some cases, gross morphological structures including gill bar synaptaculae were not captured. In our case, both histology and taxonomic training were required to scan and interpret the anatomy of *B. occidentalis.* The main advantage was that the 3D scan provided a general internal and external view of the specimen, and sufficient anatomical details to identify it to genus level.

Key characteristics of the genus *Balanoglossus* were captured in the cybertype and include nerve roots in the collar region, the hepatic sacs, and well developed genital wings with lateral septa. Some species specific characters of the cybertype include the proboscis longitudinal muscle bundles, the left proboscis pore, the well-developed ventral mesentery of the proboscis, the dorsal nerve cord of the collar lacking a lumen, the

stomochord with a thick wall and narrow lumen, a well-developed heart, blood vessel, and glomerulus (Fig. 4.2 & 4.7). The outcome of this experiment is that micro-CT scans are not suitable for the formal taxonomic treatment of acorn worm species, but are an excellent tool to provide a quick identification of known species. A CT-scanned specimen, when combined with geographical range data, is an excellent method for non-specialists to quickly and economically determine their local acorn worm biodiversity.

4.10 Acknowledgments

Thanks to The Integrated Quantitative Biology Initiative (IQBI) funded by the Canadian Foundation of Innovation (CFI) project 33122 for their Zeiss Xradia Versa 520 and to Dr. Rui Tahara. Thanks to the Object Research Systems which provided us with a free of charge licence of the Dragonfly software for non-commercial use. This work was supported by a NSERC Discovery grant to CBC.

4.11 data availability

The micro-CT scan files used to create the 3D cybertype with Dragonfly from ORS is available at: https://doi.org/10.5281/zenodo.5103093.

5 Conclusion Générale

5.1 Motivation et questions principales

La motivation première de ma thèse était de faire avancer nos connaissances sur la biominéralisation chez les hémichordés, son évolution et son implication dans l'évolution des deutérostomes. Hemichordata est un embranchement regroupant 140 espèces (Cameron, 2016) d'invertébrés marins retrouvés sur toutes les latitudes et à toutes les profondeurs. Ce groupe est souvent considéré comme étant celui qui ressemble le plus à l'ancêtre commun des deutérostomes, étant donné qu'il partage des caractéristiques avec les chordés et les échinodermes, comme décrit dans le chapitre 1. De plus, les entéropneustes ont peu changé morphologiquement depuis 505 millions d'années (Cameron, 2018). Hemichordata est donc un groupe clé pour comprendre l'évolution de deux groupes d'animaux très distincts et diversifiés soit les échinodermes et les chordés. Ce groupe reçoit d'ailleurs beaucoup d'attention des chercheurs en biologie développementale, mais certains aspects de sa biologie sont négligés (Cameron, 2002; Lowe *et al.*, 2004; Miyamoto & Saito, 2007; Cameron & Perez, 2012; Kaul-Strehlow & Stach, 2013; Miyamoto & Wada, 2013; Cameron, 2018). Depuis la découverte d'osselets chez deux espèces d'entéropneustes par Cameron & Bishop (2012), aucune nouvelle recherche n'a été menée sur ce sujet. Je me suis alors donné pour but de répondre à plusieurs questions concernant ce phénomène. Est-ce un phénomène répandu chez les entéropneustes? À quoi ressemble les osselets chez d'autres espèces? La forme varie-t-elle au sein d'une même espèce? Sont-ils tous fait de la même matière? Quand et comment se développent-ils? À quoi peuvent-ils servir?

J'ai également mené à terme une étude qui fut commencée comme projet Honnors par Xavier Guilbeault-Mayers (deuxième auteur de l'article du chapitre 3). Les données de

cette étude stagnaient depuis 2015 et étaient loin d'être publiées. Mener à terme ce projet m'a permis d'étudier un autre tissu dur et extracellulaire des hémichordés, et le principal trait partagé entre les hémichordés et les chordés, les branchies. Ce trait serait peut-être même ancestral aux bilatériens si les deutérostomes s'avèrent être paraphylétique (Kapli *et al.*, 2021). Chez les hémichordés et les céphalocordés, les branchies sont très nombreuses et on assume qu'elles sont symétriques à l'âge adulte. Toutefois, aucune recherche n'a réellement quantifié leur symétrie au sein d'une population. Comme plusieurs asymétries sont présentes dans les branchies des deutérostomes, notamment, chez les échinodermes fossiles et les céphalocordés larvaires, ce projet avait pour but de répondre aux questions suivantes : Les branchies sont-elles vraiment symétriques chez les hémichordés et les céphalocordés adultes? Les branchies étaient-elles symétriques chez l'ancêtre commun des deutérostomes? Quel était le rôle original des branchies? Reste-il une trace de l'asymétrie larvaire chez les céphalocordés adultes?

5.2 Ce que l'on sait maintenant sur la biominéralisation des hémichordés

Grâce à mes récentes recherches, je peux affirmer que la formation d'osselets de carbonate de calcium est un phénomène répandu chez les entéropneustes. En effet, j'ai trouvé des osselets chez toutes les espèces d'entéropneuste que j'ai étudiées. On connait maintenant les osselets de 10 espèces d'entéropneuste réparties parmi trois des quatre familles. Ceci suggère que la biominéralisation est un trait ancestral chez ce groupe. Toutefois, on ne sait pas encore si les membres de l'autre classe d'hémichordé, Pterobranchia, ont des osselets, et, s'ils n'en ont pas, est-ce une perte ou est-ce que l'origine de la biominéralisation s'est fait après la divergence des deux classes?

Ces osselets sont tous de taille relativement semblable, soit de 5 à 30 microns, et certaines formes sont partagées parmi les espèces. Les osselets sont bilobés avec une symétrie axiale chez sept espèces. Chez deux autres, ils sont organisés autour d'un axe central sans être bilobés. Chez la dernière espèce avec des osselets connus, ceux-ci sont sphériques. En plaçant les osselets sur les arbres phylogénétique les plus récents, il apparait que la forme bilobée soit l'état ancestral (Fig. 2.4). Au sein de la famille Harrimaniidae la taille des trabécules est aussi caractéristique des genres et les genres plus apparentés ont des osselets plus semblables. De plus, au sein de cette famille, la forme dite « en brocoli » est caractéristique du genre *Saccoglossus*. On connait les osselets d'un seul membre de la famille Spengelidae, *Schizocardium californicum*. Chez ce dernier les osselets sont globuleux avec des excroissances polyédriques qu'on ne retrouve chez aucune autre espèce. Pour les Ptychoderidae, il semble que les osselets globuleux, sphériques ou bilobés, soient ancestraux et que les formes uniques trouvées chez les membres du genre *Balanoglossus* soient des états dérivés.

Tous les osselets d'hémichordés sont faits de carbonate de calcium. Selon les espèces, le carbonate de calcium est sous forme de calcite, d'aragonite ou de vatérite. Le polymorphe le plus fréquent est la calcite retrouvée chez cinq espèces. L'aragonite est présente chez trois espèces et la vatérite chez une seule. Il est donc plus parcimonieux de considérer que la calcite représente l'état ancestral des osselets. Ceci est d'autant plus intéressant que les osselets d'échinodermes sont toujours faits de calcite.

La biominéralisation semble être, en effet, un phénomène répandu chez les entéropneustes. Les formes des osselets sont variées bien que la forme bilobée soit la plus fréquente et la taille très semblable. Plusieurs formes peuvent être présente dans une même espèce. Chez

toutes les espèces, les osselets possèdent une certaine porosité, sauf *Harrimania planktophilus*. Cette porosité peut être très réduite comme chez *Glossobalanus berkeleyi* ou être un réseau de cavités très semblable au stéréome des échinodermes comme chez *Saccoglossus*, *Balanoglossus aurantiacus* et *Schizocardium californicum*. Tous les osselets sont faits de carbonate de calcium, mais de polymorphe différents selon les espèces. On peut donc déduire que les osselets des entéropneustes ancestraux était globuleux, bilobés, isolés, faits de carbonate de calcium et poreux. Les questions du développement et de la fonction restent en suspens.

5.3 Ce qui n'a pas pu être déterminé

Plusieurs expériences ont été faites, mais ont dû être exclues des articles parce que leurs résultats étaient négatifs et non-publiables. Ces expériences devaient être tentées, car elles auraient pu élucider plusieurs questions sur les osselets des hémichordés. Bien que ces expériences aient donné des résultats négatifs, il sera pertinent de les réexplorer quand des solutions aux problèmes techniques auront été trouvées.

5.3.1 Le protéome des osselets

J'ai tenté, par trois fois, d'isoler et de séquencer les protéines qui seraient présentes dans la matrice des osselets d'hémichordés, mais ces expériences n'ont pas pu mettre de protéines matricielles en évidence. La pertinence de ces expériences vient du fait que des gènes homologues à des gènes biominéralisateurs d'échinodermes sont présents dans le génome de *Saccoglossus kowalevskii*, mais nous ne savons rien de leur expression chez ce

dernier. Si ces protéines étaient présentes dans les osselets d'hémichordés, comme elles le sont chez les échinodermes, l'homologie entre les deux serait prouvée au-delà du doute raisonnable. Il est donc très important d'explorer cette hypothèse. Toutefois, les trois tentatives n'ont rien donné de concluant.

Pour tenter de mettre en évidence la présence de protéines matricielles, j'ai isolé des osselets, les ai déminéralisés puis ai fait séquencer la matière résiduelle. La méthode et les résultats détaillés sont disponible à l'annexe B. Les trois séquençages n'ont pas été conclusifs. Seuls quelques peptides ont été identifiés et aucun qui ne correspondait, ne serait-ce qu'un peu, avec une protéine liée à la biominéralisation. Le génome utilisé pour identifier ces peptides est le génome complet de *Saccoglossus kowalevskii* (Skow_1.1, représentation complète, ~1,6 Gb), l'espèce utilisée pour isoler les protéines. Si des protéines matricielles sont en effet présentes, le problème vient de la méthode d'isolation et du faible nombre de peptide séquencés, mais pas du génome de référence. Je me suis basé sur l'étude des protéines du squelette d'oursin par Mann *et al.* (2008), mais les osselets d'oursin sont beaucoup plus gros et faciles à acquérir que ceux d'hémichordés. J'ai donc augmenté le nombre de vers à chaque nouvelle tentative afin d'avoir une plus grande masse de protéines et ainsi plus de chance de les séquencer, mais les résultats sont restés non concluants.

De ces résultats, deux conclusions sont possibles : soit il n'y a pas de matrice protéique dans les osselets, soit la méthode d'isolation est trop agressive chimiquement et détruit la matrice protéique. Nous ne pouvons pas encore trancher entre les deux et, jusqu'à ce qu'une méthode d'isolation d'osselets n'utilisant pas de produit violent, tel l'eau de javel utilisé ici, cette piste doit être mise sur pause.

5.3.2 La fonction des osselets

Plusieurs expériences d'immunohistochimie ont été faites pour tenter de mettre en évidence la présence de cils, de nerfs ou de fibres musculaires autour des osselets. Toutes ces expériences ont donné des résultats négatifs et non probants, donc ils ne sont pas présentés ici. Le problème principal de ces expériences est que les osselets ne sont pas visibles au microscope tant que les cellules autour ne sont pas digérées. De fait, il est impossible de caractériser leur entourage avec précision. De plus, les tissus d'entéropneuste font beaucoup d'auto-fluorescence, donc discerner le bruit d'une vraie structure s'avère d'autant plus difficile. Les résultats préliminaires ne montrent aucun cil, nerf ou muscle particulier près des protubérances dermiques où les osselets sont censés être formés. Cela démontrerait que les osselets n'ont probablement pas de fonction sensorielle ou locomotrice. Cependant, les problèmes mentionnés plus haut rendent les résultats non-probant et les conclusions impossibles. Ces expériences ont donc dû être exclues.

Pour tenter de résoudre ces problèmes, j'ai fait appel à un laboratoire muni d'un Scanner aux rayons-X afin d'obtenir une reconstruction virtuelle en 3D d'un ver (X-ray Micro-CT scan). En utilisant une teinture non acide je pensais arriver à voir les osselets dans un animal entier ainsi que leur orientation. L'importance d'une teinture non acide est que les osselets de carbonate de calcium se dissolvent dans les solutions acides. Il s'avère que la résolution atteignable avec cette machine n'a pas suffi pas à identifier les osselets de cette façon. Même en prélevant un carré d'épiderme de seulement 2 mm de côté pour optimiser la résolution maximale, elle reste insuffisante. Il faut donc mettre cette piste de recherche sur pause également.

Lorsque les progrès technologiques permettront de voir les osselets dans un spécimen entier, ou presque, nous pourrons alors envisager de reprendre cette voie de recherche. Par exemple en utilisant des anticorps contre les cils, les nerfs ou les muscles, liés à un agent de contraste pour caractériser efficacement l'entourage des osselets et élucider leur(s) fonction(s).

Même si la résolution ne permet pas de voir les osselets dans les vers, on voit très bien la majorité de leurs caractéristiques morphologiques. Nous avons donc décidé, avec Christopher B. Cameron et Noura Jabr, de rentabiliser ces expériences et ces données en testant la viabilité de cette technique en taxonomie des entéropneustes. Cette piste a mené à l'élaboration du chapitre 4.

5.3.3 Le développement précoce des osselets de *Saccoglossus kowalevskii*

J'ai acquis et cultivé des embryons de *Saccoglossus kowalevskii* afin de découvrir à quel âge les osselets apparaissent, s'ils ressemblent déjà à ceux des adultes et comment ils se développent. La méthode d'acquisition et de culture est décrite à la section 2.3.

Saccoglossus kowalevskii est une espèce idéale pour étudier le développement des osselets pour plusieurs raisons. Premièrement, elle est très facile à acquérir en grande quantité et à reproduire. Deuxièmement, c'est une espèce modèle dont les embryons sont très étudiés déjà. Troisièmement, elle possède deux types d'osselets distincts qui semblent être simplement deux stades de développement. Cette dernière caractéristique n'est retrouvée chez aucun autre genre jusqu'à présent et demande plus d'études.

Lors des deux essais de culture, mes embryons ont atteint le stade maximal de trois fentes branchiales et de six fentes branchiales, respectivement. N'ayant pas trouvé d'ossicule lors de la première culture, j'ai laissé la seconde vieillir beaucoup plus avant d'en tester la présence. Même dans ces vers plus vieux, aucun osselet ne fut trouvé. L'absence d'osselets à ces stades suggère toutefois qu'ils se développent plus tard. Pour savoir avec précision quand apparaissent les osselets il faudra répéter cette expérience et laisser les vers devenir encore plus vieux, mais le temps requis pour élever une telle culture m'empêche de répéter cette expérience dans le cadre de mes études doctorales.

5.4 L'origine de la biominéralisation des ambulacraires

Les premiers osselets d'hémichordés qui furent analysés pour leur composition chimique étaient fait d'aragonite (Cameron & Bishop, 2012), mais on sait maintenant que la plupart sont formés de calcite. Comme le squelette des échinodermes est toujours fait de calcite à haute teneur en Mg, il semblait peu probable qu'il soit homologue à un squelette d'aragonite. Ce point a été soulevé comme un fait prouvant l'absence d'homologie entre les deux biominéraux (Zamora & Rahman, 2014). Cependant, il semble que les osselets d'hémichordés soient ancestralements fait de calcite comme chez les échinodermes. Cette similitude renforce l'hypothèse de l'homologie entre les deux structures. Comme une telle variation de polymorphe est absente chez les échinodermes, deux scénarios sont alors possibles. Soit un plus grand contrôle du polymorphe a été acquis chez les échinodermes, soit ce contrôle a été perdu chez les hémichordés.

Morphologiquement, les osselets d'hémichordés semblent être plésiomorphiques par rapport au groupe des ambulacraires. Tel que discuté au chapitre 2.5, les échinodermes ont déjà un squelette très exhaustif et des formes variées durant la mer de calcite du début du cambrien où ils ont supposément acquis leur squelette. Les deux phylums ambulacraires ont divergé durant l'édiacarien, donc si les osselets sont homologues, ils devaient être déjà présents avant la divergence des groupes. Chez cet ancêtre les osselets devaient être petits, simples et variables. Les échinodermes auraient ensuite évolué leur squelette à partir de ces petits osselets.

Les osselets des hémichordés sont poreux ou creux chez toutes les espèces observées sauf *H. planktophilus*. Ces pores ou cavités ne peuvent toutefois pas être appelés des vrais stéréomes bien qu'ils soient semblables. Le vrai stéréome est formé de la fusion de plusieurs osselets en un réseau complexe. Comme nous ne savons pas comment les osselets se développent chez les hémichordés, il n'est pas exclu que leur porosité soit possiblement causée par la fusion de plus petits cristaux, mais nous ne pouvons pas l'affirmer avec certitude. Considérant cela, nous favorisons une hypothèse dans laquelle les osselets du dernier ancêtre commun des ambulacraires avait des osselets microscopiques, simples, isolés, poreux et faits principalement de calcite à faible teneur en magnésium, comme ceux des entéropneustes récents.

5.5 L'origine des branchies des deutérostomes

Les fentes branchiales pharyngiennes sont une synapomorphie des deutérostomes. Elles relient le pharynx au mieux extérieur et sont présente chez les hémichordés, les chordés et

les échinodermes fossiles. L'homologie entre les branchies des trois groupes est bien supportée par la morphologie comparée, le développement moléculaire, la génomique et le registre fossile tel qu'expliqué dans le chapitre 3.2. Chez les céphalocordés et les tuniciers, les branchies servent à l'alimentation par filtration (Ruppert *et al.*, 2000; Bone *et al.*, 2003). Cette fonction fut perdue chez les vertébrés (Baker *et al.*, 2015). Les échinodermes fossiles les plus anciens se nourrissaient aussi par filtration et avaient des branchie (Rahman *et al.*, 2015). Les échinodermes récents n'ont pas de branchie pharyngienne et leurs larves non plus. Chez les hémichordés, la classe Pterobranchia se nourrit de particules en suspension avec ses bras et tentacules et présente des branchies vestigiales ou absentes. La classe Enteropneusta possède encore des branchies, mais ses membres peuvent se nourrir par filtration ou ingérer le substrat directement.

L'asymétrie et le bruit développemental permettent de déterminer que les branchies servaient à l'alimentation par filtration chez l'ancêtre commun des entéropneustes. *Saccoglossus bromophenolossus* démontre un niveau d'asymétrie fluctuante plus élevé et une plus grande quantité d'erreur de développement que *Protoglossus graveolens*. Ces deux espèces vivent de façon sympatrique, sont de taille semblable et sont relativement proches phylogénétiquement. La grande différence entre les deux est que *S. bromophenolossus* est détritivore uniquement et que *P. graveolens* est détritivore et filtreur. On en conclu que les branchies de *S. bromophenolosus* montrent des signes de vestigialité parce qu'ils ont perdu leur fonction ancestrale primaire : l'alimentation par filtration.

Les branchies démontrent une asymétrie fluctuante chez *Branchiostoma floridae* avec un biais probablement hérité de leur stade larvaire. *Branchiostoma floridae* a un faible niveau d'asymétrie fluctuante. La majorité (64%) des individus sont parfaitement symétriques,

mais lorsqu'ils ne le sont pas, il y a plus de branchies du côté gauche dans 77% des cas. Ce biais est probablement lié à l'asymétrie larvaire du développement des branchies. Afin de prouver cette hypothèse, il faudrait faire la même étude de la symétrie chez les autres genres de céphalocordés, puisque l'asymétrie du développement branchial est différente pour chaque genre. Les branchies de *Branchistoma* apparaissent sur le côté droit (Lankester & Willey, 1890; Willey, 1891; Boorman & Shimeld, 2002; Holland & Onai, 2012), celles d'*Asymmetron* apparaissent légèrement à gauche (Holland & Holland, 2010; Igawa *et al*., 2017) et le développement de celles d'*Epigonichtys* est inconnu.

Les branchies de l'ancêtre commun des deutérostomes étaient probablement symétriques et servait à l'alimentation par filtration.Tous les autres états sont dérivés de celui-ci. Les échinodermes ont probablement perdu leurs branchies quand le système ambulacraire est devenu le principal moyen de nutrition comme les ptérobranches qui n'ont plus de branchies et se nourrissent avec des tentacules ciliés.

5.6 Taxonomie traditionnelle et avancés technologiques

Les tests immunohistochimiques que j'ai menés pour étudier les fonctions possibles des osselets ont tous donné des résultats négatifs. Aucune association avec des neurones, des cils ou des fibres musculaires n'a pu être mise en évidence. J'ai également fait un micro-scan tomographique informatisé ou micro-CT-scan d'un entéropneuste pour voir la disposition et l'orientation des osselets in-situ, mais il a été impossible de voir les osselets dans ces scans. Toutefois, grâce à ces scans j'ai pu prouver l'efficacité de cette technique en taxonomie.

La micro-CT-scan aux rayons X est une technique efficace et pratique pour l'étude morphologique des hémichordés, mais ne peut pas remplacer l'histologie traditionnelle complètement. D'un côté, cette nouvelle technique n'endommage pas les spécimens qui peuvent donc être réobservés au fur des avancées technologiques. De plus, la nature numérique des données créées permet de les partager mondialement comme les séquences génomiques et moléculaires le sont déjà. Finalement, elle est beaucoup plus rapide et facile à faire que l'histologie traditionnel. Malheureusement, comme les images obtenues sont monochromatiques, et la résolution inférieure avec les rayons X, l'histologie reste nécessaire pour bien interpréter les résultats. Toutefois, la taxonomie des hémichordés est bien documentée et permet de se passer de l'histologie tant que l'espèce observée ne diffère pas trop des espèces connues (Cameron *et al.*, 2010; Deland *et al.*, 2010; Cameron & Perez, 2012; Cameron & Ostiguy, 2013; Jabr *et al.*, 2018). Pour les spécimens rares ou uniques La micro-CT-scan aux rayons X serait donc une alternative suffisante et préférable aux études histologiques.

5.7 Les hémichordés et l'évolution des deutérostomes

Les hémichordés sont un groupe essentiel pour bien comprendre l'évolution des deutérostomes. Leurs osselets semblent être plésiomorphiques pour les ambulacraires. Le squelette dermique ne serait alors pas une apomorphie des échinodermes. Le stéréome pourrait aussi être retiré de la liste des apomorphies des échinodermes, mais plus d'études sont requises pour l'affirmer. Rechercher les osselets chez les ptérobranches et les Torquaratoridae sera également nécessaire pour comprendre les tendances évolutives des osselets face à une taille corporelle réduite, à la vie colonialle et aux grandes profondeurs.

Certaines études récentes placent les Xenacoelomorpha comme groupe-frère des ambulacraires (Kapli *et al.*, 2021). Si tel est le cas, peut-être y a-t-il un lien évolutif entre les osselets dermiques des ambulacraires et les statolithes des Xenacoelomorpha.

L'étude de la symétrie pharyngienne des hémichordés supporte l'hypothèse selon laquelle les deutérostomes ancestraux étaient symétriques. Un certain débat existe sur l'origine des asymétries des deutérostomes et certains auteurs pensent que le deutérostome ancestral était asymétrique (Sato & Holland, 2008). Par rapport aux fentes pharyngiennes, cela ne semble ne pas être le cas. L'asymétrie des échinodermes fossiles est explicable par une vestigialisation liée à un changement de mode d'alimentation, et celle des céphalocordés semble être une conséquence de leur développement unique. Des études développementales du genre *Epigonichthys* et une quantification de l'asymétrie d'*Epigonichthys* et d'*Asymmetron* pourraient nous aider à comprendre l'origine exacte de ces asymétries.

Les deutérostomes sont un groupe qui reçois beaucoup d'attention, mais il ne faut pas étudier seulement les vertébrés et les oursins. Les hémichordés démontrent bien comment les petits embranchements peuvent nous apprendre beaucoup sur les plus grands et l'importance de s'intéresser à eux. Plusieurs découvertes fondamentales restent à faire, il faut simplement se donner la peine de regarder et ne pas se laisser arrêter parce qu'un sujet n'est pas populaire ou non-commercialisable.

6 références

Addadi, L., & Weiner, S. (1997). Biomineralization: A pavement of pearl. *Nature, 389*(6654), 912-915. https://doi.org/10.1038/40010

Agassiz, A. (1873). The history of *Balanoglossus* and Tornaria. *Memoirs of the American Academy of Arts and Sciences, 9*, 421-436. https://doi.org/10.2307/25058009

Aizenberg, J., Lambert, G., Weiner, S., & Addadi, L. (2002). Factors involved in the formation of amorphous and crystalline calcium carbonate: a study of an ascidian skeleton. *Journal of the American Chemical Society, 124*(1), 32-39. https://doi.org/10.1021/ja016990l

Aizenberg, J., Tkachenko, A., Weiner, S., Addadi, L., & Hendler, G. (2001). Calcitic microlenses as part of the photoreceptor system in brittlestars. *Nature, 412*(6849), 819. https://doi.org/10.1038/35090573

Baeumler, N., Haszprunar, G., & Ruthensteiner, B. (2008). 3D interactive microanatomy of Omalogyra atomus (Philippi, 1841) (Gastropoda). Zoosymposia, 1, 101-118. https://doi.org/10.11646/zoosymposia.1.1.9

Baker, D. W., Sardella, B., Rummer, J. L., Sackville, M., & Brauner, C. J. (2015). Hagfish: Champions of CO2 tolerance question the origins of vertebrate gill function. *Scientific reports, 5*(1), 1-8. https://doi.org/10.1038/srep11182

Balser, E. J., & Ruppert, E. E. (1990). Structure, ultrastructure, and function of the preoral heart-kidney in *Saccoglossus kowalevskii* (Hemichordata, Enteropneusta) including new data on the stomochord. *Acta Zoologica, 71*(4), 235-249. https://doi.org/10.1111/j.1463-6395.1990.tb01082.x

Belichov, D. V. (1971). Kishechnodyshashie (Enteropneusta) Kurilo-Kamchatskoj Vpadiny (Tuskarory), Glossobalanus tuscarorae n. sp. Vop. Zool., Ser. 2, Kazan Pedagogical Univ, 61, 3-38.

Belton, P. S., Tanner, S. F., Cartier, N., & Chanzy, H. (1989). High-resolution solid-state carbon-13 nuclear magnetic resonance spectroscopy of tunicin, an animal cellulose. *Macromolecules, 22*(4), 1615-1617. https://doi.org/10.1021/ma00194a019

Benito, J., Fernández, I., & Pardos, F. (1993). Fine structure of the hepatic sacculations of *Glossobalanus minutus* (Enteropneusta, Hemichordata). *Acta Zoologica, 74*(2), 77-86. https://doi.org/10.1111/j.1463-6395.1993.tb01224.x

Berman, A., Addadi, L., Kvick, Å., Leiserowitz, L., Nelson, M., & Weiner, S. (1990). Intercalation of sea urchin proteins in calcite: study of a crystalline composite material. *Science, 250*(4981), 664-667. https://doi.org/10.1126/science.250.4981.664

Bone, Q., Carre, C., & Chang, P. (2003). Tunicate feeding filters. *Marine Biological Association of the United Kingdom. Journal of the Marine Biological Association of the United Kingdom, 83*(5), 907. https://doi.org/10.1017/S002531540300804Xh

Boorman, C. J., & Shimeld, S. M. (2002). The evolution of left–right asymmetry in chordates. *Bioessays*, *24*(11), 1004-1011. https://doi.org/10.1002/bies.10171

Borromeo, L., Zimmermann, U., Andò, S., Coletti, G., Bersani, D., Basso, D., ... & Garzanti, E. (2017). Raman spectroscopy as a tool for magnesium estimation in Mg‐calcite. *Journal of Raman Spectroscopy, 48*(7), 983-992. https://doi.org/10.1002/jrs.5156)

Bottjer, D. J., Davidson, E. H., Peterson, K. J., & Cameron, R. A. (2006). Paleogenomics of echinoderms. *Science, 314*(5801), 956-960. https://doi.org/10.1126/science.1132310

Braun, K., Kaul-Strehlow, S., Ullrich-Lüter, E., & Stach, T. (2015). Structure and ultrastructure of eyes of tornaria larvae of *Glossobalanus marginatus*. *Organisms Diversity & Evolution, 15*(2), 423-428. https://doi.org/10.1007/s13127-015-0206-x

Brenzinger, B., Haszprunar, G., & Schrödl, M. (2013). At the limits of a successful body plan–3D microanatomy, histology and evolution of Helminthope (Mollusca: Heterobranchia: Rhodopemorpha), the most worm-like gastropod. Frontiers in Zoology, 10(1), 37. https://doi.org/10.1186/1742-9994-10-37

Bridges, T. S., & Woodwick, K. H. (1994). Comparative morphology and function of hepatic caeca in four enteropneusts. *Acta Zoologica, 75*(4), 371-378. https://doi.org/10.1111/j.1463-6395.1994.tb00973.x

Burdon-Jones, C. (1962). The feeding mechanism of Balanoglossus gigas. *Boletim da Faculdade de Filosofia, Ciências e Letras, Universidade de São Paulo. Zoologia*, *24*(24), 255-279. https://doi.org/10.11606/issn.2526-3382.bffclzoologia.1962.120589

Byrne, M., Martinez, P., & Morris, V. (2016). Evolution of a pentameral body plan was not linked to translocation of anterior Hox genes: the echinoderm HOX cluster revisited. *Evolution & development, 18*(2), 137-143. https://doi.org/10.1111/ede.12172

Cameron, C. B. (2016). A comprehensive list of extant hemichordate species with links to images. (your guide to 'global worming'). Accessed at: https://www.webdepot.umontreal.ca/Usagers/cameroc/MonDepotPublic/Cameron/Species.html on 2021-02-21

Cameron, C. B. (2002). Particle retention and flow in the pharynx of the enteropneust worm *Harrimania planktophilus*: the filter-feeding pharynx may have evolved before the chordates. *The Biological Bulletin, 202*(2), 192-200. https://doi.org/10.2307/1543655

Cameron, C. B. (2002). The anatomy, life habits, and later development of a new species of enteropneust, *Harrimania planktophilus* (Hemichordata: Harrimaniidae) from

Barkley Sound. *The Biological Bulletin 202*(2), 182-191. https://doi.org/10.2307/1543654

Cameron, C. B. (2005). A phylogeny of the hemichordates based on morphological characters. *Canadian Journal of Zoology*, *83*(1), 196-215. https://doi.org/10.1139/z04-190

Cameron, C. B. (2016). *Saccoglossus testa* from the Mazon Creek fauna (Pennsylvanian of Illinois) and the evolution of acorn worms (Enteropneusta: Hemichordata). *Palaeontology*, *59*(3), 329-336. https://doi.org/10.1111/pala.12235

Cameron, C. B. (2018). Treatise on invertebrate paleontology, part V, chapter 2, class Enteropneusta: introduction, morphology, life habits, systematic descriptions, and future research. *Treatise Online, 109*, 1-22.

Cameron, C. B., & Bishop, C. D. (2012). Biomineral ultrastructure, elemental constitution and genomic analysis of biomineralization-related proteins in hemichordates. *Proceedings of the Royal Society B: Biological Sciences, 279*(1740), 3041-3048. https://doi.org/10.1098/rspb.2012.0335

Cameron, C. B., & Ostiguy, A. (2013). Three new species of *Glossobalanus* (Hemichordata: Enteropneusta: Ptychoderidae) from western North America. *Zootaxa, 3630*(1), 143-154. http://doi.org/10.11646/zootaxa.3630.1.5

Cameron, C. B., & Perez, M. (2012). Spengelidae (Hemichordata: Enteropneusta) from the Eastern Pacific including a new species, *Schizocardium californicum*, from California. *Zootaxa, 3569*(1), 79-88. https://doi.org/10.11646/zootaxa.3569.1.6

Cameron, C. B., Deland, C., & Bullock, T. H. (2010). A revision of the genus *Saccoglossus* (Hemichordata: Enteropneusta: Harrimaniidae) with taxonomic descriptions of five new species from the Eastern Pacific. *Zootaxa, 2483*(1), 1-22. https://doi.org/10.11646/zootaxa.2483.1.1

Cannon, J. T., Kocot, K. M., Waits, D. S., Weese, D. A., Swalla, B. J., Santos, S. R., & Halanych, K. M. (2014). Phylogenomic resolution of the hemichordate and echinoderm clade. *Current Biology, 24*(23), 2827-2832. https://doi.org/10.1016/j.cub.2014.10.016

Cannon, J. T., Rychel, A. L., Eccleston, H., Halanych, K. M., & Swalla, B. J. (2009). Molecular phylogeny of hemichordata, with updated status of deep-sea enteropneusts. *Molecular Phylogenetics and Evolution, 52*(1), 17-24. https://doi.org/10.1016/j.ympev.2009.03.027

Caron, J. B., Conway Morris, S., & Shu, D. (2010). Tentaculate fossils from the Cambrian of Canada (British Columbia) and China (Yunnan) interpreted as primitive deuterostomes. *Public Library of Sciences One*, *5*(3), e9586. https://doi.org/10.1371/journal.pone.0009586

Caron, J. B., Morris, S. C., & Cameron, C. B. (2013). Tubicolous enteropneusts from the Cambrian period. *Nature, 495*(7442), 503-506. https://doi.org/10.1038/nature12017

Cedhagen, T., & Hansson, H. G. (2012). Biology and distribution of hemichordates (Enteropneusta) with emphasis on Harrimaniidae and description of *Protoglossus bocki* sp. nov. from Scandinavia. *Helgoland Marine Research, 67*(2), 251. https://doi.org/10.1007/s10152-012-0320-5

Chen, C., Linse, K., Copley, J. T., & Rogers, A. D. (2015). The 'scaly-foot gastropod': a new genus and species of hydrothermal vent-endemic gastropod (Neomphalina: Peltospiridae) from the Indian Ocean. *Journal of Molluscan Studies, 81*(3), 322-334. https://doi.org/10.1093/mollus/eyv013

Davies, T. G., Rahman, I. A., Lautenschlager, S., Cunningham, J. A., Asher, R. J., Barrett, P. M., ... & Donoghue, P. C. (2017). Open data and digital morphology. *Proceedings of the Royal Society B: Biological Sciences*, *284*(1852), 20170194. https://doi.org/10.1098/rspb.2017.0194

Dawydoff, C. (1909). Beobachtungen über den Regenerationsprozeß bei den Enteropneusten. *Zeitschrift für wissenschaftliche Zoology, 93*, 237–305. https://www.biodiversitylibrary.org/page/9778546

De Coster, G., Van Dongen, S., Malaki, P., Muchane, M., Alcántara-Exposito, A., Matheve, H., & Lens, L. (2013). Fluctuating asymmetry and environmental stress: understanding the role of trait history. *Public Library of Science One*, *8*(3). https://doi.org/10.1371/journal.pone.0057966

Deland, C., Cameron, C. B., Rao, K. P., Ritter, W. E., & Bullock, T. H. (2010). A taxonomic revision of the family Harrimaniidae (Hemichordata: Enteropneusta) with descriptions of seven species from the Eastern Pacific. *Zootaxa, 2408*(1), 1-30. https://doi.org/10.11646/zootaxa.2408.1.1

Dilly, P. N. (1985). The habitat and behaviour of *Cephalodiscus gracilis* (Pterobranchia, Hemichordata) from Bermuda. *Journal of Zoology, 207*(2), 223-239. https://doi.org/10.1111/j.1469-7998.1985.tb04926.x

Dilly, P. N. (1986). Modern pterobranchs: observations on their behaviour and tube building. *Geological Society, London, Special Publications, 20*(1), 261-269. https://doi.org/10.1144/GSL.SP.1986.020.01.27

Dilly, P. N. (2014). *Cephalodiscus* reproductive biology (Pterobranchia, Hemichordata). *Acta Zoologica, 95*(1), 111-124. https://doi.org/10.1111/azo.12015

Dingerkus, G., & Uhler, L. D. (1977). Enzyme clearing of alcian blue stained whole small vertebrates for demonstration of cartilage. *Stain technology*, *52*(4), 229-232. https://doi.org/10.3109/10520297709116780

Dominguez, P., Jacobson, A. G., & Jefferies, R. P. (2002). Paired gill slits in a fossil with a calcite skeleton. Nature, 417(6891), 841. https://doi.org/10.1038/nature00805

Donoghue, P. C. J., Sansom, I. J., & Downs, J. P. (2006). Early evolution of vertebrate skeletal tissues and cellular interactions, and the canalization of skeletal

development. *Journal of Experimental Zoology Part B: Molecular and Developmental Evolution, 306*(3), 278-294. https://doi.org/10.1002/jez.b.21090

Dorken, M. E., Neville, K. J., & Eckert, C. G. (2004). Evolutionary vestigialization of sex in a clonal plant: selection versus neutral mutation in geographically peripheral populations. *Proceedings of the Royal Society of London. Series B: Biological Sciences*, *271*(1555), 2375-2380. https://doi.org/10.1098/rspb.2004.2875

Duboc, V., Röttinger, E., Lapraz, F., Besnardeau, L., & Lepage, T. (2005). Left-right asymmetry in the sea urchin embryo is regulated by nodal signaling on the right side. *Developmental cell*, *9*(1), 147-158. https://doi.org/10.1016/j.devcel.2005.05.008

Duncan, P. B. (1987). Burrow structure and burrowing activity of the funnel‐feeding enteropneust Balanoglossus aurantiacus in Bogue Sound, North Carolina, USA. *Marine Ecology, 8*(1), 75-95. (1987) https://doi.org/10.1111/j.1439-0485.1987.tb00176.x

Emlen, J. M., Freeman, D. C., & Graham, J. H. (1993). Nonlinear growth dynamics and the origin of fluctuating asymmetry. *Genetica*, *89*(1-3), 77-96. https://doi.org/10.1007/BF02424507

Endler, J. A. (1986). *Natural selection in the wild* (No. 21). Princeton, NJ: Princeton University Press.

Ettensohn, C. A. (2014). Horizontal transfer of the msp130 gene supported the evolution of metazoan biomineralization. *Evolution & Development, 16*(3), 139-148. https://doi.org/10.1111/ede.12074

Ezhova, O. V., & Malakhov, V. V. (2020). Axial complex of Crinoidea: Comparison with other Ambulacraria. *Journal of Morphology, 281*(11), 1456-1475. https://doi.org/10.1002/jmor.21259

Ezhova, O. V., & Malakhov, V. V. (2015). The nephridial hypothesis of the gill slit origin. *Journal of Experimental Zoology Part B: Molecular and Developmental Evolution, 324*(8), 647-652. https://doi.org/10.1002/jez.b.22645

Ezhova, O. V., & Malakhov, V. V. (2020, September). Is the Gill Skeleton of Acorn Worms (Enteropneusta) Similar to the Gill Skeleton of Amphioxus (Cephalochordata)?. *Doklady Biological Sciences 494*(1), 232-235). https://doi.org/10.1134/S001249662005004X

Ezhova, O. V., Lavrova, E. A., & Malakhov, V. V. (2013). Microscopic anatomy of the axial complex in the starfish *Asterias rubens* (Echinodermata, Asteroidea). *Biology Bulletin, 40*(8), 643-653. https://doi.org/10.1134/S1062359013080049

Falini, G., Albeck, S., Weiner, S., & Addadi, L. (1996). Control of aragonite or calcite polymorphism by mollusk shell macromolecules. *Science, 271*(5245), 67-69. https://doi.org/10.1126/science.271.5245.67

Fauchald, K. (1977). The polychaete worms. Definitions and keys to the orders, families and genera. *Natural History Museum of Los Angeles County, Science Series, 28.*

Faulwetter, S., Vasileiadou, A., Kouratoras, M., Dailianis, T., & Arvanitidis, C. (2013). Micro-computed tomography: Introducing new dimensions to taxonomy. ZooKeys, (263), 1. https://doi.org/10.3897/zookeys.263.4261

Fritzenwanker, J. H., Gerhart, J., Freeman Jr, R. M., & Lowe, C. J. (2014). The Fox/Forkhead transcription factor family of the hemichordate *Saccoglossus kowalevskii*. *EvoDevo, 5*(1), 1-26. https://doi.org/10.1186/2041-9139-5-17

Gerhart, J., Lowe, C., & Kirschner, M. (2005). Hemichordates and the origin of chordates. *Current Opinion in Genetics & Development*, *15*(4), 461-467. https://doi.org/10.1016/j.gde.2005.06.004

Gillis, J. A., Fritzenwanker, J. H., & Lowe, C. J. (2012). A stem-deuterostome origin of the vertebrate pharyngeal transcriptional network. *Proceedings of the Royal Society of London B: Biological Sciences, 279*(1727), 237-246. https://doi.org/10.1098/rspb.2011.0599

Girard, C. F. (1853). Descriptions of new nemerteans and planarians from the coast of the Carolinas. *Proceedings of the Academy of Natural Sciences of Philadelphia, 6*, 365-367.

Giray, C., & King, G. M. (1996). *Protoglossus graveolens*, a new hemichordate (Hemichordata: Enteropneusta: Harrimanidae) from the Northwest Atlantic. *Proceedings of the Biological Society of Washington, 109*(3), 430-445.

Gonzalez, P., & Cameron, C. B. (2009). The gill slits and pre-oral ciliary organ of *Protoglossus* (Hemichordata: Enteropneusta) are filter-feeding structures. *Biological Journal of the Linnean Society, 98*(4), 898-906. https://doi.org/10.1111/j.1095-8312.2009.01332.x

Graham, J. H., Raz, S., Hel-Or, H., & Nevo, E. (2010). Fluctuating asymmetry: methods, theory, and applications. *Symmetry*, *2*(2), 466-540. https://doi.org/10.3390/sym2020466

Grande, C., Martín-Durán, J. M., Kenny, N. J., Truchado-García, M., & Hejnol, A. (2015). Evolution, divergence and loss of the Nodal signalling pathway: new data and a synthesis across the Bilateria. *International Journal of Developmental Biology*, *58*(6-7-8), 521-532. https://doi.org/10.1387/ijdb.140133cg

Guthrie, R. D. (1965). Variability in characters undergoing rapid evolution, an analysis of Microtus molars. *Evolution*, *19*(2), 214-233. https://doi.org/10.2307/2406375

Halanych, K. M. (1993). Suspension feeding by the lophophore-like apparatus of the pterobranch hemichordate *Rhabdopleura normani. The Biological Bulletin, 185*(3), 417-427. https://doi.org/10.2307/1542482

Hart, M. W., Miller, R. L., & Madin, L. P. (1994). Form and feeding mechanism of a living *Planctosphaera pelagica* (phylum Hemichordata). *Marine Biology, 120*(4), 521-533. https://doi.org/10.1007/BF00350072

Hawe, A., & Haszprunar, G. (2014). 3D-microanatomy and histology of the hydrothermal vent gastropod Lurifax vitreus Warén & Bouchet, 2001 (Heterobranchia: Orbitestellidae) and comparisons with Ectobranchia. Organisms Diversity & Evolution, 14(1), 43-55. https://doi.org/10.1007/s13127-013-0155-1

Heller, J. (2015). *Sea Snails. A Natural History. 1st ed*. Switzerland: Springer International Publishing. https://doi.org/10.1007/978-3-319-15452-7

Holland N. D., Clague D. A., Gordon D. P., Gebruk A., Pawson D. L., & Vecchione M. (2005). 'Lophenteropneust' hypothesis refuted by collection and photos of new deep-sea hemichordates. Nature 434, 374–376. https://doi.org/10.1038/nature03382

Holland N. D., Jones W. J., Ellena J., Ruhl H. A., & Smith K.L. (2009). A new deep-sea species of epibenthic acorn worm (Hemichordata, Enteropneusta). Zoosystema 31, 333–346. https://doi.org/10.5252/z2009n2a6

Holland N. D., Kuhnz L. A., & Osborn K. J. (2012a). Morphology of a new deep-sea acorn worm (class Enteropneusts, phylum Hemichordata): a part-time demersal drifter with externalized ovaries. Journal of Morphology 273, 661–671. https://doi.org/10.1002/jmor.20013

Holland N. D., Osborn K. J., & Kuhnz L. A. (2012b). A new deep-sea species of harrimaniid enteropneust (Hemichordata). Proceedings of the Biological Society of Washington 125, 228–240. https://doi.org/10.2988/12-11.1

Holland, L. Z., & Onai, T. (2012). Early development of cephalochordates (amphioxus). *Wiley Interdisciplinary Reviews: Developmental Biology, 1*(2), 167-183. https://doi.org/10.1002/wdev.11

Holland, N. D., & Holland, L. Z. (2010). Laboratory spawning and development of the Bahama lancelet, *Asymmetron lucayanum* (Cephalochordata): fertilization through feeding larvae. *The Biological Bulletin, 219*(2), 132-141. https://doi.org/10.1086/BBLv219n2p132

Holland, N. D., Jones, W. J., Ellena, J., Ruhl, H. A., & Smith, K. L. (2009). A new deep-sea species of epibenthic acorn worm (Hemichordata, Enteropneusta). *Zoosystema, 31*(2), 333-346. https://doi.org/10.5252/z2009n2a6

Horst, C. J. (1939). Hemichordata. Klassen und Ordnungen des Tierreichs wissenschaftlich dargestellt in Wort und Bild. Leipzig, Akademische Verlagsgesellschaft, 4(4).

Humphreys, T., Sasaki, A., Uenishi, G., Taparra, K., Arimoto, A., & Tagawa, K. (2010). Regeneration in the hemichordate *Ptychodera flava*. *Zoological Science, 27*(2), 91–95. https://doi.org/10.2108/zsj.27.91

Igawa, T., Nozawa, M., Suzuki, D. G., Reimer, J. D., Morov, A. R., Wang, Y., Henmi, Y., & Yasui, K. (2017). Evolutionary history of the extant amphioxus lineage with shallow-branching diversification. *Scientific reports*, *7*(1), 1-14. https://doi.org/10.1038/s41598-017-00786-5

Inouye, M. (1976). Differential staining of cartilage and bone in fetal mouse skeleton by alcian blue and alizarin red S. *official journal of Congeital Anomalies Research Association of Japan*, *16*(3), 171-173. https://doi.org/10.24540/cgafa.16.3_171

Jabr, N., Archambault, P., & Cameron, C. B. (2018). Biogeography and adaptations of torquaratorid acorn worms (Hemichordata: Enteropneusta) including two new species from the Canadian Arctic. *Canadian Journal of Zoology, 96*(11), 1221-1229. https://doi.org/10.1139/cjz-2017-0214

Jefferies, R. P. (2001). Cephalochordata (Lancelets). *Essentials of life science.* https://doi.org/10.1038/npg.els.0001530

Jefferies, R. P., Brown, N. A., & Daley, P. E. (1996). The early phylogeny of chordates and echinoderms and the origin of chordate left–right asymmetry and bilateral symmetry. *Acta Zoologica, 77*(2), 101-122. https://doi.org/10.1111/j.1463-6395.1996.tb01256.x

Kaji, T., Reimer, J. D., Morov, A. R., Kuratani, S., & Yasui, K. (2016). Amphioxus mouth after dorso-ventral inversion. *Zoological letters*, *2*(1), 2. https://doi.org/10.1186/s40851-016-0038-3

Kapli, P., Natsidis, P., Leite, D. J., Fursman, M., Jeffrie, N., Rahman, I. A., ... & Telford, M. J. (2021). Lack of support for Deuterostomia prompts reinterpretation of the first Bilateria. *Science Advances, 7*(12), eabe2741.

Kaul-Strehlow, S., & Stach, T. (2013). A detailed description of the development of the hemichordate *Saccoglossus kowalevskii* using SEM, TEM, Histology and 3D-reconstructions. *Frontiers in zoology 10*(1), 1-31. https://doi.org/10.1186/1742-9994-10-53

Kerr, A. M., & Kim, J. (1999). Bi-penta-bi-decaradial symmetry: A review of evolutionary and developmental trends in holothuroidea (echinodermata). *Journal of Experimental Zoology, 285*(2), 93-103. https://doi.org/10.1002/(SICI)1097-010X(19990815)285:2<93::AID-JEZ1>3.0.CO;2-9

Khor, J. M., Guerrero-Santoro, J., & Ettensohn, C. A. (2019). Genome-wide identification of binding sites and gene targets of Alx1, a pivotal regulator of echinoderm skeletogenesis. *Development, 146*(16). https://doi.org/10.1242/dev.180653

Kingsley, R. J. (1990). Calcium carbonate spicules in the invertebrates. *Skeletal biomineralization: patterns, processes and evolutionary trends,5*, 27-33. https://doi.org/10.1029/SC005p0027

Kirschvink, J. L., & Hagadorn, J. W. (2000). 10 A grand unified theory of biomineralization. *The Biomineralisation of Nano-and Micro-Structures*, Wiley, Weinheim, Germany, pp. 139-150.

Knight-Jones, E. W. (1953). Feeding in *Saccoglossus* (Enteropneusta). *Proceedings of the Zoological Society of London*, *123*(3), 637-654. https://doi.org/10.1111/j.1096-3642.1953.tb00192.x

Komsta., L and Novomestky., F. (2015). moments: Moments, cumulants, skewness, kurtosis and related tests. R package version 0.14. Retrieved from https://CRAN.R-project.org/package=moments

Kuwano, H. (1902). On a new Enteropneust from Misaki, Balanoglossus misakiensis n. sp. 日本動物学彙報, 4(2), 77-84.

Lahti, D. C., Johnson, N. A., Ajie, B. C., Otto, S. P., Hendry, A. P., Blumstein, D. T., Richard GCoss, R. G., Donohue, K., & Foster, S. A. (2009). Relaxed selection in the wild. *Trends in ecology & evolution*, *24*(9), 487-496. https://doi.org/10.1016/j.tree.2009.03.010

Lambert, G. (1992). Ultrastructural aspects of spicule formation in the solitary ascidian *Herdmania momus* (Urochordata, Ascidiacea). *Acta Zoologica, 73*(4), 237-245. https://doi.org/10.1111/j.1463-6395.1992.tb01088.x

Lambert, G., & Lambert, C. C. (1997). Extracellular formation of body and tunic spicules in the New Zealand solitary ascidian *Pyura pachydermatina* (Urochordata, Ascidiacea). *Acta Zoologica, 78*(1), 51-60. https://doi.org/10.1111/j.1463-6395.1997.tb01126.x

Lambert, G., Lambert, C. C., & Lowenstam, H. A. (1989). Protochordate biomineralization. *Skeletal biomineralization: patterns, processes and evolutionary trends, 5*, 165-173. https://doi.org/10.1029/SC005p0165

Lankester, E. R., & Willey, A. (1890). Memoirs: The development of the atrial chamber of Amphioxus. *Journal of Cell Sciences, 2*(123), 445-466.

Le Roy, N., Jackson, D. J., Marie, B., Ramos-Silva, P., & Marin, F. (2014). The evolution of metazoan α-carbonic anhydrases and their roles in calcium carbonate biomineralization. *Frontiers in Zoology, 11*(1), 75. https://doi.org/10.1186/s12983-014-0075-8

Legendre, P., & Legendre, L. F. (2012). *Numerical ecology*. Oxford, UK: Elsevier.Lester, S. M. (1985). *Cephalodiscus* sp.(Hemichordata: Pterobranchia): observations of functional morphology, behavior and occurrence in shallow water around Bermuda. *Marine Biology, 85*(3), 263-268. https://doi.org/10.1007/BF00393246

Legg, D. A., Garwood, R. J., Dunlop, J. A., & Sutton, M. (2012). A taxonomic revision of orthosternous scorpions from the English Coal-measures aided by X-ray Micro-Tomography (XMT). Palaeontologia Electronica, 15(2), 1-16.

Lenth, R. (2019). emmeans: Estimated Marginal Means, aka Least-Squares Means. R package version 1.3.3. Retrieved from https://CRAN.R-project.org/package=emmeans

Lester, S. M. (1985). *Cephalodiscus* sp.(Hemichordata: Pterobranchia): observations of functional morphology, behavior and occurrence in shallow water around Bermuda. *Marine Biology, 85*(3), 263-268. https://doi.org/10.1007/BF00393246

Li, Y., Kocot, K. M., Tassia, M. G., Cannon, J. T., Bernt, M., & Halanych, K. M. (2018). Mitogenomics reveals a novel genetic code in Hemichordata. *Genome biology and evolution, 11*(1), 29-40. https://doi.org/10.1093/gbe/evy254

Lowe, C. J., Clarke, D. N., Medeiros, D. M., Rokhsar, D. S., & Gerhart, J. (2015). The deuterostome context of chordate origins. *Nature, 520*(7548), 456. https://doi.org/10.1038/nature14434

Lowe, C. J., Tagawa, K., Humphreys, T., Kirschner, M., & Gerhart, J. (2004). Hemichordate embryos: procurement, culture, and basic methods. *Methods in Cell Biology, 74*, 171-194. https://doi.org/10.1016/S0091-679X(04)74008-X

Lowe, C. J., Wu, M., Salic, A., Evans, L., Lander, E., Stange-Thomann, N., Griber, C. E., Gerhart, J., & Kirschner, M. (2003). Anteroposterior patterning in hemichordates and the origins of the chordate nervous system. *Cell, 113*(7), 853-865. https://doi.org/10.1016/S0092-8674(03)00469-0

Lukinykh, A. I., Ezhova, O. V., Krylenko, S. V., Galkin, S. V., Gebruk, A. V., & Malakhov, V. V. (2018). Discovery of Trunk Coelomoducts in Hemichordata. *Doklady Biological Sciences, 483*(1), 228-230. https://doi.org/10.1134/S0012496618060042

Luo, Y. J., & Su, Y. H. (2012). Opposing Nodal and BMP signals regulate left–right asymmetry in the sea urchin larva. *Public Library of Science Biology, 10*(10), e1001402. https://doi.org/10.1371/journal.pbio.1001402

Luo, Y. J., Takeuchi, T., Koyanagi, R., Yamada, L., Kanda, M., Khalturina, M., ... & Satoh, N. (2015). The *Lingula* genome provides insights into brachiopod evolution and the origin of phosphate biomineralization. *Nature communications, 6*, 8301. https://doi.org/10.1038/ncomms9301

Maletz, J. (2014). The classification of the Pterobranchia (Cephalodiscida and Graptolithina). *Bulletin of Geosciences, 89*(3). https://doi.org/10.3140/bull.geosci.1465

Mann, K., Poustka, A. J., & Mann, M. (2008). In-depth, high-accuracy proteomics of sea urchin tooth organic matrix. *Proteome Science, 6*(1), 33. https://doi.org/10.1186/1477-5956-6-33

Massin, C., & Lane, D. J. W. (1991). Description of a new species of sea cucumber (Stichopodidae, Holothuroidea, Echinodermata) from the Eastern Indo-Malayan Archipelago: *Thelenota rubralineata* n. sp. *Micronesica, 24*(1), 57-64.

Mayer, G., & Bartolomaeus, T. (2003). Ultrastructure of the stomochord and the heart–glomerulus complex in *Rhabdopleura compacta* (Pterobranchia): phylogenetic implications. *Zoomorphology, 122*(3), 125-133. https://doi.org/10.1007/s00435-003-0078-z

Mayorova, T. D., Smith, C. L., Hammar, K., Winters, C. A., Pivovarova, N. B., Aronova, M. A., ... & Reese, T. S. (2018). Cells containing aragonite crystals mediate responses to gravity in *Trichoplax adhaerens* (Placozoa), an animal lacking neurons and synapses. *Public library of Sciences one, 13*(1), e0190905. https://doi.org/10.1371/journal.pone.0190905

McEdward, L. R., & Miner, B. G. (2001). Larval and life-cycle patterns in echinoderms. *Canadian Journal of Zoology, 79*(7), 1125-1170. https://doi.org/10.1139/z00-218

Merker, S., Gruhl, A., & Stach, T. (2014). Comparative anatomy of the heart–glomerulus complex of *Cephalodiscus gracilis* (Pterobranchia): structure, function, and phylogenetic implications. *Zoomorphology, 133*(1), 83-98. https://doi.org/10.1007/s00435-013-0200-9

Metscher, B. D. (2009). MicroCT for comparative morphology: simple staining methods allow high-contrast 3D imaging of diverse non-mineralized animal tissues. *BMC physiology*, *9*(1), 1-14. https://doi.org/10.1186/1472-6793-9-11

Michels, J. (2013). Confocal laser scanning microscopy-detailed three-dimensional morphological imaging of marine organisms. *Imaging Marine Life*, E.G. Reynaud (Ed.). https://doi.org/10.1002/9783527675418.ch4

Mitchell, C. E., Melchin, M. J., Cameron, C. B., & Maletz, J. (2013). Phylogenetic analysis reveals that *Rhabdopleura* is an extant graptolite. *Lethaia, 46*(1), 34-56. https://doi.org/10.1111/j.1502-3931.2012.00319.x

Miyamoto, N., & Saito, Y. (2007). Morphology and development of a new species of Balanoglossus (Hemichordata: Enteropneusta: Ptychoderidae) from Shimoda, Japan. Zoological science, 24(12), 1278-1285. https://doi.org/10.2108/zsj.24.1278

Miyamoto, N., & Wada, H. (2013). Hemichordate neurulation and the origin of the neural tube. *Nature Communications, 4*(1), 1-8. https://doi.org/10.1038/ncomms3713

Møller, A. P., & Swaddle, J. P. (1997). *Asymmetry, developmental stability and evolution*. Oxford, UK: Oxford University Press.

Monniot, F., & Monniot, C. (2008). Compléments sur la diversité des ascidies (Ascidiacea, Tunicata) de l'ouest Pacifique tropical. *Zoosystema, 30*(4), 799-872.

Morgulis, M., Gildor, T., Roopin, M., Sher, N., Malik, A., Lalzar, M., … & de-Leon, S. B. T. (2019). Possible cooption of a VEGF-driven tubulogenesis program for biomineralization in echinoderms. *Proceedings of the National Academy of Sciences, 116*(25), 12353-12362. https://doi.org/10.1073/pnas.1902126116

Morino, Y., Koga, H., & Wada, H. (2016). The conserved genetic background for pluteus arm development in brittle stars and sea urchin. *Evolution & development, 18*(2), 89-95. https://doi.org/10.1111/ede.12174

Murdock, D. J. (2020). The 'biomineralization toolkit' and the origin of animal skeletons. *Biological Reviews, 95*(5), 1372-1392. https://doi.org/10.1111/brv.12614

Murdock, D. J., & Donoghue, P. C. (2011). Evolutionary origins of animal skeletal biomineralization. *Cells Tissues Organs, 194*(2-4), 98-102. https://doi.org/10.1159/000324245

Nakajima, Y., Humphreys, T., Kaneko, H., & Tagawa, K. (2004). Development and neural organization of the tornaria larva of the Hawaiian hemichordate, *Ptychodera flava. Zoological science, 21*(1), 69-79. https://doi.org/10.2108/0289-0003(2004)21[69:DANOOT]2.0.CO;2

Nakano, H., Miyazawa, H., Maeno, A., Shiroishi, T., Kakui, K., Koyanagi, R., ... & Kohtsuka, H. (2017). A new species of *Xenoturbella* from the western Pacific Ocean and the evolution of *Xenoturbella. BioMed Central evolutionary biology, 17*(1), 245. https://doi.org/10.1186/s12862-017-1080-2

Nanglu, K., Caron, J. B., Morris, S. C., & Cameron, C. B. (2016). Cambrian suspension-feeding tubicolous hemichordates. *BioMed Central Biology, 14*(1), 56-65. https://doi.org/10.1186/s12915-016-0271-4

Nehrke, G., Poigner, H., Wilhelms‐Dick, D., Brey, T., & Abele, D. (2012). Coexistence of three calcium carbonate polymorphs in the shell of the Antarctic clam *Laternula elliptica*. *Geochemistry, Geophysics, Geosystems, 13*(5). https://doi.org/10.1029/2011GC003996

Nishikawa, T. (2004). A new deep-water lancelet (Cephalochordata) from off Cape Nomamisaki, SW Japan, with a proposal of the revised system recovering the genus *Asymmetron*. *Zoological Science, 21*(11), 1131–1136. https://doi.org/10.2108/zsj.21.1131

O'Donnell, M. J., Todgham, A. E., Sewell, M. A., Hammond, L. M., Ruggiero, K., Fangue, N. A., ... & Hofmann, G. E. (2010). Ocean acidification alters skeletogenesis and gene expression in larval sea urchins. *Marine Ecology Progress Series, 398,* 157-171. https://doi.org/10.3354/meps08346

Ogasawara, M., Wada, H., Peters, H., & Satoh, N. (1999). Developmental expression of Pax1/9 genes in urochordate and hemichordate gills: insight into function and evolution of the pharyngeal epithelium. *Development, 126*(11), 2539-2550. https://doi.org/10.1242/dev.126.11.2539

Okai, N., Tagawa, K., Humphreys, T., Satoh, N., & Ogasawara, M. (2000). Characterization of gill-specific genes of the acorn worm *Ptychodera flava*.

Developmental Dynamics, *217*(3), 309-319. https://doi.org/10.1002/(SICI)1097-0177(200003)217:3<309::AID-DVDY9>3.0.CO;2-2

Osborn K.J., Kuhnz L.A., Priede I.J., Urata M., Gebruk A.V. and Holland N.D. (2012) Diversification of acorn worms (Hemichordata, Enteropneusta) revealed in the deep sea. Proceedings of the Royal Society, B 279, 1646–1654. https://doi.org/10.1098/rspb.2011.1916

Osborn, K. J., Gebruk, A. V., Rogacheva, A., & Holland, N. D. (2013). An externally brooding acorn worm (Hemichordata, Enteropneusta, Torquaratoridae) from the Russian Arctic. The Biological Bulletin, 225(2), 113-123. https://doi.org/10.1086/BBLv225n2p113

Osborn, K. J., Kuhnz, L. A., Priede, I. G., Urata, M., Gebruk, A. V., & Holland, N. D. (2011). Diversification of acorn worms (Hemichordata, Enteropneusta) revealed in the deep sea. *Proceedings of the Royal Society of London B: Biological Sciences, 279*(1733), 1646-1654. https://doi.org/10.1098/rspb.2011.1916

Ou, Q., Morris, S. C., Han, J., Zhang, Z., Liu, J., Chen, A., Zhang, X., & Shu, D. (2012). Evidence for gill slits and a pharynx in Cambrian vetulicolians: implications for the early evolution of deuterostomes. *BMC biology*, *10*(1), 1-15. https://doi.org/10.1186/1741-7007-10-81

Palmer, A. R., & Strobeck, C. (1986). Fluctuating asymmetry: measurement, analysis, patterns. *Annual review of Ecology and Systematics 17*(1), 391-421. https://doi.org/10.1146/annurev.es.17.110186.002135

Pennington, J. T., & Strathmann, R. R. (1990). Consequences of the calcite skeletons of planktonic echinoderm larvae for orientation, swimming, and shape. *The Biological Bulletin, 179*(1), 121-133. https://doi.org/10.2307/1541746

Peterson, K. J., & Eernisse, D. J. (2016). The phylogeny, evolutionary developmental biology, and paleobiology of the Deuterostomia: 25 years of new techniques, new discoveries, and new ideas. *Organisms Diversity & Evolution*, *16*(2), 401-418. https://doi.org/10.1007/s13127-016-0270-x

Philippe, H., Brinkmann, H., Copley, R. R., Moroz, L. L., Nakano, H., Poustka, A. J., Wallberg, A., Peterson, K. J., & Telford, M. J. (2011). Acoelomorph flatworms are deuterostomes related to *Xenoturbella*. *Nature*, *470*(7333), 255-258. https://doi.org/10.1038/nature09676

Pinheiro, J., Bates, D., DebRoy, S., Sarkar, D., & R Core Team (2018). nlme: Linear and Nonlinear Mixed Effects Models. R package version 3.1-137. Retrieved from https://CRAN.R-project.org/package=nlme

Porter, S. M. (2010). Calcite and aragonite seas and the de novo acquisition of carbonate skeletons. Geobiology, 8(4), 256-277. https://doi.org/10.1111/j.1472-4669.2010.00246.x

Priede I. J., Osborn K. J., Gebruk A. V., Jones D., Shale D., Rogacheva A., & Holland N. D. (2012). Observations on torquaratorid acorn worms (Hemichordata, Enteropneusta) from the North Atlantic with descriptions of a new genus and three new species. Invertebrate Biology 131, 244–257. https://doi.org/10.1111/j.1744-7410.2012.00266.x

R Core Team (2018). R: A language and environment for statistical computing. R Foundation for Statistical Computing, Vienna, Austria. Retrieved from https://www.R-project.org/

Rahman, I. A., Zamora, S., Falkingham, P. L., & Phillips, J. C. (2015). Cambrian cinctan echinoderms shed light on feeding in the ancestral deuterostome. *Proceedings of the Royal Society of London B: Biological Sciences, 282*(1818), 20151964. https://doi.org/10.1098/rspb.2015.1964

Rao, K. P. 1955. Morphogenesis during regeneration in an enteropneust. *Journal of Animal Morphology and Physiology, 1*, 1–7.

Rehkämper, G., Welsch, U., & Dilly, P. N. (1987). Fine structure of the ganglion of *Cephalodiscus gracilis* (Pterobranchia, Hemichordata). *Journal of Comparative Neurology, 259*(2), 308-315. https://doi.org/10.1002/cne.902590210

Ren, D., Feng, Q., & Bourrat, X. (2013). The co-effect of organic matrix from carp otolith and microenvironment on calcium carbonate mineralization. *Materials Science and Engineering: C, 33*(6), 3440-3449. https://doi.org/10.1016/j.msec.2013.04.031

Ricketts, E. F., Calvin, J., Hedgpeth, J. W., & Phillips, D. W. (1985). Between pacific tides. Stanford University Press.

Ries, J. B. (2010). Geological and experimental evidence for secular variation in seawater Mg/Ca (calcite-aragonite seas) and its effects on marine biological calcification. *Biogeosciences, 7*(9), 2795. https://doi.org/10.5194/bg-7-2795-2010

Ritter, W. (1902). The movements of the Enteropneusta and the mechanisms by which they are accomplished. *The Biological Bulletin, 3*, 255-261. https://doi.org/10.2307/1535545

Rott, H. (2003). *Developmental instability: causes and consequences*. Oxford, UK: Oxford University Press.

Röttinger, E., & Lowe, C. J. (2012). Evolutionary crossroads in developmental biology: hemichordates. *Development*, *139*(14), 2463-2475. https://doi.org/10.1242/dev.066712

Röttinger, E., DuBuc, T. Q., Amiel, A. R., & Martindale, M. Q. (2015). Nodal signaling is required for mesodermal and ventral but not for dorsal fates in the indirect developing hemichordate, Ptychodera flava. *Biology open, 4*(7), 830-842. https://doi.org/10.1242/bio.011809

Roux, M., Messing, C. G., & Améziane, N. (2002). Artificial keys to the genera of living stalked crinoids (Echinodermata). *Bulletin of Marine Science, 70*(3), 799-830.

Ruppert, E. E. (2005). Key characters uniting hemichordates and chordates: homologies or homoplasies?. *Canadian journal of zoology, 83*(1), 8-23. https://doi.org/10.1139/z04-158

Ruppert, E. E., & Balser, E. J. (1986). Nephridia in the larvae of hemichordates and echinoderms. *The Biological Bulletin, 171*(1), 188-196. https://doi.org/10.2307/1541916

Ruppert, E. E., & Balser, E. J. (2001). Nephridia in the larvae of hemichordates and echinoderms. *The Biological Bulletin, 171*(1), 188-196. https://doi.org/10.2307/1541916

Ruppert, E. E., Nash, T. R., & Smith, A. J. (2000). The size range of suspended particles trapped and ingested by the filter-feeding lancelet *Branchiostoma floridae* (Cephalochordata: Acrania). *Journal of the Marine Biological Association of the United Kingdom, 80*(2), 329-332. https://doi.org/10.1017/S0025315499001903

Rychel, A. L., & Swalla, B. J. (2007). Development and evolution of chordate cartilage. *Journal of Experimental Zoology Part B: Molecular and Developmental Evolution, 308*(3), 325-335. https://doi.org/10.1002/jez.b.21157

Rychel, A. L., & Swalla, B. J. (2008). Anterior regeneration in the hemichordate *Ptychodera flava*. *Developmental Dynamics*, *237*(11), 3222-3232. https://doi.org/10.1002/dvdy.21747

Rychel, A. L., & Swalla, B. J. (2009). Regeneration in hemichordates and echinoderms. In *Stem cells in marine organisms* (pp. 245-265). Springer, Dordrecht. https://doi.org/10.1007/978-90-481-2767-2_10

Rychel, A. L., Smith, S. E., Shimamoto, H. T., & Swalla, B. J. (2006). Evolution and development of the chordates: collagen and pharyngeal cartilage. *Molecular Biology and Evolution, 23*(3), 541-549. https://doi.org/10.1093/molbev/msj055

Sato, A., & Holland, P. W. (2008). Asymmetry in a pterobranch hemichordate and the evolution of left–right patterning. *Developmental dynamics: an official publication of the American Association of Anatomists, 237*(12), 3634-3639. https://doi.org/10.1002/dvdy.21588

Sato, A., Nagasaka, S., Furihata, K., Nagata, S., Arai, I., Saruwatari, K., ... & Nagasawa, H. (2011). Glycolytic intermediates induce amorphous calcium carbonate formation in crustaceans. *Nature Chemical Biology, 7*(4), 197. https://doi.org/10.1038/nchembio.532

Satoh, N. (2008). An aboral-dorsalization hypothesis for chordate origins. *Genesis*, *46*(11), 614-622. https://doi.org/10.1002/dvg.20416

Satoh, N., Tagawa, K., Lowe, C. J., Yu Jr, K., Kawashima, T., Takahashi, ... & Gerhart, J. (2014). On a possible evolutionary link of the stomochord of hemichordates to

pharyngeal organs of chordates. *Genesis, 52*(12), 925-934. https://doi.org/10.1002/dvg.22831

Saucède, T., Mooi, R., & David, B. (2003). Combining embryology and paleontology: origins of the anterior-posterior axis in echinoids. *Comptes Rendus Palevol, 2*(6-7), 399-412. https://doi.org/10.1016/j.crpv.2003.09.017

Simakov, O., Kawashima, T., Marlétaz, F., Jenkins, J., Koyanagi, R., Mitros, T., Hisata, K., Bredeson, J., Shoguchi, E., Gyoja, F., Yue, J. X., Chen, Y. C., Freeman, R. M., Sasaki, A., Hikosaka-Katayama, T., Sato, A., Fujie, M., Baughman, K. W., Levine, J., Gonzalez, P., Cameron, C. B., Fritzenwanker, J. H., Pani, A. M., Goto, H., Kanda, M., Arakaki, N., Yamasaki, S., Qu, J., Cree, A., Ding, Y., Dinh, H. H., Dugan, S., Holder, M., Jhangiani, S. N., Kovar, C. L., Lee, S. L., Lewis, L. R., Morton, D., Nazareth, L. V., Okwuonu, J., Santibanez, J., Chen, R., Richards, S., Muzny, D. M., Gillis, A., Peshkin, L.,Wu, M., Humphreys, T., Su, Y. H., Putnam, N. H., Schmutz, J., Fujiyama, A., Yu, J. K., Tagawa, K., Worley, K. C., Gibbs, R. A., Kirschner, M. W., Lowe, C. J., Satoh, N., Rokhsar, D. S., & Gerhart, J. 2015. Hemichordate genomes and deuterostome origins. *Nature, 527*(7579): 459–465, https://doi.org/10.1038/nature16150

Smith, A. B. (1980). Stereom microstructure of the echinoid test. *Special Papers in Palaeontology*, *25*, 1–324.

Smith, A. B. (2005). The pre‐radial history of echinoderms. *Geological Journal, 40*(3), 255-280. https://doi.org/10.1002/gj.1018

Smith, A. B. (2008). Deuterostomes in a twist: the origins of a radical new body plan. *Evolution & Development, 10*(4), 493-503. https://doi.org/10.1111/j.1525-142X.2008.00260.x

Smith, A. B., Zamora, S., & Alvaro, J. J. (2013). The oldest echinoderm faunas from Gondwana show that echinoderm body plan diversification was rapid. *Nature Communications, 4*, 1385. https://doi.org/10.1038/ncomms2391

Spengel, J. W. (1893). Die Enteropneusten des Golfes von Neapel. Fauna und Flora des Golfes von Neapel. Zool. Stat. Mono., 18, 1-758.

Spengel, J. W. (1901). Die Benennung der Enteropneusten-Gattungen. Zoologische Jahrbücher, Abteilung fuer Systematik Oekologie und Geographie der Tiere, 15, 209–218.

Spengel, J. W. (1932). *Planctosphaera pelagica.* Scientific Results “Michael Sars” North Atlantic Deep-Sea Expedition, 5, 1-27.

Stach, T. (2013). Larval anatomy of the pterobranch *Cephalodiscus gracilis* supports secondarily derived sessility concordant with molecular phylogenies. *Naturwissenschaften, 100*(12), 1187-1191. https://doi.org/10.1007/s00114-013-1117-3

Stach, T., Gruhl, A., & Kaul-Strehlow, S. (2012). The central and peripheral nervous system of *Cephalodiscus gracilis* (Pterobranchia, Deuterostomia). *Zoomorphology, 131*(1), 11-24. https://doi.org/10.1007/s00435-011-0144-x

Stock, S. R. (2014). Sea urchins have teeth? A review of their microstructure, biomineralization, development and mechanical properties. *Connective Tissue Research, 55*(1), 41-51. https://doi.org/10.3109/03008207.2013.867338

Strano, F., Micaroni, V., Beli, E., Mercurio, S., Scarì, G., Pennati, R., & Piraino, S. (2019). On the larva and the zooid of the pterobranch *Rhabdopleura recondita* Beli, Cameron and Piraino, 2018 (Hemichordata, Graptolithina). *Marine Biodiversity, 49*(4), 1657-1666. https://doi.org/10.1007/s12526-018-0933-2

Strathmann, R., & Bonar, D. (1976). Ciliary feeding of tornaria larvae of *Ptychodera flava* (Hemichordata: Enteropneusta). *Marine Biology, 34*(4), 317-324. https://doi.org/10.1007/BF00398125

Tague, R. G. (1997). Variability of a vestigial structure: first metacarpal in *Colobus guereza* and *Ateles geoffroyi*. *Evolution*, *51*(2), 595-605. https://doi.org/10.1111/j.1558-5646.1997.tb02446.x

Tamm, S. L. (2014). Formation of the statolith in the ctenophore *Mnemiopsis leidyi*. *The Biological Bulletin, 227*(1), 7-18. https://doi.org/10.1086/BBLv227n1p7

Tassia, M. G., Cannon, J. T., Konikoff, C. E., Shenkar, N., Halanych, K. M., & Swalla, B. J. (2016). The Global Diversity of Hemichordata. *Public library of Sciences one, 11*(10), e0162564. https://doi.org/10.1371/journal.pone.0162564

Turbeville, J. M., Schulz, J. R., & Raff, R. A. (1994). Deuterostome phylogeny and the sister group of the chordates: evidence from molecules and morphology. *Molecular biology and evolution, 11*(4), 648-655. https://doi.org/10.1093/oxfordjournals.molbev.a040143

Tweedell, K. S. (1961). Regeneration of the enteropneust, *Saccoglossus kowalevskii*. *The Biological Bulletin*, *120*(1), 118-127. https://doi.org/10.2307/1539342

Vinogradova, E., Ruíz-Zepeda, F., Plascencia-Villa, G., & José-Yacamán, M. (2016). Calcitic microlens arrays in *Archaster typicus*: Microstructural evidence for an advanced photoreception system in modern starfish. *Zoomorphology, 135*(1), 83-87. https://doi.org/10.1007/s00435-015-0276-5

Vo, M., Mehrabian, S., Etienne, S., Pelletier, D., Cameron, C. B. (2019). The hemichordate pharynx and gill pores impose functional constraints at small and large body sizes, *Biological Journal of the Linnean Society*, *127*(1), 75–87. https://doi.org/10.1093/biolinnean/blz005.

Vserossijskij, S., & Bjalynickij-Birulja, A. A. (1928). Trudy tret'ego Vserossijskogo S" ezda Zoologov, Anatomov i Gistologov: v Leningrade 14-20 dekabrija 1927 g. Izd. Glavnogo Upravlenija Nauk. Učreždenij.

Westfall, P. H. (2014). Kurtosis as peakedness, 1905–2014. RIP. *The American Statistician, 68*(3), 191-195. https://doi.org/10.1080/00031305.2014.917055

Willey, A. (1891). Memoirs: The Later Larval Development of Amphioxus. *Journal of Cell Science, 2*(126), 183-234.

Willey, A. (1894). *Amphioxus and the ancestry of the vertebrates*. Macmillan and Co., New-York.

Willey, A. (1899). Memoirs: Remarks on some recent work on the protochorda, with a condensed account of some fresh observations on the enteropneusta. *Journal of Cell Science*, *2*(166), 223-244.

Willey, A. (1931). *Glossobalanus berkeleyi*, a new enteropneust from the West Coast. *Transactions of the Royal Society of Canada, 5*, 19-28.

Wilt, F. H., Killian, C. E., & Livingston, B. T. (2003). Development of calcareous skeletal elements in invertebrates. *Differentiation, 71*(4-5), 237-250. https://doi.org/10.1046/j.1432-0436.2003.7104501.xGet

Wlizla, M. (2011). *Evolution of nodal signaling in deuterostomes: insights from Saccoglossus kowalevskii*. Ph.D. thesis (University of Chicago, USA).

Wood, R. A., Zhuravlev, A. Y., Sukhov, S. S., Zhu, M. Y., & Zhao, F. C. (2017). Demise of Ediacaran dolomitic seas marks widespread biomineralization on the Siberian Platform. *Geology, 45*(1), 27-30. https://doi.org/10.1130/G38367.1

Woodwick, K. H., & Sensenbaugh, T. (1985). Saxipendium coronatum, new genus, new species (Hemichordata: Enteropneusta): the unusual spaghetti worms of the Galapagos Rift hydrothermal vents. Proceedings of the Biological Society of Washington, 98(2), 351-365.

Woosley, R. J., Millero, F. J., & Grosell, M. (2012). The solubility of fish-produced high magnesium calcite in seawater. *Journal of Geophysical Research: Oceans, 117*(C4). https://doi.org/10.1029/2011JC007599

Worsaae, K., Sterrer, W., Kaul-Strehlow, S., Hay-Schmidt, A. & Giribet, G. (2012) An anatomical description of a miniaturized acorn worm (Hemichordata, Enteropneusta) with asexual reproduction by paratomy. Public Library of Sciences ONE, 7(11), e48529. http://doi.org/10.1371/journal.pone.0048529

Yoshimura, K., Morino, Y., & Wada, H. (2019). Regeneration of the acorn worm pygochord with the implication for its convergent evolution with the notochord. *Development, growth & differentiation, 61*(2), 158-165. https://doi.org/10.1111/dgd.12581

Yu, J. K., Holland, L. Z., & Holland, N. D. (2002). An amphioxus nodal gene (AmphiNodal) with early symmetrical expression in the organizer and mesoderm and later asymmetrical expression associated with left–right axis formation. *Evolution & development, 4*(6), 418-425. https://doi.org/10.1046/j.1525-142X.2002.02030.x

Zamora, S., & Rahman, I. A. (2014). Deciphering the early evolution of echinoderms with Cambrian fossils. *Palaeontology, 57*(6), 1105-1119. https://doi.org/10.1111/pala.12138

Zamora, S., Rahman, I. A., & Smith, A. B. (2012). Plated Cambrian bilaterians reveal the earliest stages of echinoderm evolution. *Public Library of Sciences One, 7*(6), e38296. https://doi.org/10.1371/journal.pone.0038296

Zhao, Y., & Li, J. (2014). Excellent chemical and material cellulose from tunicates: diversity in cellulose production yield and chemical and morphological structures from different tunicate species. *Cellulose, 21*(5), 3427-3441. https://doi.org/10.1007/s10570-014-0348-6

Ziegler, A., Ogurreck, M., Steinke, T., Beckmann, F., Prohaska, S., & Ziegler, A. (2010). Opportunities and challenges for digital morphology. *Biology direct*, *5*(1), 1-9. https://doi.org/10.1186/1745-6150-5-45

Zuur, A., Ieno, E. N., Walker, N., Saveliev, A. A., & Smith, G. M. (2009). *Mixed effects models and extensions in ecology with R*. New York, NY: Springer Science & Business Media.

Annexe A. Figures supplémentaires du chapitre 2

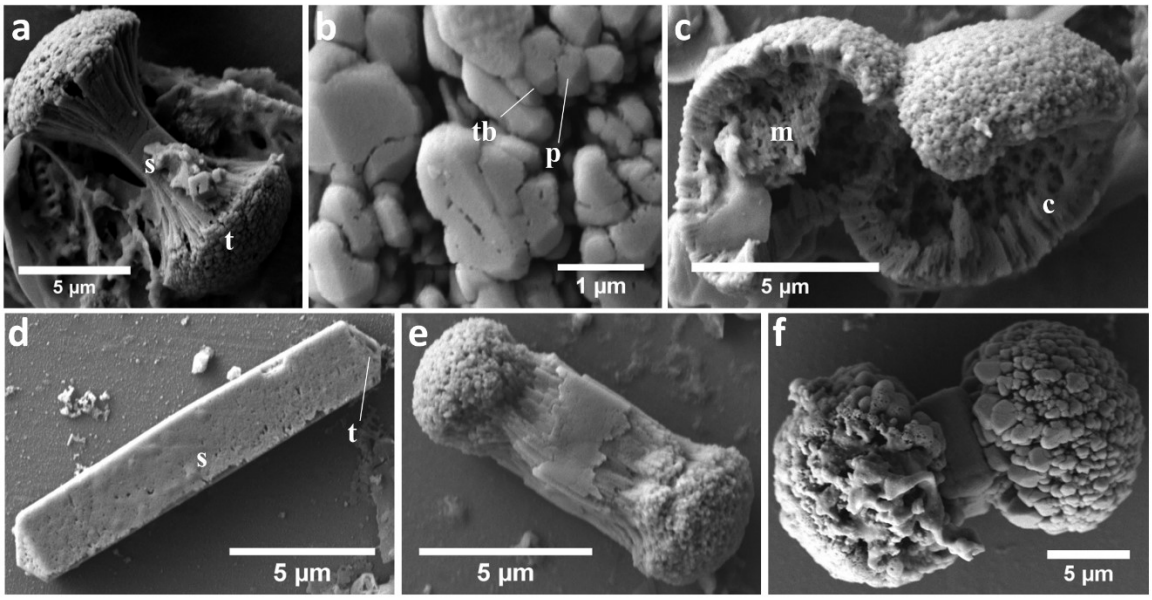

Figure S1. Scanning electron micrographs of ossicles from *Saccoglossus kowalevskii*. **a**. Sideview of a typical ‘’double-broccoli’’ ossicle formed of a prismatic shaft (s) and two terminal lobes (t). **b**. Close up on a terminal lobe showing the arrangement and spacing of trabeculae (tb). The trabeculae end in a point (p). **c**. Broken terminal lobes showing the brick-like arrangement of the cortex (c) and the porous medulla (m). **d**. Sideview of a typical ‘’prism-ossicle’’ formed of a prismatic shaft (s) and pyramidal tips (t). Most of the ossicle is the shaft. The surface of both the shaft and tip is porous. **e & f**. ‘’broccoli-ossicle’’ with small and large terminal lobes showing the variation in their possible size.

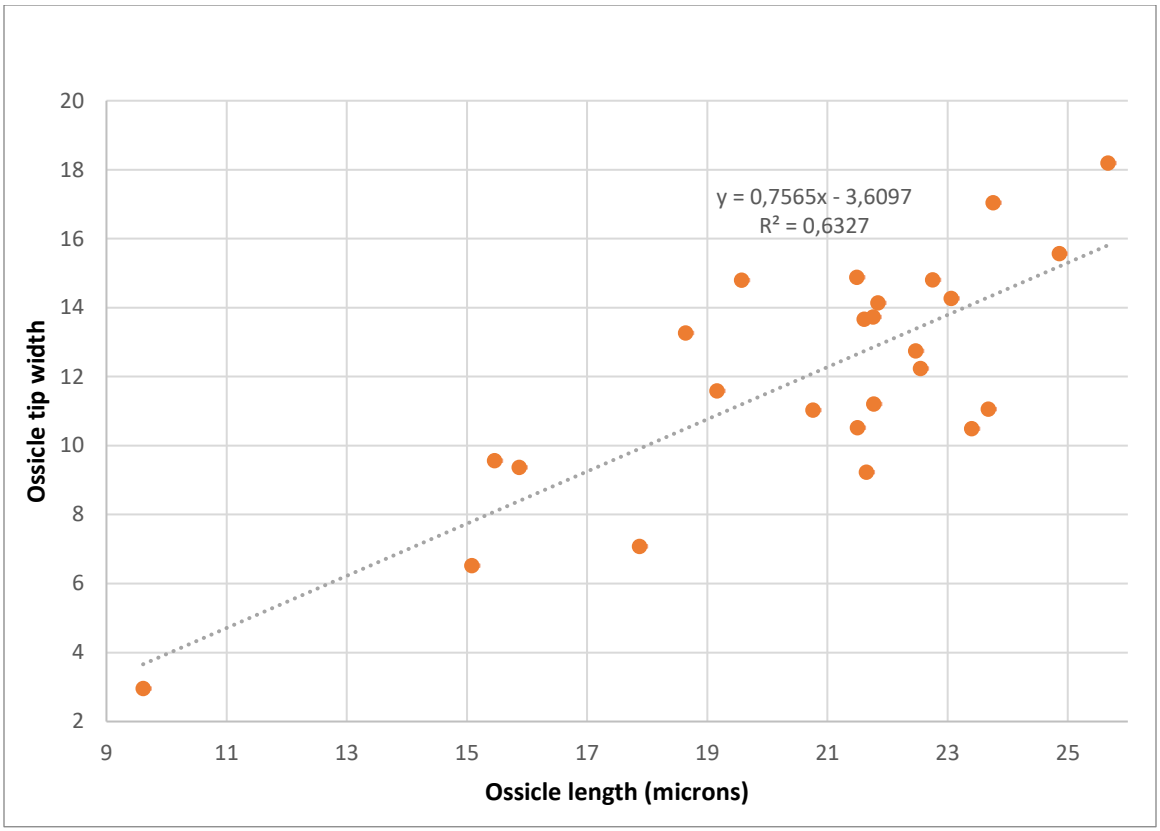

Figure S2. *Saccoglossus kowalevskii* ossicle width and length proportion.

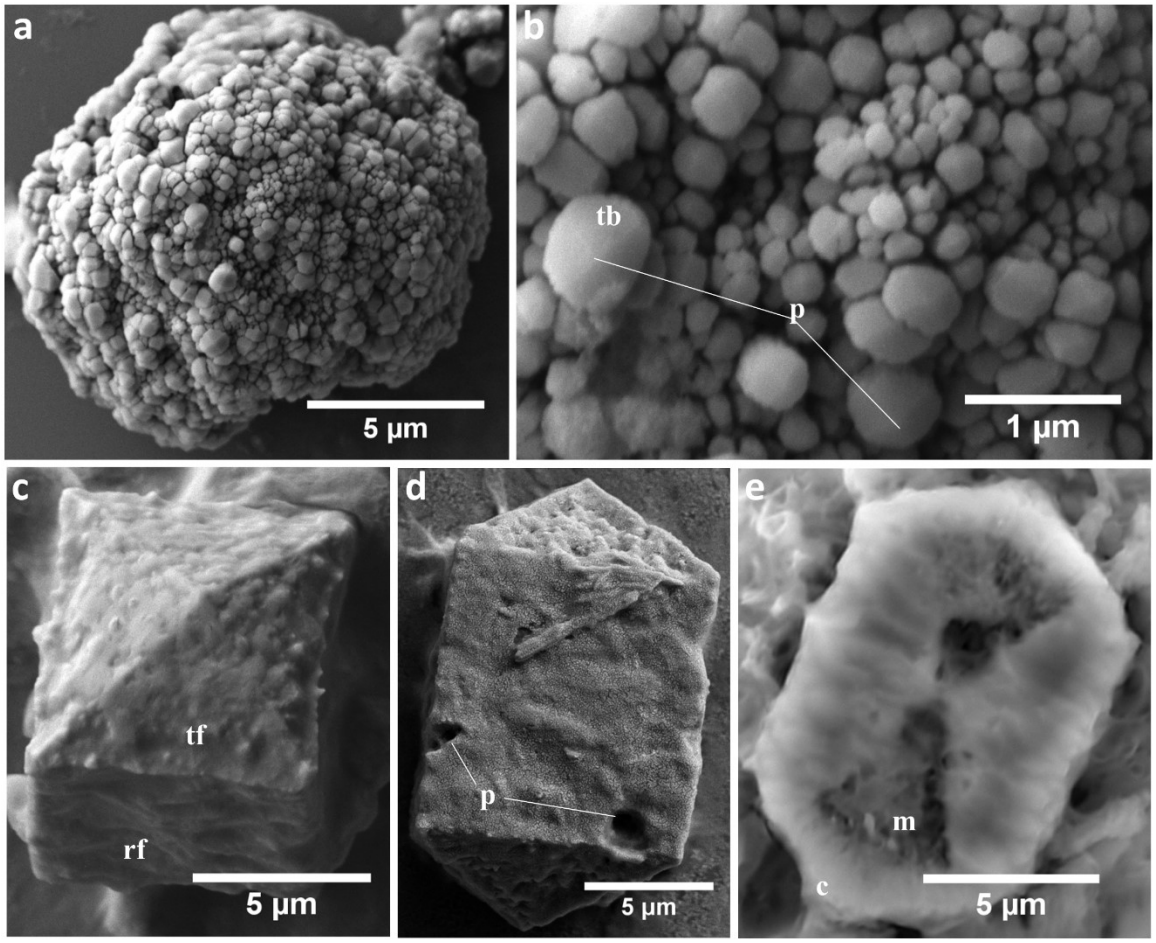

Figure S3. Scanning electron micrographs of ossicles from *Saccoglossus pusillus*. **a**. Lone terminal lobe from a ‘’broccoli-ossicle’’ **b**. Close up on the same terminal lobe showing the arrangement and spacing of trabeculae (tb). The trabeculae end in a low point (p) and are rounded in cross-section. **c**. Angled view of a typical ‘’prism-ossicle’’. The triangular faces (tf) are rough, and the rectangular faces (rf) are wrinkly. This ossicle has no crack. **d**. ‘’Prism-ossicle’’ with pores (p). This ossicle shows the typical shape of a squared prism with pyramidal ends **e**. ‘’Prism-ossicle’’ with a bowtie shape crack. The crack shows a dense cortex (c) and a porous medulla (m).

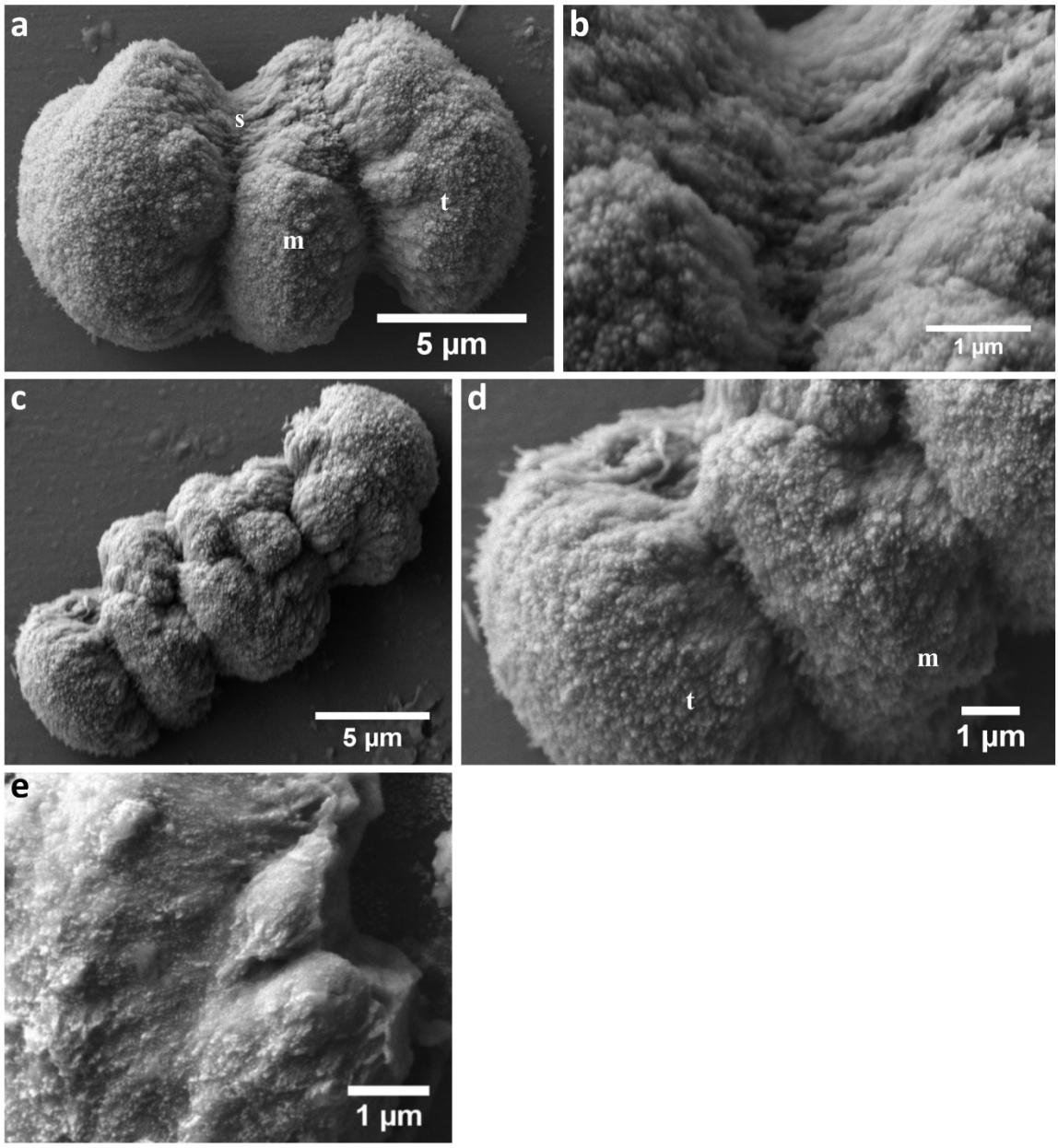

Figure S4. Scanning electron micrographs of ossicles from *Harrimania planktophilus*. **a**. Sideview of a typical ossicle (m. medial lobe; s. shaft; t. terminal lobe). **b**. Close-up on the shaft region of **a** showing its laminar organisation. **c**. The largest ossicle found in this specie. The shaft is completely outgrown by medial lobes. **d**. Close-up of both a medial and terminal lobe. Their structure is identical. Individual trabeculae are indistinguishable. **e**. Broken terminal lobe of the ossicle shown in **d**. There are no pores in the inside structure of the ossicle.

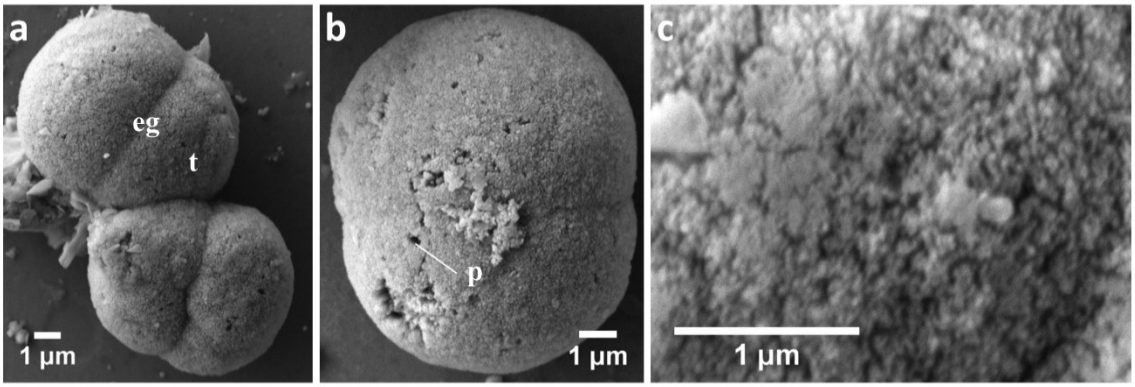

Figure S5. Scanning electron micrographs of ossicles from *Protoglossus graveolens*. **a**. Two typical ossicles formed of two terminal lobes (t) separated by an equatorial groove (eg). **b**. A bigger ossicle showing many pores (p). **c**. Close-up on a terminal lobe. Individual trabeculae are indistinguishable.

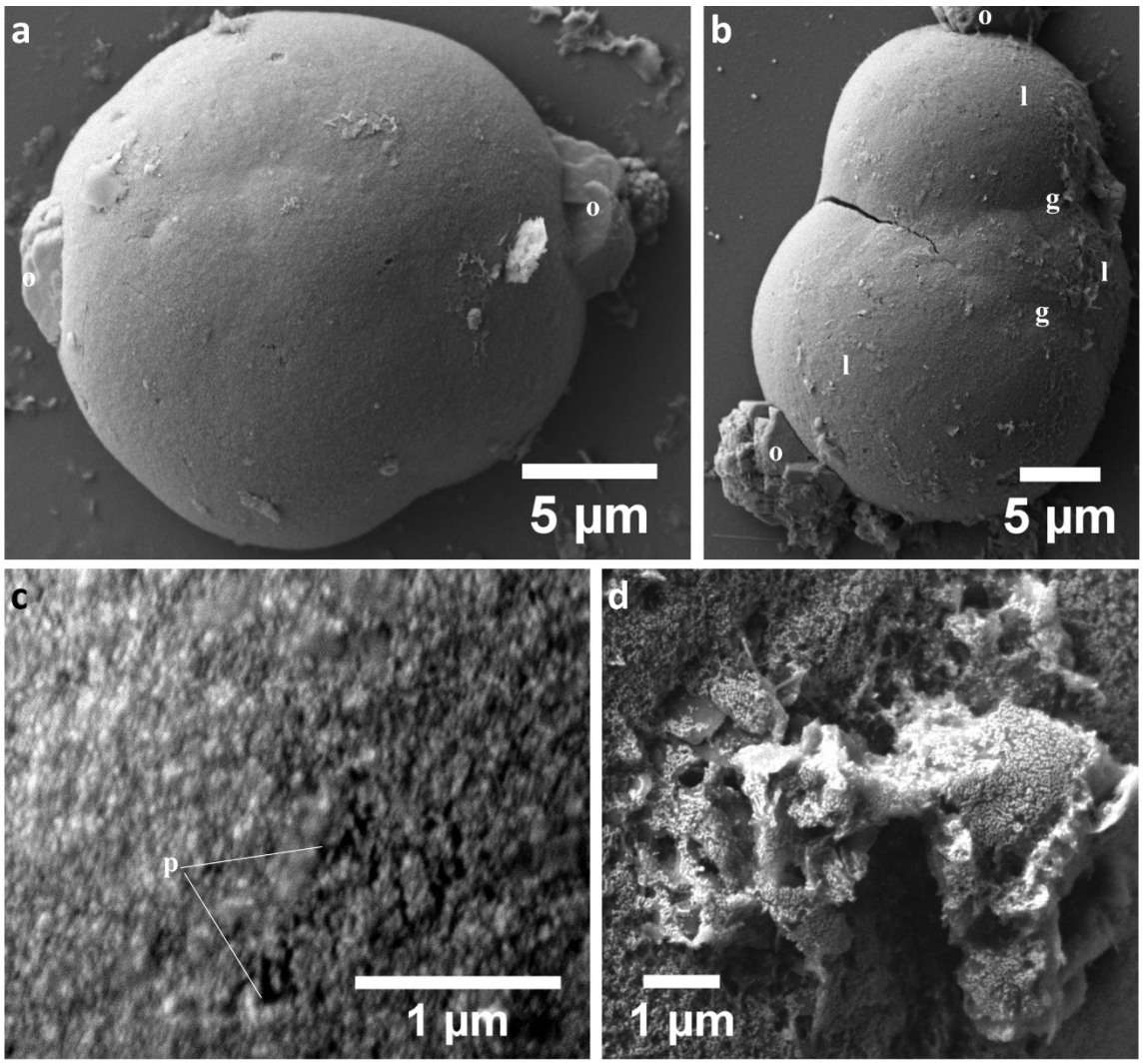

Figure S6. Scanning electron micrographs of ossicles from *Schizocardium californicum* **a**. An ossicle with a single lobe. A polyhedral outgrowth (o) is present a both ends. **b**. An ossicle with three lobes (l). Each lobe is separated by a groove (g). Polyhedral outgrowths are present. **c**. Close-up on the surface of a lobe. The lobes are an aggregate of smaller crystals among which pores (p) are present. **d**. Close-up on a broken polyhedral outgrowth showing the porous inner organisation of the ossicle.

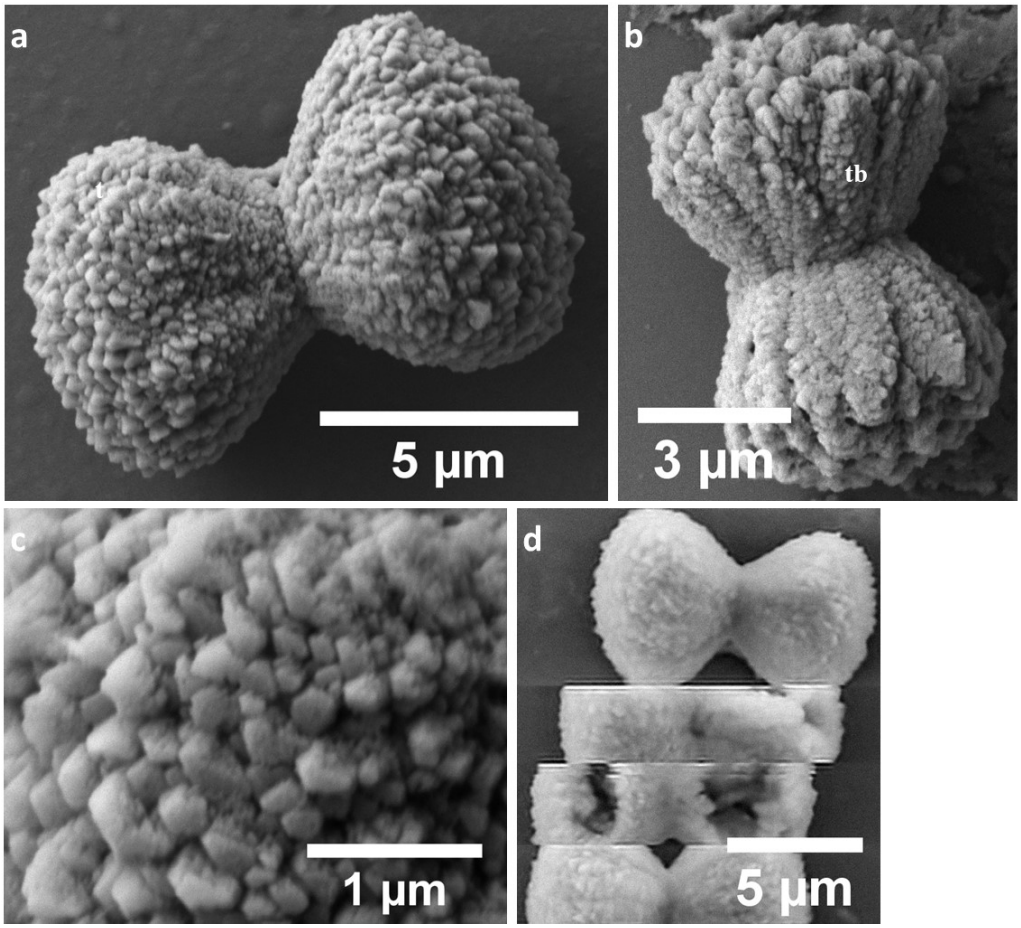

Figure S7. Scanning electron micrographs of ossicles from *Balanoglossus occidentalis*. **a**. Sideview of a typical ossicle formed of two conical terminal lobes (t) joined at their point. **b**. A smaller ossicle showing clear trabeculae (tb). **c**. Close-up on the terminal lobe of **a** showing the aggregation of polyhedral crystals. **d**. Micrograph of **a** that moved because of charging effects. A cavity can be seen in both terminal lobes.

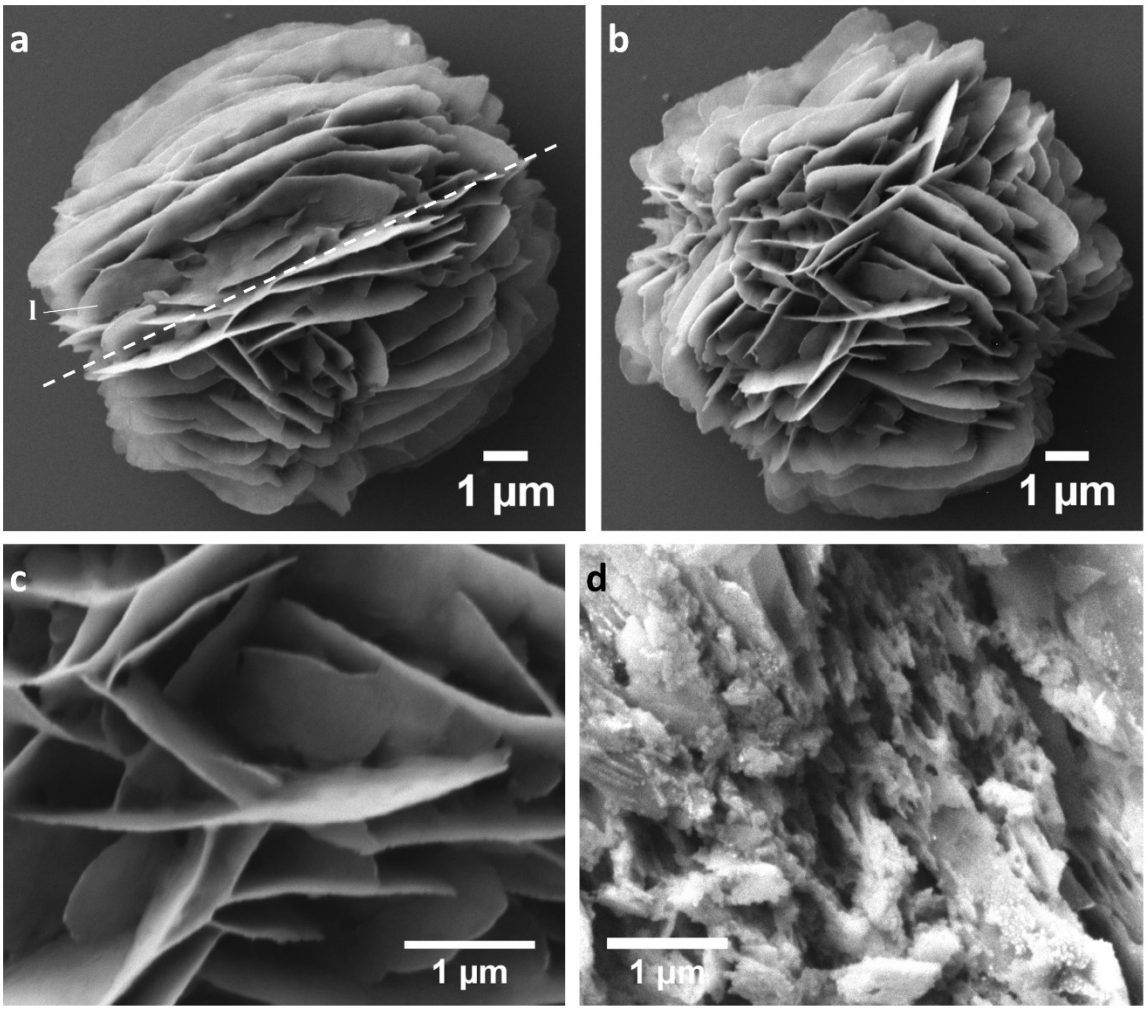

Figure S8. Scanning electron micrographs of ossicles from *Balanoglossus aurantiacus* **a**. A typical ossicle with an axis (dashed line) around which the lamellae (l) are organised. **b**. An ossicle without such axis. **c**. Close-up on the lamellae showing how they intersect in a network fashion. **d**. Close-up on a broken ossicle showing the inner network of pores.

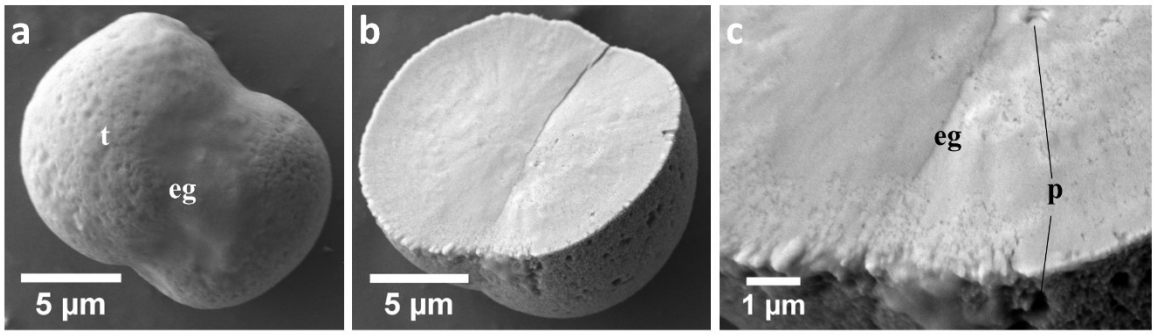

Figure S9. Scanning electron micrographs of ossicles from *Glossobalanus berkeleyi* **a**. A typical ossicle formed of two spherical terminal lobes (t) joined by an equatorial groove (eg). **b**. A broken ossicle. The inside of the ossicle is filled. **c**. Close-up of the edge of the broken ossicle. Minute pores (p) can be seen inside the ossicle.

Annexe B. Méthode et résultats de séquençage protéomique

Méthode

Les échantillons d'osselets pour le séquençage du protéome provenaient de ceux isolés dans le ver *Saccoglossus kowalevskii* pendant l'élaboration du chapitre 2. Lors des trois essais 53, 107 et 120 vers furent digérés pour isoler les osselets comme décrit dans la méthodologie du chapitre 2. En me basant sur la méthodologie de Mann *et al.* (2008), ces osselets furent décalcifiés dans une solution d'acide acétique à 50% pendant toute une nuit à 4°C. Les échantillons furent ensuite rincés deux fois avec des solutions d'acide acétique à 10% et deux fois avec des solutions d'acide acétique à 5% en utilisant des tubes à dialyse (Spectra/Por6, poids moléculaire seuil de 1000). Les échantillons ont ensuite été séchés à l'air et ont donné 15 mg, 30 mg et 25 mg de matière sèche respectivement. Les échantillons secs furent envoyés à l'Institut de Recherche en Immunologie et Cancérologie (IRIC) à Montréal pour y être séquencés. Là, les échantillons furent dilués avec 100 µl d'une solution de 50mM de bicarbonate d'ammonium, 5mM de hydroclorure de Tris(2-carboxyethyl) phosphine (Thermo Fisher Scientific, San Jose, CA), 20mM de 2-chloroactamide et agité par vortex pendant 1 h à 37°C. 1 µg de trypsine fut ajouté à la solution et la digestion eu lieu pendant 8h à 37°C. Les échantillons de peptides furent séchés et solubilisés dans une solution de 5% acétonitrile et 0.2% acide formique. Les échantillons furent mis dans des filtres pré-colonne C4 (Optimize Technologies, Oregon City, OR) connectés directement à la valve de commutation. Les échantillons furent séparés sur une colonne à phase inverse (150 µm de diamètre intérieur par 150 mm de longueur) avec un gradient de 10 à 30% de la solution acétonitrile et acide formique et un flot de 600 nL/min sur un Ultimate 3000 nano-LC connecté à un Q-Exactive Plus (Thermo

Fisher Scientific, San Jose, CA). Chaque spectre de masse (MS), acquis avec une résolution de 70000, fut suivi par 12 spectres tandem-MS (MS-MS) sur les ions précurseurs, avec plusieurs charges, les plus abondants.

Les spectre Tandem-MS furent performés par dissociation induite par collision (HCD) avec une énergie de collision de 27%. Les données furent traitées avec PEAKS X (Bioinformatics Solutions, Waterloo, ON) et une base de données Uniprot d'entéropneuste ou de ptérobranche. Les tolérances de masse sur les ions précurseurs et les ions fragments étaient de 10 ppm et 0.01 Da, respectivement. Les modifications post-traductionnelles sélectionnées étaient la carbamidométylation (C), l'oxydation (M), la déamination (NQ), l'acétylation (9N-term) et la phosphorylation (STY). Les données furent visualisées avec le programme Scaffold 4.3.0 (seuil de protéine, 99%, avec au moins deux peptides identifiés et un taux de fausse découverte [FDR] de 1% pour les peptides).

Résultats

Dans le premier essai de séquençage, la seule protéine détectée était un transporteur d'acide aminée (OS=*Saccoglossus kowalevskii*, OX=10224, A0A0U2SRB9_SACKO, 15 spectres, couverture de 6%). Trois protéines furent identifiées avec le deuxième essai, une histone H4 (OS=*Balanoglossus clavigerus* OX=560604, F8J4K4_BALCL, 6 spectres, couverture de 31%), un facteur d'élongation 1-alpha (OS=*Saccoglossus kowalevskii* OX=10224, Q6PTG5_SACKO, 5 spectres, couverture de 6%) et La sous-unité beta de l'ATP synthase (OS=*Saccoglossus kowalevskii* OX=10224, Q6PTG8_SACKO, 3 spectres, couverture de 9%). La troisième tentative a identifié uniquement une Chaine lourde de myosine (OS=Saccoglossus kowalevskii OX=10224, 4 spectres, couverture de 4%).